

**Blends of Maleated Elastomer and Nylon  
and Their Mechanical Properties**

**マレイン酸変性エラストマー/ナイロンブレンドとその力学的特性**

**A Thesis Presented to  
WASEDA UNIVERSITY**

**2003.7**

**Osamu OKADA**

**岡田 治**

# **CONTENTS**

## **Chapter 1 Introduction**

- 1.1 Compatibilization
  - 1.2 Compatibilizers
  - 1.3 Reactive compatibilization
  - 1.4 Toughened nylons
  - 1.5 Factors for toughening of nylon 6
  - 1.6 Characterization of fracture behavior
  - 1.7 Thermoplastic elastomers
  - 1.8 Thermoplastic elastomeric blends
  - 1.9 Polyolefin blends
  - 1.10 Phase inversion
  - 1.11 Purpose of this study
  - 1.12 Scope and organization of this dissertation
- References

## **Chapter 2 Fracture toughness of nylon 6 blends with maleated ethylene-propylene rubbers**

- 2.1 Introduction
  - 2.2 Experimental
  - 2.3 Treatment of fracture data with varying ligament size
  - 2.4 Results and discussion
    - 2.4.1 Fracture behavior of single-edge notch three-point-bend specimens
    - 2.4.2 Fracture energy by notched Izod test
    - 2.4.3 Comparison of fracture energy parameters
    - 2.4.4 Stress analysis
  - 2.5 Conclusions
- References

## **Chapter 3 Fracture toughness of blends of nylon 6 with maleated styrene/hydrogenated butadiene/styrene tri block copolymer**

3.1 Introduction

3.2 Experimental

3.3 Fracture analysis

3.4 Results and discussion

3.4.1 Morphology and notched Izod impact strength

3.4.2 Failure mode map for Dynatup impact test

3.4.3 Fracture analysis

3.4.3.1 Energy analysis

3.4.3.2 Stress analysis

3.4.4 Effect of rubber particle size on fracture parameters

3.5 Conclusions

References

## **Chapter 4 Nylon 6 as a modifier for maleated ethylene-propylene rubber**

4.1 Introduction

4.2 Experimental

4.3 Morphology

4.4 Mechanical properties

4.5 Dynamic mechanical properties

4.6 Modeling of modulus data

4.7 Conclusions

References

## **Chapter 5 Mechanical properties of blends of maleated ethylene-propylene rubber and nylon 6**

5.1 Introduction

5.2 Experimental

5.3 Morphology  
5.4 Mechanical properties  
5.5 Thermal and dynamic mechanical analysis  
5.6 Phase inversion behavior  
5.7 Conclusions  
References

## **Chapter 6 Dynamic mechanical properties of blends of nylon 6 and maleated ethylene-propylene rubber**

6.1 Analysis of Dickie model  
6.2 Results  
References

## **Chapter 7 Conclusion and development**

7.1 Thermodynamic criteria for blend miscibility  
7.2 Prediction and analysis of interfacial properties  
7.2.1 Interfacial tension and interfacial thickness  
7.2.2 Theory of droplet deformation and breakup  
7.3 Theory of interfacial properties for compatibilized blends  
7.4 Conclusions  
7.5 Future development  
References

## Terminology

### Chapter 2 and 3

$a$  : crack length

$\bar{d}_w$  : weight average particle diameter

$\bar{d}_n$  : number average particle diameter

$G_{IC}$  : critical strain energy release rate

$K_{IC}$  : critical stress intensity factor

$\ell$  : ligament length

$r_y$  : plastic zone size

$U/A$  : total specific fracture energy

$u_o$  : limiting specific fracture energy

$u_d$  : dissipative energy density

$\sigma_y$  : the yield stress

$\sigma_{max}$  : the maximum tensile stress

### Chapter 4 to 6

$E_i$  : tensile modulus

$E'$  : dynamic storage modulus

$E''$  : dynamic loss modulus

$G_i$  : shear modulus

$K_i$  : bulk modulus

$\tan \delta$  : loss tangent

$T_g$  : glass transition temperature

$V_{max}$  : maximum packing fraction

$\nu$  : Poisson's ratio

## **Chapter 1 Introduction**

Polymer blends can be a convenient technique to generate materials with superior properties by combination of desirable properties of different polymers in relatively low cost compared to synthesis of new molecules. Generally, polymers in blends tend to form separate phases and generate interface between two phases, because they are thermodynamically immiscible [1]. When the interaction energy for mixing between polymers is unfavorable, interfacial tension between the phases increases and interpenetration between phases decreases [2]. Large interfacial tension prevents fine dispersion of the phases during melt blending and cause unstable morphology. Little interpenetration results in poor adhesion between the phases and inferior mechanical properties of the blends [3].

It has been found that problems of interface of such incompatible blends can be solved by the addition of appropriate block or graft copolymers, i.e., compatibilizers [4-14]. Compatibilization technique provides a finer and more stable morphology and a stronger interface. Compatibilization has been achieved by addition of block copolymer, reactive compatibilization, IPN technology, crosslinking the blend component [15].

### **1.1 Compatibilization**

Copolymer could be anchored into homopolymer phases, if the copolymer segments are long enough to be entangled with surrounding chains [16-18]. Creton et al investigated Critical molecular weight for block copolymer reinforcement of interface in blends of polystyrene (PS) and poly(2-vinylpyridine) (PVP) [19]. It is suggested that at least one average entanglement between the PVP block and the PVP homopolymer is necessary to generate good stress transfer at the interface. Failure mechanism of polymer interface reinforced with block copolymer is also investigated [20]. They investigated the effect of the PVP block degree of polymerization and the areal density of block copolymer chains at the interface on the critical release energy rate and on the fracture mechanisms. The effectiveness of the reinforcement and the failure mechanism at the interface depend strongly on the respective molecular weights of the blocks and on the areal density of chain at the interface. Washiyama et al studied the fracture of interfaces between PS and PVP homopolymers reinforced with a series of PS-PVP block copolymers [21] [22]. Brown et al investigated the effects of thin layers of PS-poly(methylmethacrylate) (PMMA) diblock copolymers between PS and PMMA homopolymers on adhesion of two homopolymers [23]. Low molecular weight diblocks gave lower toughness than the high molecular weight diblocks.

Previous reports indicated that significant solubilization can be attained only if the homopolymer molecular weight is similar to or less than that of the corresponding segments of the copolymer [24, 25]. Recent studies suggested that block copolymer generally locate at the interface in the ideal case regardless of molecular weight [26].

## 1.2 Compatibilizers

Styrene-hydrogenated butadiene block copolymers are used as compatibilizers for the blends of polystyrene with various polyolefins such as low-density polyethylene (LDPE), high-density polyethylene (HDPE), polypropylene (PP). Di-block copolymer of Poly(cis-1,4-isoprene-b-1,4-butadiene) was used as a compatibilizer for the blends of polyisoprene (PI) and polybutadiene (PB) [27]. Various types of rubber such as ethylene-propylene diene copolymer (EPDM), natural rubber (NR), and ABS are used as compatibilizers for blends of LDPE and PS or polyvinylchloride (PVC) or PP [28]. Other examples of compatibilizers are di-block copolymers of poly(1,2 butadiene-b-1,4 butadiene) for blends of poly-1,2-butadiene and poly-1,4-butadiene [29], and poly(carbonate-s-dimethyl siloxane)sequenced multiblocks as compatibilizers for blends of polycarbonate (PC) and polydimethylsiloxane (PDMS) [30].

Mechanical properties of compatibilized blends such as blends of low-density polyethylene (LDPE) and polystyrene with various block copolymers [31-33], blends of high-density polyethylene and polystyrene with block copolymers [34-36] have been studied extensively. Failure properties were compared to the additive line and compatibilized blends show superior failure properties.

However, preformed block or graft copolymers have not been used extensively because of economical reason and difficulty in meeting of requirement of molecular weight for compatibilization. Block copolymers with low molecular do not provide stability of morphology, while those with high molecular weight do not readily diffuse to the interface and have low critical micelle concentration [16].

## 1.3 Reactive compatibilization

The block or graft copolymers which are formed in situ during melt mixing are extensively used for compatibilization. Interfacial reaction occurs between functionalized polymeric components [12]. Typical examples of blends of commercial interest are the combination of polymer synthesized by condensation polymerization such as polyamides and polyesters with polymers which have functional group along chain. The former polymers have nucleophilic (i.e., electron donor) end groups such as  $\text{NH}_2$ ,  $\text{COOH}$  and  $\text{OH}$ . The latter polymers have electrophilic groups, e.g., cyclic anhydride, epoxide, oxazoline, isocyanate, and carbodiimide, which are incorporated along the chain by copolymerization, end capping, or grafting [12] [37-41]. The reactions most commonly used for compatibilization are the anhydride-amine (imidization) and epoxide-carboxylic acid reactions [42-49]. Other examples are the reaction of oxazoline ring with a nucleophile (e.g., carboxylic acid) and the reactions of carbodiimide and isocyanate with amines or carboxylic acids [12]. The

utilization of acrylic orthoesters for capping anhydrides, carboxylic acids, thiols, or hydroxyl groups are also seen in several recent patents. [70,71]

The reactions during processing occur in several way such as chain cleavage and recombination, graft copolymer formation, block copolymer formation, and covalent cross-linking. Most desired reaction is graft copolymer formation. It is not easy to control reaction using the chain cleavage and recombination, because it forms random copolymer as well as block copolymer. Factors such as intensity and time of mixing, functionality level and kinetics of reactive groups, and stability of covalent bonds to processing affect the extent of reaction of block copolymer formation [12].

The reaction of imide formation between amine end groups with cyclic anhydrides was investigated. It was reported that the cyclic anhydride reacts predominantly with the amine end groups, and not with the amide linkages in the polyamide[64, 65].

Copolymer formed by the reactive compatibilization reduces the interfacial tension, provides steric stabilization and retards coalescence. These effects of copolymer act as compatibilizer and reduce the size of dispersed-phase particles. The particle size decreases as the amount of maleic anhydride increases [38]. It was found that the MA content does not need to exceed 1% for tough blends. Other important factors for reactive compatibilization are end-group configuration, molecular weight, physical interaction and mixing time as seen in literature [50].

#### **1.4 Toughened nylons**

Typical examples of rubber toughened engineering polymers are polyamides, polyesters, epoxy resins, poly(phenylene oxide) [51], polycarbonates and polyacetals [52, 53]. Other examples are toughening of polyimides and polysulfones and polyarylether ketones. Blends of rubber modified PA-PPO [54, 55], PBT-PC, PA-PC, PET-PBT and PET-PC have developed for materials with high strength, high heat deformation temperatures, solvent resistance and toughness.

Nylons have been used for numerous engineering applications because they have desirable properties such as high strength and modulus, excellent chemical and abrasion resistance, high melting point, low coefficient of friction, and toughness. However, nylons tend to break in a brittle manner for notched specimen and at low temperatures. Applications of nylons were limited because of the poor resistance to crack propagation.

Toughening of nylons such as PA-6 and PA-66 have been investigated extensively [56-62]. Reactive processing of nylon with 5 to 20 wt% of an acid-functional elastomer is typical approach to toughening of nylon. The examples of elastomers are maleic anhydride

modified ethylene/propylene elastomers (EPR-g-MA, EPDM-g-MA), styrene/ethylene/butylene/styrene block copolymers (SEBS-g-MA), and emulsion-made core-shell rubbers.

### **1.5 Factors for toughening of nylon 6**

Toughness of blends depends on rubber concentration, rubber particle size, and type of rubber. Wu showed that transition from ductile to brittle behavior occurs at a critical particle size for a constant rubber amount [63, 64]. Supertough blends in which Izod impact strength is larger than 800 J/m are yielded, for a fixed rubber content of about 20%, when the rubber particle size is larger than a lower limit of about 0.1  $\mu\text{m}$ , but smaller than an upper limit of about 1  $\mu\text{m}$  [64].

Wu [58] has shown that toughness of nylon/rubber blends increases when the interparticle distance or ligament thickness is reduced to below a critical value. Cavitation of the rubber particles relieves the triaxial stress state ahead of a growing crack and permits the matrix to shear yield [65]. Shear yielding in the matrix dissipates considerable energy during the fracture process [66-68]. The upper limit on particle size apparently defines a critical interparticle distance (ligament thickness) of the matrix that allows percolation of a shear-yield condition in the material [58].

It has been suggested that extremely small particles are unable to cavitate [59, 60], which would explain the lower limit on particle size. Volume strain to cavitate which is a function of particle diameter increases as the particle size decreases. Lower limit of particle size is occurred when the sample fails by yield or fracture before it reaches the very high critical strain to cavitate.

The ductile-to-brittle transition temperature decreases as the particle size decreases, but it increases at extremely small particles [63, 64]. The effect of rubber modulus on toughness has been examined [25][20]. Blends of rubbers with lower modulus indicate lower ductile-to-brittle transition temperatures and higher room temperature toughness at constant rubber volume or particle size.

### **1.6 Characterization of fracture behavior**

Toughness may be defined as the ability to resist fracture by absorbing energy and is usually expressed in terms of the work done in forming a unit area of fracture surface. Typically, the toughness values for rigid polymers range from 50  $\text{J m}^{-2}$  in highly cross-linked epoxy resins to 80  $\text{kJ m}^{-2}$  for toughened nylon blends. The notched Izod impact test and the notched Charpy test are the most widely used for evaluating the fracture toughness of thermoplastics. They are easy to carry out and calculate the impact strength. The results are reproducible because of the presence of a rounded notch tip of defined radius.

However, the data is measured only for the same specimens and depends on the geometry. Reproducibility for transition region is rather poor. More precise method that is independent from geometry is necessary. It has been shown that standard Charpy or Izod toughness does not functionally depend on material variables. It is also reported that comparison of standard Izod toughness does not show intrinsic material property [69].

Fracture mechanics approaches can separate the effects of specimen geometry from those based on the intrinsic material properties. Fracture mechanics differentiates elastic from plastic fracture and separates the initiation and propagation in the total toughness [70].

Linear elastic fracture mechanics (LEFM) is used for characterization of fracture behavior of brittle polymers [71]. There are two approaches, i.e., the stress intensity approach and the energy approach [72, 73].

Nonlinear fracture mechanics for ductile polymers is based on the J-integral concept. The J-integral is a path-independent contour integral and is applied to elastic-plastic materials under either linear or nonlinear elastic deformation which precedes crack growth. It describes the stresses, strains and displacements of any path around a single crack [27-30]. The J-integral is expressed for a two-dimensional crack.

However, current method for J-integral measurement is restricted to quasistatic loading only. It is difficult and expensive to use J-integral method [59, 60]. It is necessary to establish a more useful and powerful method for characterization of fracture toughness of ductile polymers. Essential work of fracture (EWF) has been developed based on Broberg's unified theory of fracture for this purpose.

The total work of fracture,  $W_f$ , consists of both the dissipative work,  $W_p$ , in the outer plastic zone, which is geometry dependent, and the essential work,  $W_e$ , in the inner autonomous zone called the fracture process zone (FPZ), which is a material property. In quasistatic crack growth,

$$W_f = W_e + W_p$$

$$w_f = w_e + w_p l$$

where  $w_f$  is the specific total work of fracture ( $=W_f/l$ ),  $w_p$  is the geometry dependent plastic-zone shape factor, and  $w_e$  is the specific nonessential plastic work of fracture. Plotting  $w_f$  against  $l$  yields a straight line whose y-intercept is  $w_e$  and whose slope equals  $w_p$ . Equation above provides a sound theoretical basis for a simple experimental method to determine  $w_e$

from experiments on the total work of fracture using a range of ligament lengths and different specimen geometries [69, 80].

Mai et.al. showed that the notch-tip plastic constraint increases as the ligament length decreases relative to the thickness. Plane-stress conditions occur when  $l/B$  is large enough. The plane-stress/plan-strain transition often occurs at  $l/B = 3$  to 5 for many ductile materials. Mai also pointed out that the plane-strain condition will be reached with further decreasing of the ligament length, if the thickness satisfies the condition specified in the ASTM E813 standard for JIC measurement,

$$B \geq 25 \frac{w_{le}}{y}$$

where  $w_{le}$  is the plane-strain specific essential work of fracture.

Wu et al. applied the EWF method to impact measurement of ductile polymer blends using SENB specimens [23,59, 60]. Vu-Khahn shows the following equation [83]:

$$U = G_i A + T_a A^2 / 2$$

Wildes et al. [94] showed that the specific total fracture energy  $U/A$  is expressed as

$$U/A = u_o + u_d \ell$$

where  $u_o$  is the limiting specific fracture energy and  $u_d$  is the dissipative energy density.

### 1.7 Thermoplastic elastomers

Elastomer-plastic blends are commercially and scientifically important technologies [74]. In the elastomer-plastic blends, plastic particles are used as modifiers and organic fillers to replace standard reinforcing or nonreinforcing fillers. PE was blended with EPDM in order to improve mechanical and electrical properties [75]. It was also reported that oil resistance, ozone and electrical properties were improved by mixing PE in butyl rubber. It was reported that PE acts as a reinforcing agent for IR, if PE is chemically bound to the rubber matrix [76]. Blends of BR and polyolefin have also studied using mixing process [77]. Physical properties of blends of polystyrene (PS) with BR and SBR were studied. It is found that tensile strength was determined by blend ratio, whereas hardness, elongation, set and resilience were controlled by continuity of the PS phase. Several studies were made with PS-SBR blends [78] and PS-NR blends [79].

### 1.8 Thermoplastic elastomeric blends

The elastomer-plastic blends are also studied as thermoplastic elastomers (TPEs). Growth of production of TPEs has been increased rapidly compared to synthetic and natural rubber over the decade [80]. The primary advantages of TPE over conventional rubber are the ease of processing and the possibility of recycling and reuse. The disadvantages are the high cost

of raw materials, the inability to highly load with low cost fillers such as carbon black, poor chemical and temperature resistance and high mechanical hysteresis [81].

All TPEs have microphase separation structures that result from crystallinity, hydrogen bonding, ionic and van der Waals driving forces. One phase in these systems is the soft phase that is between glass temperature,  $T_g$ , and melting temperature,  $T_m$ . The other phase is the hard phase which is rigidly locked in place, because the service temperature is below either  $T_g$  or  $T_m$ . The relative amounts of two components control the physical properties of the TPEs.

One approach to formation of TPEs is block copolymerization. The first commercially available TPEs in the early 1960s are Kraton series from Shell Development Company. These materials are either poly(styrene-*b*-butadiene-*b*-styrene) (SBS), poly(styrene-*b*-isoprene-*b*-styrene) (SIS), poly(styrene-*b*-ethylenebutylene-*b*-styrene) (SEBS) triblock copolymers which are typically anionically polymerized. The styrene-rich phase acts as the glassy hard phase up to about 100°C. Approximately 50% of all production of TPEs are SBS, SIS and SEBS triblock copolymers. Segmented copolymers based on polyester or polyurethane are formed by condensation polymerizations [81].

Other major productions of TPEs, which account for about 30% of TPEs market, are random or block  $\alpha$ -olefin copolymers including ethylene-propylene (EP) copolymers formed by Ziegler-Natta polymerization. The physical crosslink by crystallizable hard segments is particularly interested for better processability and mechanical properties compared to the glassy hard segments. It is desired that such EP copolymers with molecular structure similar to the SBS tri-block copolymer could be directly polymerized. However, the direct polymerization of such  $\alpha$ -olefin is difficult, because Ziegler-Natta catalysts have high decay rates [82, 83] as well as high propagation rates [84, 85]. Synthesis of such polyolefin block copolymers have been investigated by several researchers [86-88].

A comb-graft copolymer with EPDM backbone and pendant crystalline poly(pivalolactone) is the exception where the crystalline domains are distinctly dispersed in the undeformed state [89, 90].

Another approach to formation of TPEs is blending of elastomers with rigid thermoplastics. The copolymers of  $\alpha$ -olefine are often blended with another homopolymer, which is typically one of the copolymer components in order to improve mechanical properties. One of examples is blends of propylene- $\alpha$ -olefin copolymers including EPDM with isotactic polypropylene. These blends show better mechanical properties than the only

copolymers. Co-crystallization behavior is reported in these systems [91].

Blends of natural rubber and polyolefin are investigated to form thermoplastic natural rubber [92]. The major components are NR and isotactic polypropylene. Those blends were prepared by mixing NR with polyolefins in an internal mixer at the temperatures about 180°C which are above the melting point of the polyolefins. The mechanical properties of these blends depend on the ratio of the two components; those with high NR content are rubbery and those with high polyolefin content are semirigid. Polyethylene, ethylene and vinyl acetate can be also used. Effects of cross-linking of the NR phase were also studied [93].

Ethylene-propylene rubber is important heat resistant rubber. Reinforcement by carbon black for EPR is weaker than for general rubber. Reinforcement of EPR by incorporation of nylon 6 via reactive processing is interesting for new approach for new type of reinforcement of rubber using resin. Also, there may be possibility of thermoplastic elastomer by nylon grafted EPR. Blends of elastomer and thermoplastic are commercially important to make thermoplastic elastomers and have been investigated by many authors. Morphology is a key factor affecting the mechanical properties of TPE blends as in the case of block copolymers.

### **1.9 Polyolefin blends**

Blends of ethylene/propylene copolymers and terpolymers with polyethylene and polypropylene are commercially important. Numerous patents have issued concerning these blends [94]. A patent application was filed for blends of crystalline polypropylene and EPM in which the EPM contained more than 50% propylene [95]. A patent covering a process for preparing a blend of natural or synthetic rubber and polypropylene, in which polypropylene was the continuous phase, was also filed [96]. The properties and applications of polyolefin thermoplastic elastomers which are commercially available have been shown in literatures[97, 98].

The morphology and other properties of blends of EPM and EPDM elastomers with polypropylene have been investigated., Lohse [99] showed that blends of crystalline polypropylene and ethylene/propylene copolymers are immiscible in 50/50 mixtures using neutron scattering techniques. Onogi and coworkers [100] showed that phase inversion occurs at polypropylene contents of 50-60% based on the analysis of modulus data and infrared dichroism studies for blends of ethylene/propylene elastomer with polypropylene. Kresge [101] indicated that EPM/polypropylene blends was cocontinuous in the range of 70-85% EPM from the results of electron micrograph studies. Kresge lists a number of patents concerned with thermoplastic elastomers prepared by polymer blending. The morphology and physical properties for blends of ethylene/propylene elastomers with polypropylene

were examined by Danesi and Porter [102]. Ranalli reviewed the properties of ethylene/propylene elastomer blends with polypropylene [103].

Dynamic vulcanization is another approach to produce TPEs based on  $\alpha$ -olefin polymers. In this process, blends that have elastomeric properties are produced via melt compounding where cross-linking reaction takes place. The dynamic vulcanizate can flow at processing temperature and is a kind of thermoplastic elastomer. If blends of polypropylene which is modified with maleic anhydride and NBR which is amine terminated are dynamically vulcanized, they should form NBR-PP block copolymer during melt mixing [104]. This copolymer acts as a compatibilizer in dynamic vulcanization.

### **1.10 Phase inversion**

Phase inversion behaviors of polymer blends are also explored [105]. Morphology of polymer blends where two polymers are mixed depends on composition. One phase is dispersed in other polymer matrix in either extreme of composition. Both two polymers are continuous in the intermediate region where phase inversion occurs. Such co-continuous morphology is investigated extensively [106].

Interpenetrating polymer networks (IPNs) [107] were proposed by Klempner et al. The concepts of IPNs have been developed for thermoset polymer systems. Gergen et al. proposed thermoplastic IPNs and reported the morphology and properties of interpenetrating network blends of S-EB-S with polypropylene, polybutylene, nylon, polybutylene terephthalate, polycarbonate and other thermoplastics [108]. The authors defined IPNs as equilibrium blends of two or more polymers where at least two of the components have three dimensional spatial continuity. The components retain their individual identities and thus the properties of both are fully expressed. Factors for polymer blends affecting properties are compositions of component, content of maleic acid, morphology, viscosity, and crystallinity.

### **1.11 Purpose of this study**

Purpose of this work is to explore three major research categories for polymer blends of nylon 6 and maleated ethylene-propylene rubber such as mechanical behavior, phase inversion behavior and fracture behavior.

### **1.12 Scope and organization of this dissertation**

Chapter 2 describes dynamic fracture behavior of blends of nylon 6 and maleated ethylene-propylene rubber. Izod impact testing and single-edge notch three-point bend (SEN3PB) instrumented Dynatup tests were examined extensively. The effects of EPR-g-MA content, ligament length, method of fracture surface measurement, sample thickness and fracture position in molded bar on the fracture behavior were investigated.

Chapter 3 explores the effects of maleated rubber type on dynamic fracture behavior using fracture mechanics approach.

Chapter 4 examines blends of nylon 6 and ethylene-propylene rubber grafted with maleic anhydride (EPR-g-MA) which were prepared using melt blending process. Nylon 6 particles have potential to reinforce matrix of EPR-g-MA due to reaction of the polyamide amine end groups with the grafted maleic anhydride. This chapter focuses on the effects of content of nylon 6 on the rheological, morphological and mechanical properties of the blends where nylon 6 is the dispersed phase.

Chapter 5 describes blends of nylon 6 with maleated ethylene-propylene rubber (EPR-g-MA) which were prepared by melt blending over the whole composition range. The reaction of the polyamide amine end groups with the grafted maleic anhydride has the potential to form thermoplastic elastomers (TPE) with controlled morphology and chemical bonding between the phases. This chapter focuses on the effects of nylon 6 content and crystallinity of the maleated rubber on morphological, thermal and mechanical properties of these blends.

Chapter 6 further explores the effect of the amount of nylon 6 on static and dynamic modulus. The dependence of modulus on polymer composition is analyzed using the theory proposed by Dickie.

Chapter 7 discusses fundamental chemical aspects of interface for polymer blends and describes basic requirements for ideal compatibilizer. Conclusions in this study are summarized.

## References

- [1] Paul DR, Bucknall CB, editors. Polymer blends: formulations and performance. New York: John Wiley & Sons, 2000.
- [2] Callaghan TA, Takakuwa K, Paul DR, Padwa AR. Polymer 1993;34:3796.
- [3] Park I, Barlow JW, Paul DR. J Polym Sci Part B: Polym Phys 1992;30:1021.
- [4] Locke CE, Paul DR. J Appl Polym Sci 1973;17:2597.
- [5] Bartensen W, Heikens D, Piet P. Polymer 1974;15:119.
- [6] Lindsey CR, Paul DR, Barlow JW. J Appl Polym Sci 1981;26:1.
- [7] Sjoerdsma SD, Blejenberg ACAM, Heikens D. Polymer 1981;22:619.
- [8] Teysse Ph. Makromol Chem, Macromol Symp 1988;22:83.
- [9] Molau GE. In: Aggarval SL, editor. Block polymers. New York: Plenum Press, 1970. p. 79.
- [10] Anastasidis JH, Gancarz I, Kobertstein JT. Macromolecules 1989;22:1449.
- [11] Shull KA, Kramer EJ. Macromolecules 1990;23:4576.
- [12] Datta S, Lohse DJ. Polymeric compatibilizers: Use and benefits. Munich: Hanser Publishers, 1996.
- [13] Sondergaard K, Lyngaae-Jorgensen J. In: Sondergaard K, Lyngaae-Jorgensen J, editors. Rheo-physics of multiphase systems: Characterization by rheo-optical techniques. Lancaster PA: Technomic Publishing Co., 1995.
- [14] Brown SB. "Reactive extrusion: A survey of chemical reactions of monomers and polymers during extrusion processing" In: Xanthos M, editor. Reactive extrusion: Principles and practice. Munich: Hanser Publishers, 1992.
- [15] Utracki LA. Polymer alloys and blends: thermodynamics and rheology, New York: Hanser Publishers, 1989.
- [16] Paul DR. In: Legge NR, Holden G, Schroeder HE, editors. Thermoplastic elastomers: 2nd edition. New York: Hanser Publishers, 1996. pp. 489-520.
- [17] Brown HR. Macromolecules 1989;22:2859.
- [18] Brown HR, Char K, Decline VR, Green PF. Macromolecules 1993;26:4155.
- [19] [Creton C, Kramer EJ, Hadziioannou G. Macromolecules 1991;24:1846.
- [20] Creton C, Kramer EJ, Hui C-Y, Brown HR. Macromolecules 1992;25:3075.
- [21] Washiyama J, Creton C, Kramer EJ. Macromolecules 1992;25:4751.
- [22] Washiyama J, Creton C, Kramer EJ, Xiao F, Hui C-Y. Macromolecules 1993;26:6011.
- [23] Brown HR, Char K, Deline VR, Green PF. Macromolecules 1993;26:4155.
- [24] Inoue T, Soen T, Hashimoto T, Kawai H. Macromolecules 1980;3:87.
- [25] Molau GE, Wittbrodt WM. Macromolecules 1968;1:260.
- [26] Lu X, Weiss RA. Macromolecules 1993;26:3615.
- [27] Cohen RE, Ramos AR. Macromolecules 1979;12:131.
- [28] Ghaffar A, Sadrmohaghegh C, Scott G. Eur Polym J 1981;17:941.
- [29] Cohen RE, Wilfong DE. Macromolecules 1982;15:370.

- [30] Trostyanskaya EB, Zemskov MB, Mikhasenok OY. *Plast Massy* 1983;11:28.
- [31] Fayt R, Jerome R, Teyssie Ph. *J. Polym. Sci., Polym. Lett* 1981;19:79.
- [32] Fayt R, Jerome R, Teyssie Ph. *J. Polym. Sci., Polym. Phys* 1981;19:1269.
- [33] Heikens D, Hoen N, Barentsen W, Piet P, Laden H. *J. Polym. Sci., Polym. Symp* 1978;62:309.
- [34] Fayt R, Jerome R, Teyssie Ph. *J. Polym. Sci., Polym. Phys* 1981;19:1269.
- [35] Fayt R, Hadjiandreou P, Teyssie Ph. *J. Polym. Sci., Polym. Chem* 1985;23:337.
- [36] Lindsey CR, Paul DR, Barlow JW. *J. Appl. Polym. Sci* 1981;26:1.
- [37] Baker WE, Saleem M. *Polym Engng Sci* 1987;27:1634.
- [38] Baker WE, Saleem M. *Polymer* 1987;28:2057.
- [39] Liu NC, Baker WE. *Adv Polym Technol* 1992;11:249.
- [40] Liu NC, Baker WE. *Adv Polymer* 1994;35:988.
- [41] Triacca VJ, Ziaee S, Barlow JW, Keskkula H, Paul DR. *Polymer* 1992;32:1401.
- [42] Keskkula H, Paul DR. In: Kohan MI, editor. *Nylon plastic handbook*. Munich: Hanser Publishers, 1995. p.414.
- [43] O'Shaughnessy B, Sawhney U. *Macromolecules* 1996;29:7230.
- [44] Fredrickson GF, Milner ST. *Macromolecules* 1996;29:7386.
- [45] Tessier M, Marechal E. *J Polym Sci Part A: Polym Chem* 1988;26:2785.
- [46] Marechal E, Coppens PG, Legras R, Dekoninck JM. *J Polym Sci Part A: Polym Chem* 1995;33:757.
- [47] Padwa AR, Sasaki Y, Wolske KA, Macosko CW. *J Polym Sci Part A: Polym Chem* 1995;33:2165.
- [48] Hale W, Keskkula H, Paul DR. *Polymer* 1999;40:365.
- [49] Guegan P, Macosko CW, Ishizone T, Hirao A, Nakahama S. *Macromolecules* 1994;27:4993.
- [50] Majumder in Paul, Bucknall, *Polymer Blends* 2000 p. 540-541.
- [51] Cooper GD, Lee GF, Katchman A, Shank CP. *Mater Technol* 1981;Spring:13.
- [52] Flexman EA, Huang DD, Snyder HL. *Polym Prepr* 1988;29(2):189.
- [53] Flexman EA. US Patent 4,804,716, 1989 (assigned to DuPont).
- [54] Hobbs SY, Dekkers MEJ, Watkins VH. *Proc 2nd Topical Conf Engineering Tech, AIChE, San Francisco* 1989.
- [55] Shibuya N, Sobajima Y, Sano H. US Patent 4,743,651, 1988 (assigned to Mitsubishi Petrochemical).
- [56] Wu S. *Polymer* 1985;26:1855.
- [57] Wu S. *Polym Engng Sci* 1987;27:335.
- [58] Wu S. *J Appl Polym Sci* 1988;35:549.
- [59] Borggreve RJM, Gaymans RJ, Schuijjer J, Ingen Housz JF. *Polymer* 1987;28:1489.
- [60] Borggreve RJM, Gaymans RJ. *Polymer* 1989;30:63.
- [61] Borggreve RJM, Gaymans RJ, Schuijjer J. *Polymer* 1989;30:71.
- [62] Borggreve RJM, Gaymans RJ, Eichenwald HM. *Polymer* 1989;30:78.

- [63] Keskkula, Rubber Toughened Engineering Plastics Collyer p. 139-140
- [64] Keskkula, in Kohan Nylon 6 p. 414-418
- [65] Bucknall CB. In: Paul DR, Bucknall CB, editors. Polymer blends: volume 2, performance. New York: John Wiley & Sons, 2000. pp. 83-117.
- [66] Gonzalez-Montiel A, Keskkula H, Paul DR. Polymer 1995;36:4587, 4605, and 4621.
- [67] Margolina A, Wu S. Polymer 1988;29:2170.
- [68] Majumder B, Keskkula H, Paul DR. J Polym Sci, Part B: Polym Phys 1994;32:2127.
- [69] Jancar J, Dibenedetto AT. Polym Engng Sci 1994;34:1799.
- [70] Mai YW. In: Paul DR, Bucknall CB, editors. Polymer blends: volume 2, performance. New York: John Wiley & Sons, 2000. pp. 17-58.
- [71] Williams JG. Fracture mechanics of polymer. Chichester, UK: Ellis Horwood, 1987.
- [72] Anderseon TL. Fracture mechanics: Fundamentals and applications. 2nd ed. Boca Raton, FL: CRC Press, 1995.
- [73] Atkins AG, Mai YW. Elastic and plastic fracture. Chichester, UK: Ellis Horwood, 1985.
- [74] Corish PJ. In: Mark JE, Erman B, Eirich ER, editors. Science and technology of rubber, second edition. San Diego: Academic Press, 1994. pp. 545-599.
- [75] Fischer WF. ACS/CIC, Div Rubber Chem, 86th Meet, 1964.
- [76] Nishioka A, Furukawa J, Yamashita S, Kotani T. J Appl Polym Sci 1970;14:1183.
- [77] Satake K. J Appl Polym Sci 1971;15:1819.
- [78] Satake K, Shinki K, Teraoka T, Ibe S. J Appl Polym Sci 1971;15:2775.
- [79] Corish PJ. In: Walsh DJ, Higgins JS, Maconnachie A, editors. Polymer blends and mixtures, Dordrecht: Martinus Nijhoff, 1985. p.453.
- [80] Reisch MS. Chem Eng News 1992;70:29.
- [81] Grady BP, Cooper SL. In: Mark JE, Erman B, Eirich ER, editors. Science and technology of rubber, second edition. San Diego: Academic Press, 1994. pp. 601-674.
- [82] Giannini U. Macromol Chem, Suppl 1981;5:216.
- [83] Galli P, Luciani L, Cecchin G. Angew Macromol Chem 1981;94:63.
- [84] Keii T. Kinetics of Ziegler-Natta polymerization . Tokyo: Kodansha, 1972.
- [85] Bool J Jr. Ziegler-Natta Polymerization . New York: Academic, 1979.
- [86] Kontos EG, Easterbrook EK, Gilbert RD. J Polym Sci 1962;61:69.
- [87] Kontos EG. US Patent 3,378,606, 1968 (assigned to Uniroyal Inc.).
- [88] Kontos EG. US Patent 3,853,969, 1974 (assigned to Uniroyal Inc.).
- [89] Thamm RC, Buck WH. J Polym Sci, Polym Chem Ed 1978;16:539.
- [90] Thamm RC, Buck WH, Caywood SW, Meyer JM, Anderson BC. Die Angew Makromol Chemie 1977;58/58:345.
- [91] Shih CK, Su ACL. In: Legge NR, Holden G, Schroeder HE, editors. Thermoplastic elastomers: a comprehensive review. New York: Hanser Publishers, 1987. pp. 91-116.
- [92] Elliot DJ, Tinker AJ. In: Robers AD, editor. Natural rubber science and technology. London: Oxford Univ Press, 1988.

- [93] Baker CSL. In: Bhowmick AK, Stephens HL, editors. Handbook of elastomers, New York: Dekker, 1988.
- [94] Wolfe JR Jr, In: Legge NR, Holden G, Schroeder HE, editors. Thermoplastic elastomers: a comprehensive review. New York: Hanser Publishers, 1987. pp. 117-131.
- [95] Holzer R, Taunus O, Mehnert K. US Patent 3,262,992, 1966 (assigned to Hercules, Inc.).
- [96] Mahlman BH. US Patent 3,665,059, 1972 (assigned to Hercules, Inc.).
- [97] Lundberg RD. In: Walker BM, editor. Hand book of thermoplastic elastomers. New York: Van Nostrand Reinhold Co., 1979. p.247.
- [98] Banks SA, Brillinger JH, Coffey CA, Puydak RC, Schmit GN, Rubber Chem Technol 1976;49:1355.
- [99] Lohse DH. Soc Plast Engng. ANTEC 1985;43:301.
- [100] Onogi S, Asada T, Tanaka T. J Polym Sci Part A-2 1969;7:171.
- [101] Kresge EN. In: Paul DR, Newman S, editors. Polymer blends, vol.2. New York: Academic Press, 1978. pp. 293-318.
- [102] Danesi S, Porter RS. Polymer 1978;19:448.
- [103] Ranalli R, Dev. Rubber Technol 1982;3:21.
- [104] Coran AY, Patel R. Rubber Chem Technol 1983;56:1045.
- [105] Favis BD. In: Paul DR, Bucknall CB, editors. Polymer blends: volume 1: formulation. New York: John Wiley & Sons, 2000. pp.501-537.
- [106] Favis BD, Chalifoux JP. Polymer 1988;29:1761.
- [107] Klempner D, Frisch HL, Frisch KC. J Elastoplastics 1971;3:2.
- [108] Gergen WP, Lutz RG, Davison S. In: Legge NR, Holden G, Schroeder HE, editors. Thermoplastic elastomers: a comprehensive review. New York: Hanser Publishers, 1987. pp. 507-540.

## Chapter 2

### Fracture toughness of nylon 6 blends with maleated ethylene-propylene rubbers

#### 2.1 Introduction

The fracture behavior of nylon 6/maleated rubber blends has been described recently in some detail [1-13]. Based on these and other reports, it is clear that the rubber phase morphology critically affects mechanical behavior. For a fixed rubber content of about 20 wt.%, super-tough blends are obtained provided the rubber particle size is greater than a lower limit of about 0.1  $\mu\text{m}$ , but smaller than an upper limit of about 1  $\mu\text{m}$  [7-9].

Maleic anhydride grafted ethylene-propylene elastomers, EPR-g-MA, are frequently used for toughening polyamides. Commercial products of this type typically contain approximately 1% by weight of grafted maleic anhydride and give rise to a rubber particle population in a nylon 6 matrix that is in a satisfactory size range for toughening. For example, two recent reports describe such blends containing rubber particles with a weight average diameter,  $\bar{d}_w$ , of about 0.4  $\mu\text{m}$  that are super-tough down to very low temperature [8-10]. However, if the rubber particle size is decreased through the use of EPR-g-MA of higher maleic anhydride content or increased by diluting the rubber phase with an unmaleated EPR, significant reductions of blend toughness can be expected at some point based on published observations for blends of nylon 6 with elastomer particles formed from a styrene/hydrogenated butadiene/styrene, SEBS, triblock copolymer [6].

It is the purpose of this chapter to examine thoroughly the fracture behavior of blends containing 20% by weight of a rubber phase formed from mixtures of maleated and unmaleated ethylene-propylene rubbers, EPR. It is of particular interest to explore the ductile-to-brittle transition as a function of the rubber particle size resulting from variation of the EPR/EPR-g-MA ratio. Various techniques and conditions of impact testing will be used. For instance, impact strength results obtained by instrumented impact testing in a single-edge notch three-point-bend (SEN3PB) configuration will be compared to the standard notched Izod strengths. Toughness parameters obtained using 1/8 in. (3.18 mm) and 1/4 in. (6.35 mm) thick specimens, with sharp notches and varying ligament lengths, are explored. These techniques provide a sensitive method of analysis of the change from ductile-to-brittle mode of fracture due to compositional and morphological variations.

**Table 1 Materials used in Chapter 2**

Polymer	Commercial designation	Characterization <sup>a</sup>	Molecular weight <sup>a</sup>	Brabender torque <sup>b</sup> (N•m)	Source
Nylon 6	Capron 8207F	End-group content: [NH <sub>2</sub> ] = 47.9 meq g <sup>-1</sup> [COOH] = 43.0 meq g <sup>-1</sup>	$\bar{M}_n = 22,000$	5.4	AlliedSignal Inc.
EPR-g-MA	Exxelor 1803	43 wt.% ethylene 53 wt.% propylene 1.14 wt.% MA	-	8.2	Exxon Chemical Co.
EPR	Vistalon 457	43 wt.% ethylene 53 wt.% propylene	$\bar{M}_n = 54,000$ $\bar{M}_w / \bar{M}_n = 2$	10.3	Exxon Chemical Co.

<sup>a</sup> Reference (14).

<sup>b</sup> Torque value taken after 10 minutes at 240 °C and 60 rpm.

**Table 2 Morphology and impact strength for 80% nylon 6 + 20% rubber blends**

Rubber phase composition	Rubber particle		Izod (J/m) 3.18 mm Thickness	Ductile-Brittle transition temperature (°C)	Dynatup (J/m)		
	$\bar{d}_w$ (μm)	Polydispersity			6.35 mm Thickness		
			Standard notch		Sharp notch		
					2 mm Ligament	10 mm Ligament	
0% EPR-g-MA + 100% EPR	1.50	3.49	153	40	148	16	63
12.5% EPR-g-MA + 87.5% EPR	1.39	1.67	142	40	161	51	96
25% EPR-g-MA + 75% EPR	1.10	1.95	334	35	181	41	106
37.5% EPR-g-MA + 62.5% EPR	0.75	1.61	405	20	275	69	277
50% EPR-g-MA + 50% EPR	0.61	1.89	672	-5	592	55	601
75% EPR-g-MA + 25% EPR	0.36	1.58	678	-20	660	55	636
100% EPR-g-MA + 0% EPR	0.24	1.75	552	-25	574	57	538

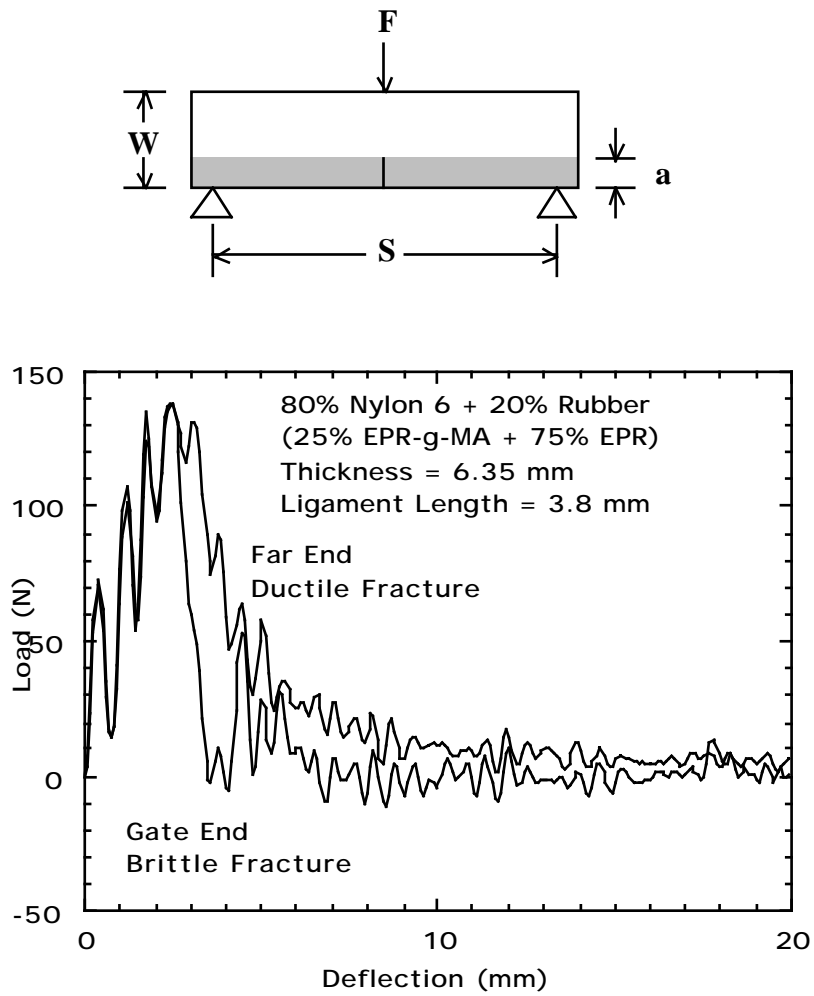


Fig. 1. Load-deflection curves obtained by Dynatup testing of thick specimens with a sharp notch and a ligament length of 3.8 mm for the blends based on a mixture of 25% EPR-g-MA and 75% EPR.

## 2.2 Experimental

Table 1 describes the materials used in this study. The nylon 6 is a commercial product of AlliedSignal designated as Capron 8207F which is a medium molecular weight grade ( $\bar{M}_n = 22,000$ ) having nearly equivalent amounts of acid and amine end groups. Blends of this nylon 6 with a dispersed phase of ethylene/propylene copolymer of varying particle size were formed by controlling the degree of maleation in the rubber phase by adjusting the ratio of EPR to EPR-g-MA. Table 2 shows the compositions of the blends studied and their characteristics.

The materials were dried in a vacuum oven for a minimum of 16 h at 80°C prior to any processing steps. The bale form of non-maleated EPR was cut into strips (2 x 4 x 5 cm<sup>3</sup>) and used to form a masterbatch of 50% EPR and 50% nylon 6 by melt blending in a 250 ml Brabender Plasticorder [14]. For the final blend all component were first vigorously mixed in a plastic bag followed by extruding twice at 240°C and 40 rpm in a Killion single screw extruder ( $L/D = 30$ ,  $D = 2.54$  cm) outfitted with an intensive mixing head. The blends were injection molded at 240°C into Izod bars (ASTM D256) that were either 3.18 mm or 6.35 mm thick using an Arburg Allrounder injection molding machine. Molded specimens were kept in a dessicator under vacuum to avoid water sorption.

The morphology of the blends was observed by a JEOL 200 CX transmission electron microscope using specimens which were microtomed at -50°C, typically in the plane parallel to the injection flow direction at the center of thick (6.35 mm) samples in the region of fracture near the gate end of an Izod bar. The nylon 6 phase was stained by exposure of thin sections to a 2% aqueous solution of phosphotungstic acid for 30 min at room temperature. The TEM was operated at an accelerating voltage of 120 kV. Rubber particle size was determined by a semi-automated digital analysis technique using IMAGE<sup>®</sup> software from the National Institutes of Health.

Instrumented impact tests were made using a Dynatup Drop Tower Model 8200 by dropping a 10 kg weight at a speed of 3.5 m/s onto the center of a specimen ( $l = 54$  mm) with a span,  $S$ , of 48 mm between supports. The specimen geometry was a SEN3PB having an original ligament length ranging typically from 2 to 10 mm with a sharp notch made by a fresh razor blade cooled in liquid nitrogen. The size of the fracture ligaments was determined by two procedures: (a) by measuring the actual length,  $\ell_a$ , of the fractured ligament (from the original crack tip to the beginning of the hinge), from which the actual fracture area can be calculated and (b) by measuring the potential length,  $\ell$ , of the ligament (from the original crack tip to the edge of the test specimen) from which the potential fracture area can be calculated. Most of the specific fracture energies reported here are based on the potential fracture area calculated by the product of specimen thickness and potential ligament length, i.e. method (b). In the case of ductile fractures, procedure (a) gives a shorter

ligament length (i.e. hinge type failure), so the fracture energy per unit area is higher. Use of procedure (b) gives a more conservative value of the specific fracture energy. The fracture energy was calculated from the load-deflection curve. Two typical load-deflection curves to be discussed later are shown in Fig. 1. They were signal-conditioned using a digital low pass filter to reduce noise vibration for both ductile and brittle fracture. Correction for drift in the baseline was made on all measurements. Energy losses caused by friction and contact of the specimen and the instrument were eliminated to determine the energy consumed due to fracture. Details of the testing procedure are described elsewhere [9,15].

### 2.3 Treatment of fracture data with varying ligament size

Impact fracture energies were measured using both Dynatup and Izod instruments employing molded test specimens of practical dimensions, i.e. 3-6 mm in thickness,  $t$ , with sharp notches. The effect of the ligament length on the fracture energy has been analyzed by two mathematically similar methods. Both of these methods are based on the ideas introduced by Broberg [16]. He suggested that the region around the crack consists of an elastic zone where the fracture initiation occurs and a plastic zone where the energy is absorbed during crack propagation. Mai and coworkers [17-19] proposed partitioning the total work of fracture  $W_f$  or  $U$  into two parts, i.e.

$$W_f = W_e + W_p \quad (1)$$

where  $W_e$  is the "essential" work of fracture while  $W_p$  is called the "non-essential" work. The first term represents the energy required to create two new surfaces, while  $W_p$  is a volume energy term and is proportional to  $\ell^2$  ( $\ell$  = ligament length). Accordingly, the total fracture work may be rewritten as the specific total fracture work  $w_f$

$$w_f = \frac{W_f}{t\ell} = w_e + w_p \ell \quad (2)$$

where  $w_p$  is a plastic zone shape factor. In this analysis  $w_p$  is not a material parameter, but is dependent on specimen geometry. Vu-Khanh [20] proposed an analogous relationship

$$\frac{U}{A} = G_i + \frac{1}{2} T_a A \quad (3)$$

where  $A$  is the area of the ligament to be broken,  $A = \ell t$ . The term  $G_i$  has been called the fracture energy at crack initiation and  $T_a$  has been identified as a tearing modulus. The interpretation of the slope and intercept terms of plots of  $U/A$  vs  $A$  is subject to some debate [19]; however, the intercept term does appear to be similar in value to the critical  $J$ -integral for fracture,  $J_{IC}$  [20].

Test conditions used in this work are similar to those used by Vu-Khanh (thick specimens in bending under high speed loading); however, the results will be analyzed

utilizing a mathematical convention similar to the "essential work of fracture" (EWF) method used by Mai et al.. Since we are using different testing conditions and sample geometries than generally used in the EWF methodology, it is not yet clear that the parameters will have exactly the meaning associated with Eq. (2). Thus, for now we adopt a different nomenclature for the intercept and slope of plots of  $w_f$  vs  $\ell$ , i.e.

$$\frac{U}{A} = u_o + u_d \ell \quad (4)$$

where  $U/A$  is the total fracture energy per unit area,  $u_o$  is called the limiting specific fracture energy and  $u_d$  is the dissipative energy density in the plastic, stress whitened, zone surrounding the fracture surface [21,22]. In ideal cases,  $u_o = w_e$  and  $u_d = w_p$ .

## 2.4 Results and discussion

The characteristics of the blends investigated in this report are summarized in Table 2. As the amount of EPR-g-MA in the rubber phase was reduced from 100 to 0% at 20% total rubber, the weight average rubber particle size,  $\bar{d}_w$ , increased from 0.24 to 1.50  $\mu\text{m}$ . The particle size polydispersity, or the  $\bar{d}_w/\bar{d}_n$  ratio, was found to be essentially constant for all blends that contained EPR-g-MA in the rubber phase; however, the blend without any reactive rubber component, i.e. 100% EPR, had a significantly higher polydispersity.

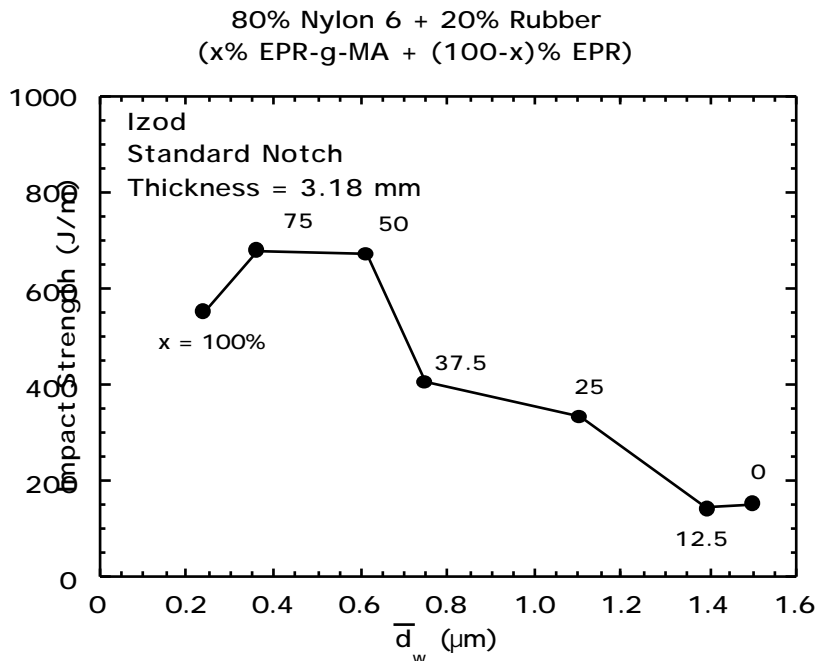


Fig. 2. Izod impact strength as a function of average rubber particle diameter for blends of 80% nylon 6 and 20% maleated EPR mixture.

Standard notched Izod impact strength was determined for the seven EPR-g-MA/EPR blends studied. The notched Izod impact strength at room temperature is plotted in Fig. 2 as a function of rubber particle size,  $\bar{d}_w$ . Super-tough behavior was observed for blends containing 50% or more of the maleated rubber component when the rubber particle diameter is below 0.61  $\mu\text{m}$ . Blends of intermediate toughness were obtained for rubber particles up to 1.1  $\mu\text{m}$  in size. For larger rubber particles, the blends were brittle.

As shown in Fig. 3, the ductile-to-brittle transition temperature is lower the higher the content of EPR-g-MA or the smaller the rubber particles. Blends containing less than 37.5% of the maleated rubber, corresponding to rubber particle diameters above 0.75  $\mu\text{m}$ , are relatively brittle at room temperature since the ductile-to-brittle transition temperature is near or higher than room temperature.

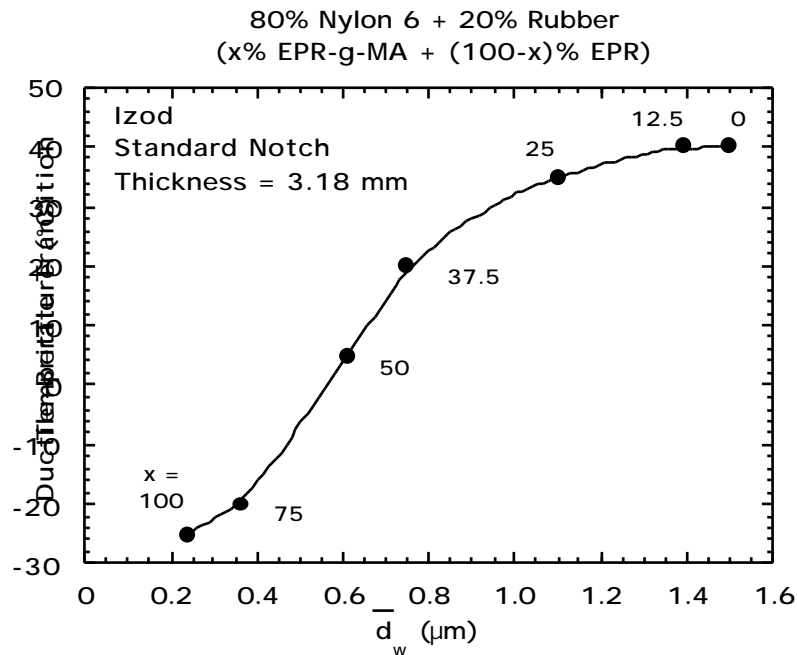


Fig. 3. Ductile-brittle transition temperature as a function of average rubber particle diameter for blends of 80% nylon 6 and 20% maleated EPR mixture.

Table 2 also shows impact fracture data for 6.35 mm thick specimens with both standard and sharp notches determined in a three-point-bending mode using the Dynatup Drop Tower. The impact fracture energies of specimens with standard notches were substantially the same as determined by the notched Izod test, cantilever mode of fracture, for blends containing 50% or more of EPR-g-MA ( $\bar{d}_w \leq 0.61 \mu\text{m}$ ). However, the largest differences in results from the Izod and Dynatup was seen for compositions with intermediate particle sizes, while at the largest two particle sizes, both methods of testing gave low impact strengths of about 150 J/m.

Impact strengths for thick specimens containing sharp notches and at two ligament lengths (2 and 10mm) measured by the Dynatup are also shown in Table 2. There was little difference between impact strength of standard notch and sharp notch specimens with 10-mm ligament length for the blends containing 37.5% or more of EPR-g-MA in the rubber phase. However, the impact strength for specimens with sharp notches was smaller than for those with standard notches when comparing the blends containing 25% or less of EPR-g-MA.

80% Nylon 6 + 20% Rubber  
 Dynatup, Sharp Notch  
 Thickness = 6.35 mm

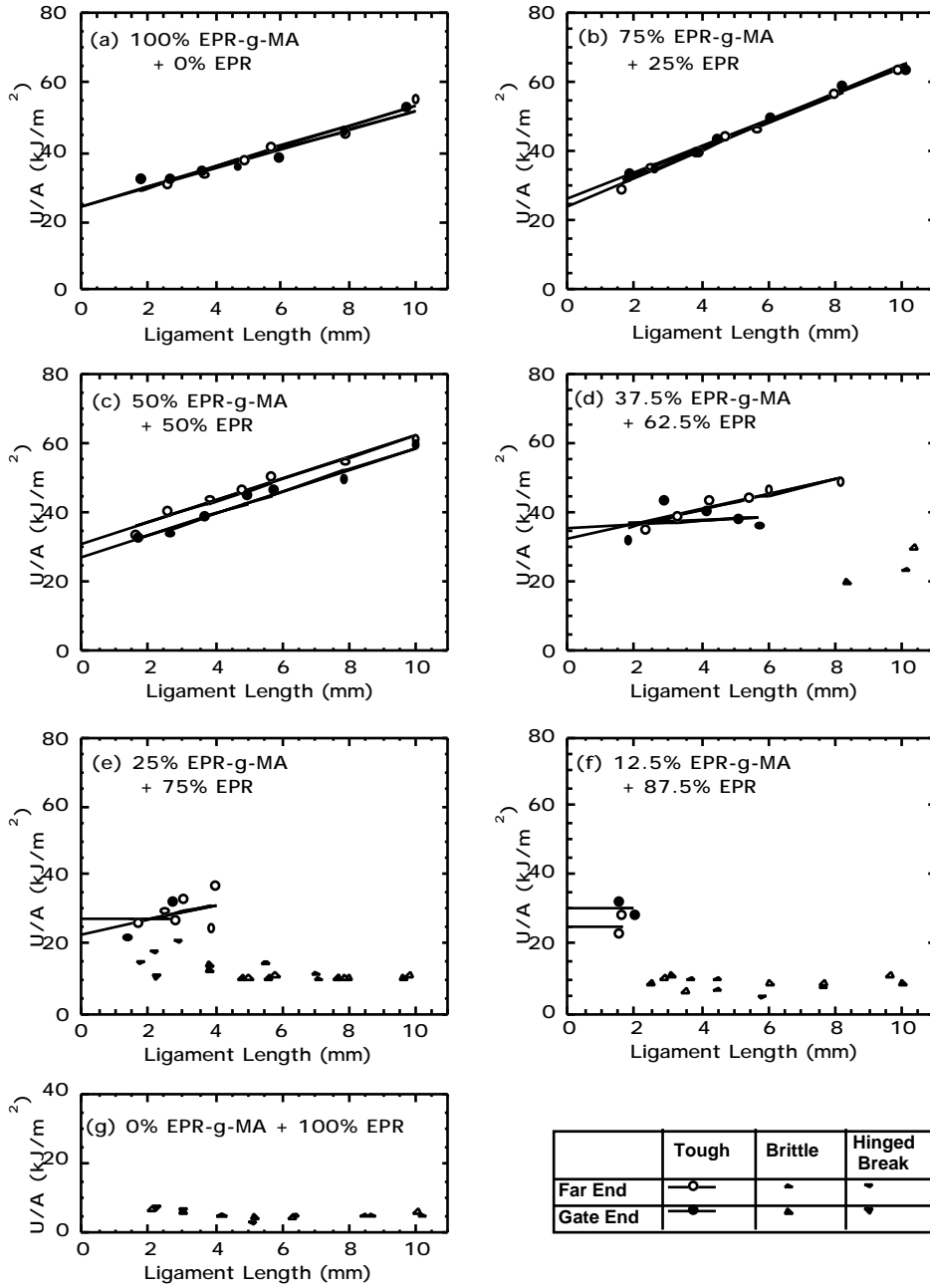


Fig. 4. Fracture energy as a function of ligament length from Dynatup measurements for blends of 80% nylon 6 and 20% rubber using x% EPR-g-MA and (100 - x)% EPR for thick specimens with a sharp notch.

The specimens with a sharp notch and short ligament lengths (2 mm) showed interesting behavior in the Dynatup test. The blend containing 0% EPR-g-MA in the rubber phase fractured in a brittle manner at low energy levels (16 J/m), while blends containing from 12.5 to 100% of EPR-g-MA fractured in a ductile manner at energy levels of 41 to 69 J/m. These blends were brittle or marginally tough at a ligament length of 10 mm, while the same blends were unexpectedly ductile at a ligament length of 2 mm. These results suggest that a ductile-to-brittle transition results from the change of ligament length for these blends.

#### **2. 4. 1 Fracture behavior of single-edge notch three-point-bend specimens**

The fracture energy measured as a function of ligament length for 6.35 mm thick specimens in a single notch, three-point-bend mode (like that illustrated at the top of Fig. 1) forms a good linear relationship when plotted as suggested by Eq. (4): the intercept and slope of such plots give the specific limiting fracture energy,  $u_o$ , and the dissipative energy density,  $u_d$ . Fig. 4 shows typical plots of  $U/A$  vs  $\ell$  for 80% nylon 6/20% rubber blends with various ratios of EPR-g-MA to EPR. In addition, the possible effect of the position of the point of fracture along the test bar, relative to the injection gate, was considered. It has been pointed out by Flexman [23-25] that toughened engineering polymers can show significant differences in fracture behavior along the length of an injection-molded bar. He has shown that differences in toughness between the gate and far ends of the bar are greatest in notched Izod tests for blend compositions that fall within a ductile-to-brittle transition region.

As shown in Fig. 4, there is a dramatic change in the relationship between specific fracture energy and ligament size as the composition of the rubber phase is altered. In blends containing high levels of EPR-g-MA, plots of  $U/A$  vs  $\ell$  are linear with little scatter of the data. For blends that contain 37.5 to 12.5% of the maleated rubber, a single straight line does not describe the results; the specific fracture energy at short ligament lengths is high (failure is ductile) while longer ligaments give much lower values (brittle failure). Obviously Eq. (4) does not describe the data over the full range of ligament length in these cases, at least with a single set of parameters. For comparison purposes, values of  $u_o$  and  $u_d$  for both ductile and brittle fracture can be computed for specimens that show both types of failure.

**Table 3 Fracture parameters from potential and actual ligament length for Dynatup measurement of far end specimens for nylon 6/rubber (80/20) blends based on mixture of x% EPR-g-MA and (100-x)% EPR**

% EPR-g-MA	$u_0$ (kJ/m <sup>2</sup> )		$u_d$ (MJ/m <sup>3</sup> )	
	Potential ligament	Actual ligament	Potential ligament	Actual ligament
12.5	25.5	28.6	0	0
25	23.3	33.7	2.1	0
37.5	31.7	39.8	2.2	1.8
50	30.8	34.0	3.1	3.3
75	24.2	31.4	4.1	3.9
100	24.1	27.1	3.1	2.9

**Table 4 The limiting specific fracture energy,  $u_0$ , for nylon 6/EPR (80/20) blends based on varying EPR-g-MA content in the rubber phase**

% EPR-g-MA	$u_0$ (kJ/m <sup>2</sup> )											
	Far end						Gate end					
	Dynatup		Izod				Dynatup		Izod			
	6.35 mm		6.35 mm		3.18 mm		6.35 mm		6.35 mm		3.18 mm	
	Ductile	Brittle	Ductile	Brittle	Ductile	Brittle	Ductile	Brittle	Ductile	Brittle	Ductile	Brittle
0	-	6.2	-	8.2	23.8	10.0	-	5.3	-	8.0	20.5	10.5
12.5	25.5	8.6	22.1	9.2	18.4	11.5	30.1	9.2	20.8	8.4	21.5	10.1
25	23.3	11.6	12.5	12.9	17.8	20.1	27.0	11.6	23.3	12.1	23.0	11.3
37.5	31.7	30.2	17.5	-	16.5	-	35.8	21.9	19.7	-	21.5	13.7
50	30.8	-	21.8	-	13.2	-	26.9	-	20.9	-	17.8	-
75	24.2	-	12.9	-	12.7	-	25.8	-	13.5	-	15.4	-
100	24.1	-	16.1	-	10.1	-	24.7	-	13.9	-	12.7	-

**Table 5** The dissipative energy density,  $u_d$ , for nylon 6/EPR (80/20) blends based on varying EPR-g-MA content in the rubber phase

% EPR-g-MA	$u_d$ (MJ/m <sup>3</sup> )											
	Far end						Gate end					
	Dynatup		Izod				Dynatup		Izod			
	6.35 mm		6.35 mm		3.18 mm		6.35 mm		6.35 mm		3.18 mm	
	Ductile	Brittle	Ductile	Brittle	Ductile	Brittle	Ductile	Brittle	Ductile	Brittle	Ductile	Brittle
0	-	0.0	-	0.0	0.0	0.0	-	0.0	-	0.0	0.0	0.0
12.5	0.0	0.0	0.0	0.0	1.7	0.0	0.0	0.0	0.0	0.0	0.0	0.0
25	2.1	0.0	3.2	0.0	3.3	0.0	0.0	0.0	0.0	0.0	0.0	0.0
37.5	2.2	0.0	3.5	-	4.5	-	0.5	0.0	2.3	-	1.4	0.0
50	3.1	-	5.0	-	5.7	-	3.2	-	4.8	-	3.3	-
75	4.0	-	6.0	-	6.4	-	3.9	-	5.7	-	4.6	-
100	2.9	-	2.3	-	6.6	-	2.7	-	2.6	-	5.4	-

**Table 6 Fracture parameters from Dynatup for nylon 6/rubber (80/20) blends based on varying EPR-g-MA content in the rubber phase**

% EPR-g-MA	$\sigma_y$ (MPa)	$K_{IC}$ , Plane-strain stress intensity factor (MPa•m <sup>1/2</sup> )	Transition ligament length (mm)
0	-	2.7	2.2
12.5	-	3.2	2.3
25	-	3.5	3.8
37.5	109.3	5.3	7.5
50	101.0	-	-
75	100.3	-	-
100	96.5	-	-

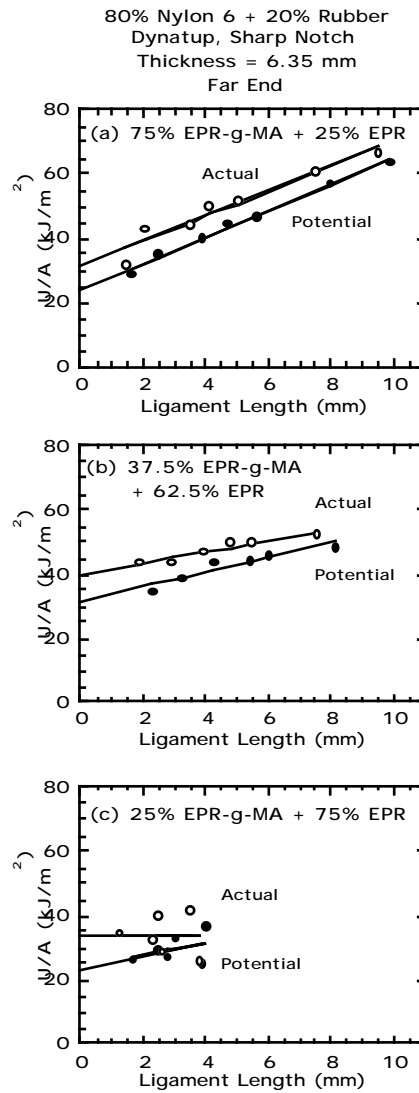


Fig. 5. Fracture energy as a function of potential and actual ligament from Dynatup measurements for blends based on (a) 75% EPR-g-MA, (b) 37.5% EPR-g-MA and (c) 25% EPR-g-MA in the rubber phase.

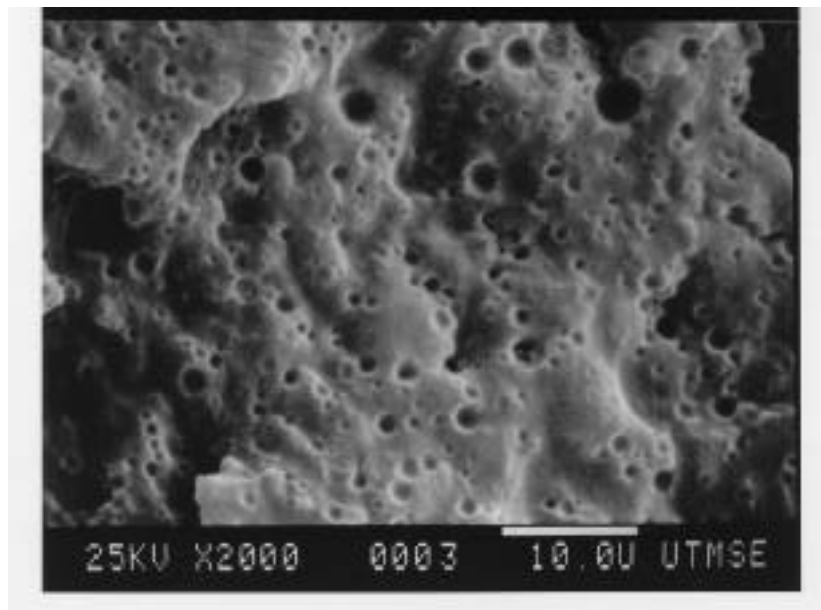
As described earlier, method (a) excludes the hinge portion and uses only the ligament that is fractured; naturally this gives higher values of  $U/A$  than when the ligament length is obtained by method (b). Fig. 5 compares  $U/A$  vs  $\ell$  plots obtained from methods (a) and (b) for three selected compositions. The ligament areas represented in Fig. 4 are based on the potential ligament length, i.e. method (b). The fracture parameters obtained by the two methods are listed in Table 3. While the numerical values of these parameters depend on whether  $\ell$  or  $\ell_a$  is used, the trends are similar.

Tables 4 and 5 show the numerical values of the intercepts and slopes, i.e.  $u_0$  and  $u_d$  obtained from the plots like those in Fig. 4. They reveal that the blends containing 50% or more EPR-g-MA are uniformly ductile and have  $u_0$  values in the range of 24-31 kJ/m<sup>2</sup> while

the  $u_d$  values range from 2.7-4.0 MJ/m<sup>3</sup>. For the ductile blends, both the gate and far end specimens are uniformly tough at all ligament lengths tested; however, the blends containing 37.5% EPR-g-MA or less show a more complicated fracture behavior. It is apparent that as the proportion of unmaleated rubber increases the blends become more brittle. The greatest deviation from the behavior typical of the most ductile blends is seen for EPR-g-MA/EPR ratios of 25/75 and 12.5/87.5. Here, the test specimens with the largest ligaments show low values of total specific fracture energy, i.e.  $U/A$ , typical of brittle materials, while those with the smallest ligaments show higher levels. Plots of specific fracture energy vs ligament size with negative slopes have been reported for high impact polystyrene [26], toughened nylon 6,6 [26] and nylon 6/ABS blends [27]. However, the present results are more dramatic in that they represent a transition from ductile to brittle fracture as might occur in a transition from plane stress to plane strain conditions. Indeed, Wu and Mai [28] have reported such a transition with ligament length; however, they found ductile (plane stress) behavior at large ligament lengths and brittle (plane strain) behavior at small ligament lengths; the opposite of what is observed here.

To further explore the change in mechanism of deformation with ligament size, fracture surfaces of several marginally tough compositions were examined by scanning electron microscopy. Different specimens of the blend based on 25% EPR-g-MA in the rubber phase gave either relatively low (brittle, ▲) or high (tough, ○) impact energies at a ligament length of about 3.8 mm as seen in Fig. 4e. It is apparent from the scanning electron photomicrographs of fracture surfaces in Fig. 6 that a sample which shows brittle behavior experiences no matrix yielding at a distance of 2.5 mm from the crack initiation while the sample exhibiting ductile fracture shows extensive yielding and matrix deformation. Fig. 1 compares load-deflection curves for specimens of this composition that show ductile and brittle behavior. The load-deflection traces are identical up to the maximum load of about 140 N; after this, the more ductile specimen shows higher deflection by about 1 mm, apparently due to higher resistance to crack propagation. Its load-deflection trace remains noticeably above that of the brittle specimen indicating a higher total fracture energy. Accordingly, the delayed crack initiation and a crack propagation mode modified by the extensive matrix deformation and yielding (Fig. 6b) account for the higher fracture energy.

(a)



(b)

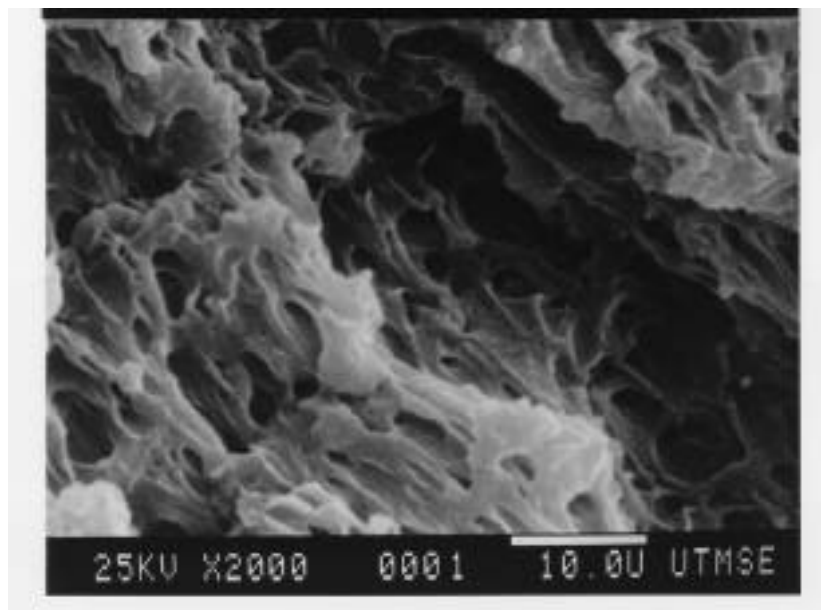


Fig. 6. SEM photomicrographs showing the fracture surface of (a) brittle and (b) ductile fracture for thick specimens with a 3.8 mm ligament length for blends based on 25% EPR-g-MA and 75% EPR mixture.

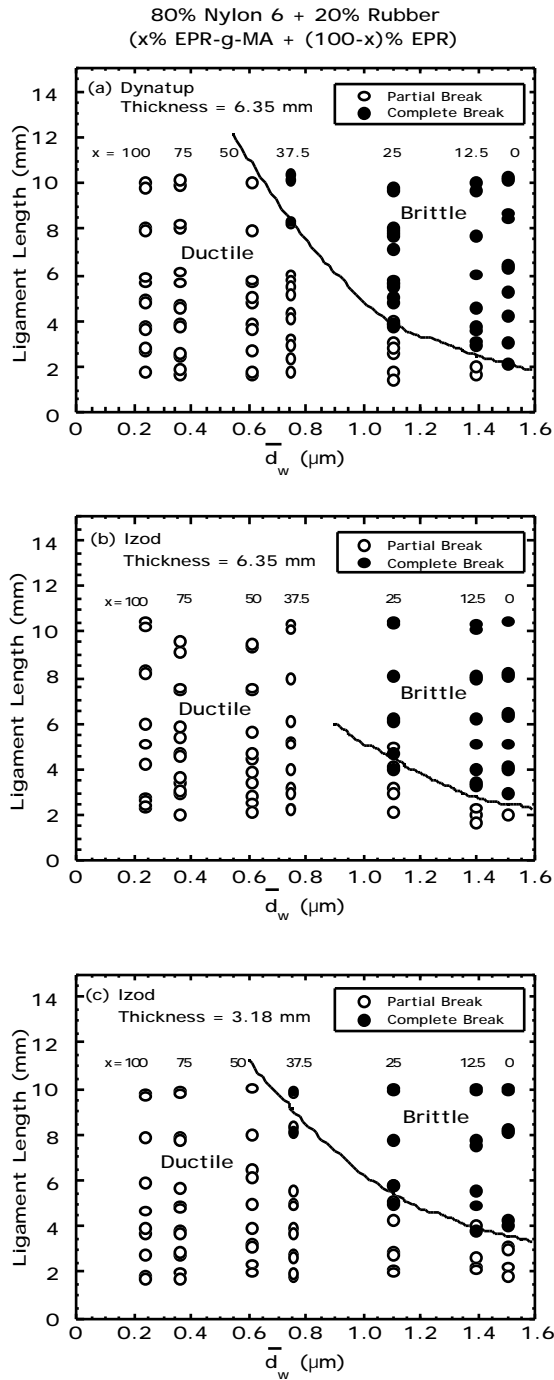


Fig. 7. Failure mode as a function of ligament length and average rubber particle diameter for blends of 80% nylon 6 and 20% maleated EPR mixture measured by: (a) Dynatup for thick specimens, (b) Izod for thick specimens and (c) Izod for thin specimens. Note that all the specimens had sharp notches.

80% Nylon 6 + 20% Rubber  
 Izod, Sharp Notch  
 Thin and Thick Specimens

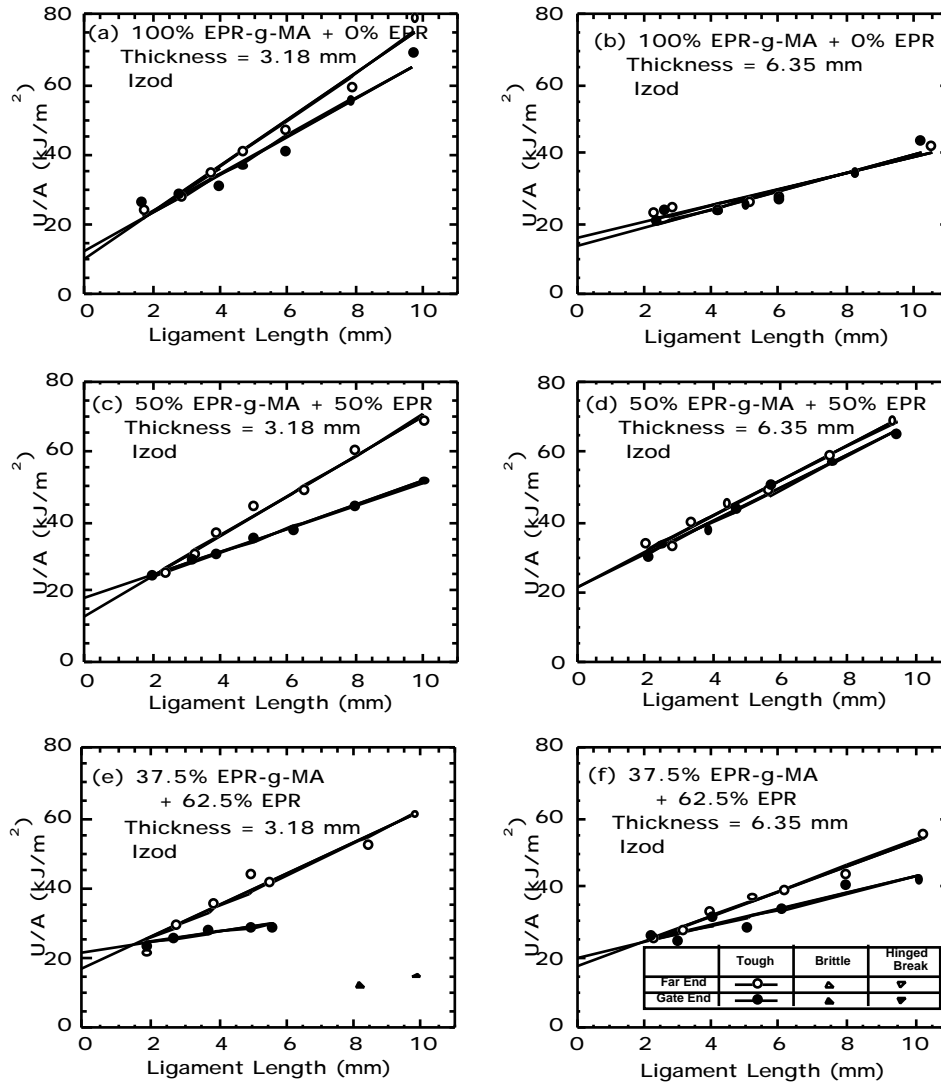


Fig. 8. Fracture energy as a function of ligament length for Izod measurements on thin and thick specimens with a sharp notch for 80% nylon 6 and 20% maleated EPR mixture.

#### 2. 4. 2 Fracture energy by notched Izod test

The Izod test (cantilever configuration) was also used to determine the fracture energy as a function of ligament length for specimens with sharp notches for comparison with the fracture behavior in the single-edge notch three-point-bend configuration using the Dynatup. The impact fracture energies for the two tests are compared in Table 2; there is good agreement with similar results reported previously [6-8, 10].

Standard notched Izod data are presented in Fig. 2 (as a function of rubber particle size) and in Fig. 3 to show the effect of particle size on the ductile-brittle transition temperature. Fig. 7 shows how the mode of impact fracture (ductile or brittle) of specimens with sharp notches depends on ligament length, sample thickness, and blend morphology. In these diagrams, specimens that exhibited complete break with relatively low specific fracture energy are classified as brittle, while those that exhibited a partial break with high specific fracture energy were considered to have experienced ductile failure. As seen in Fig. 7, rather similar ductile-to-brittle boundaries are obtained from Dynatup and Izod (3.18 or 6.35 mm) testing. No complete, or brittle, breaks were observed when the ligament lengths were of the order of 2 mm or less, even for the more brittle compositions containing 12.5% and 25% EPR-g-MA in the rubber phase. Table 6 shows the transition ligament length for the Dynatup test at which the ductile-to-brittle transition occurred. The value of the transition ligament length increased with increasing amount of EPR-g-MA in the blend, i.e. with decreasing rubber particle size. Kudva et al. [22] have qualitatively explained the transition from ductile to brittle failure as ligament length increases for transitional materials; the basis for this argument will be expanded on later.

#### 2. 4. 3 Comparison of fracture energy parameters

The Izod fracture data for specimens of two thickness (both with sharp notches) are shown in the form of  $U/A$  vs  $\ell$  plots in Fig. 8. The fracture energy parameters  $u_o$  and  $u_d$  obtained from the Izod and Dynatup (Fig. 4) experiments using various test conditions and specimens are summarized in Tables 4 and 5. The parameters obtained from observed ductile failures for the gate end specimens are plotted in Figs. 9 and 10 as a function of the average rubber particle size. In general, values obtained from Izod and Dynatup testing show similar trends. The parameter  $u_o$  seems to generally increase with rubber particle size while  $u_d$  goes through a maximum and then decreases. The values of  $u_o$  from Dynatup testing are larger than those from the Izod test (Fig. 9a); whereas, the opposite is true for  $u_d$  (Fig. 9b). For a given test configuration,  $u_o$  is effectively independent of sample thickness while  $u_d$  surprisingly appears to be slightly larger for thicker samples. The differences in  $u_o$  between specimens from the gate and far ends of injection molded bars are relatively insignificant for all specimens (Fig. 10a); however, for large rubber particles the values of  $u_d$  are substantially greater for specimens from the far end of the bar (Fig. 10b). For gate end specimens, there is a good correlation between Dynatup impact strength for the standard

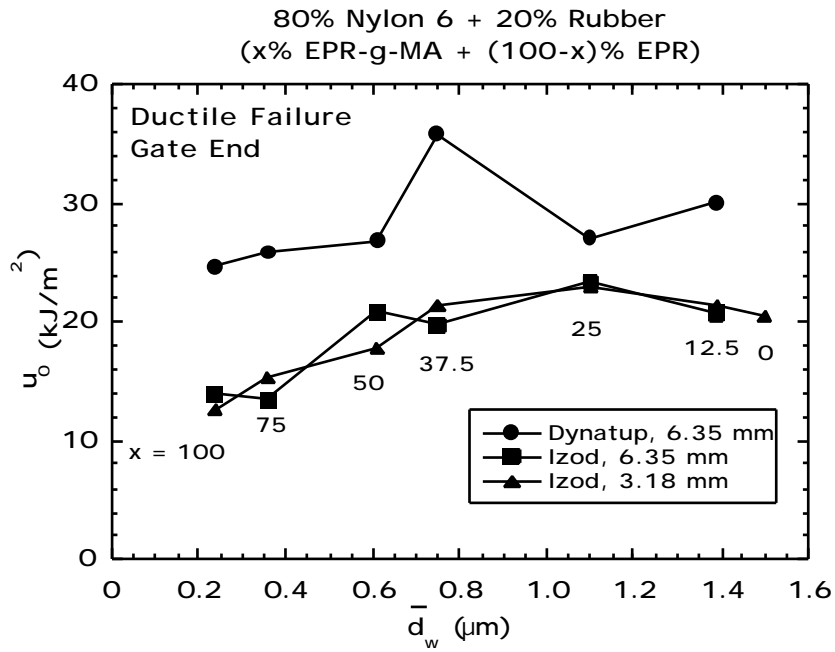
notched specimens and  $u_d$  (See Fig. 11); however, for far end specimens, the relation is not so direct. Compositions that contain 50% or more of EPR-g-MA are uniformly tough in all situations; i.e. when the weight average rubber particle size is 0.61  $\mu\text{m}$  or less. Blends that contain less EPR-g-MA (i.e. have larger rubber particles and are marginally tough) are more sensitive to sample dimensions, location in the bar, and test configuration.

#### 2. 4. 4 Stress analysis

As mentioned earlier, Kudva et al. [22] have qualitatively explained the change from ductile to brittle failure as the ligament length increases in terms of the intersection of classical equations describing failure by ductile yielding and brittle crack propagation. McCrum et al. [29] outline the basic argument in terms of simple tension for a specimen with variable crack length; Kudva et al. argued similarly using the analogous equations for bending. The purpose here is to extend this type of analysis using quantitative information from experimental Dynatup force-displacement plots like those in Fig. 1 for a bar loaded in three-point bending (see diagram at top of Fig. 1). The region just below the load goes from a maximum compressive stress at the top of the bar to a maximum tensile stress at the bottom. For a bar without a crack, the maximum tensile stress (at the bottom of the bar) is

$$\sigma_{\max} = \frac{3SF}{2tW^2} \quad (5)$$

according to linear elastic theory [29], where  $S$  is the span,  $t$  is thickness and  $W$  is width. Substitution of the peak load,  $F$ , from Dynatup plots (see Fig. 1) into this relation gives a quantity that we will call the failure stress. The results of such calculations are shown in Fig. 12 as a function of the normalized crack length  $a/W$  for the various blends. The open circles represent failures judged to be ductile while the closed circles denote failures judged to be brittle.



80% Nylon 6 + 20% Rubber (x% EPR-g-MA + (100-x)% EPR)

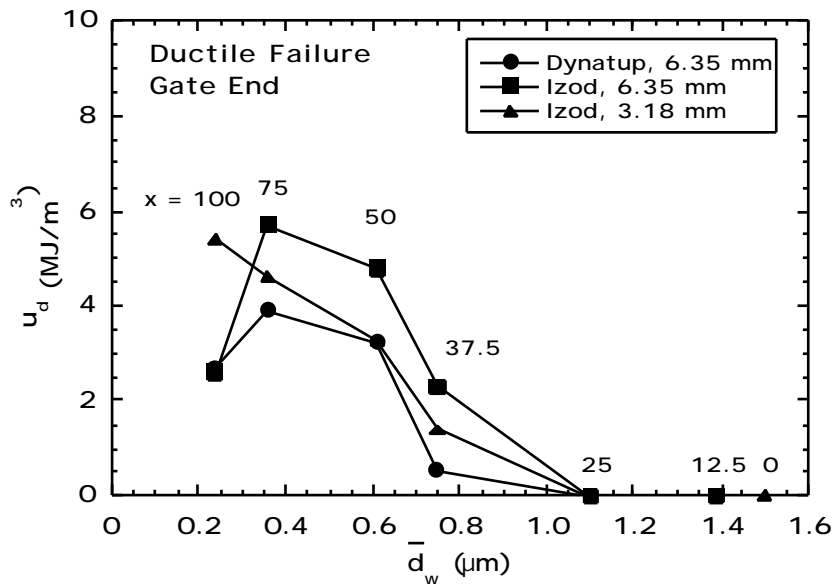
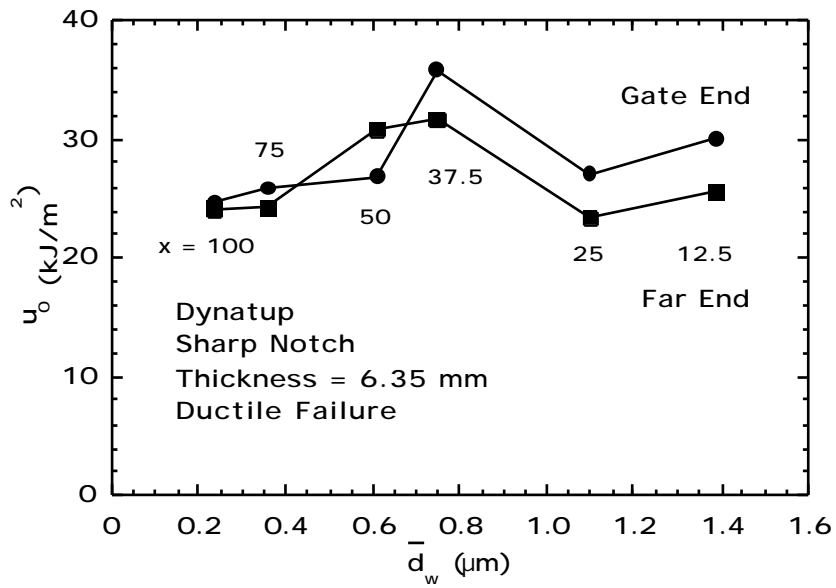


Fig. 9. Fracture parameters for nylon6/maleated EPR blends (20% rubber) (a)  $u_0$  vs rubber particle size (b)  $u_d$  vs rubber particle size; specimens were obtained from the gate end of the moldings.

80% Nylon 6 + 20% Rubber (x% EPR-g-MA + (100-x)% EPR)



80% Nylon 6 + 20% Rubber (x% EPR-g-MA + (100-x)% EPR)

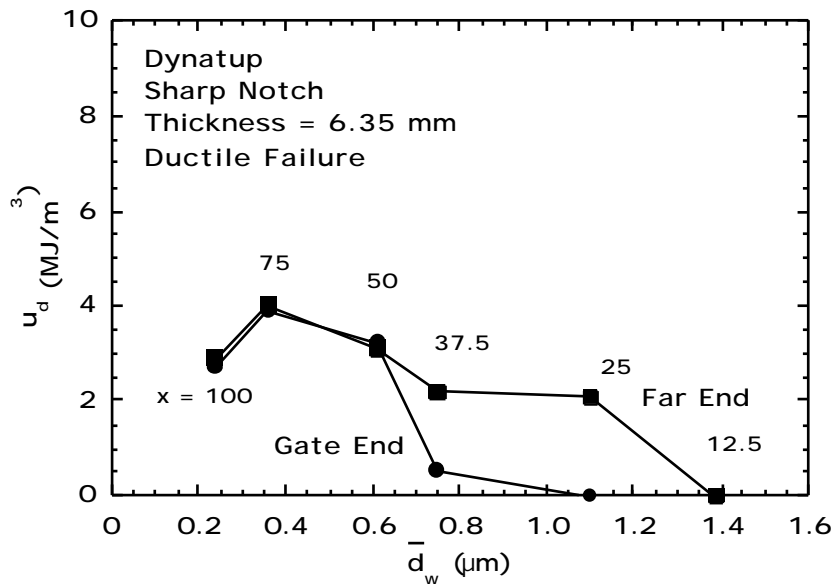


Fig. 10. Comparison of fracture parameters obtained from gate and far ends of 6.35mm injection molded bars.

80% Nylon 6 + 20% Rubber (x% EPR-g-MA + (100-x)% EPR)

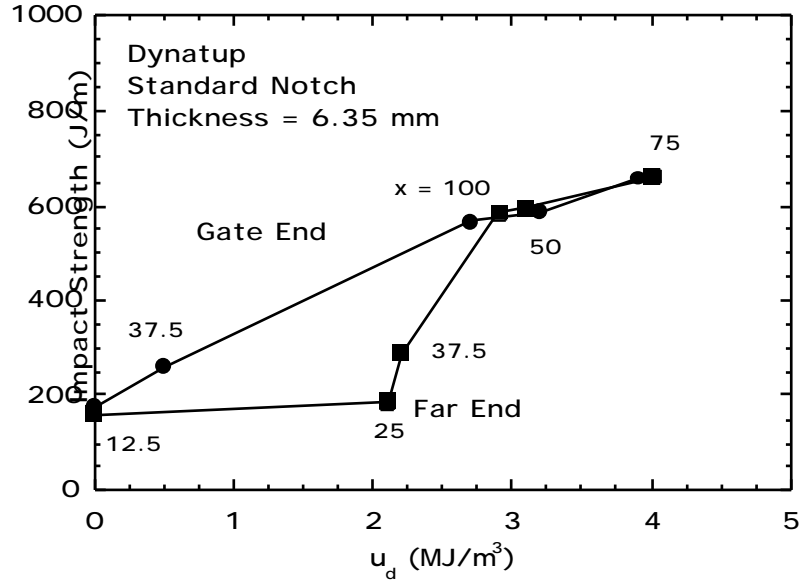


Fig. 11. Dynatup impact strength (standard notch) vs dissipative energy density ( $u_d$ ) for 6.35 mm thick specimens of varying rubber phase composition.

Of course, the presence of a crack of length,  $a$ , in the bar leads to a more complicated stress pattern and can alter the mode of failure. By the so-called “net section” argument, the tensile stress at the position of the crack tip is given by

$$\sigma_{\max}(a) = \sigma_{\max}(0) \frac{W - a}{W} \quad (6)$$

where  $\sigma_{\max}(0)$  is the stress from Eq. (5) where there is no crack, i.e.  $a = 0$ . The stress given by Eq. (6) amounts to the linear elastic result (Eq. 5) for a bar of width  $(W - a)$ , i.e. the maximum tensile stress if the shaded material at the top of Fig. 1 were ignored. Thus, if ductile failure occurs by tensile yielding at a stress of  $\sigma_y$ , then the calculated failure stress from Eq. (5) should be [30]

$$\text{failure stress} = \sigma_y \frac{W - a}{W} \quad (7)$$

On the other hand, linear elastic fracture mechanics predicts that under plane-strain conditions brittle failure should occur at [31]

$$\text{failure stress} = \frac{K_{IC}}{Y\sqrt{a}} \quad (8)$$

where  $K_{IC}$  is the critical stress intensity factor and  $Y$  is a geometdcal factor given by

$$Y = 1.93 - 3.07(a/W) + 14.53(a/W)^2 - 25.11(a/W)^3 + 25.80(a/W)^4 \quad (9)$$

Plane-strain conditions are expected when  $a/W \leq 0.6$ . According to Kudva et al. [22] the failure stress given by Eq. (7) is smaller than that from Eq. (8) for short ligament (long cracks) and vice versa for long ligaments (short cracks). This explains in a qualitative way the ductile-to-brittle transition with ligament length shown in Fig. 7. Here, we compare these models with the experimental data to estimate the parameters  $\sigma_y$  and  $K_{IC}$ .

The solid lines in Fig. 12 represent the best fit of Eq. (7) to all the data where ductile failure was exhibited. This model does a satisfactory job of describing the results. For Fig. 12e and f there are too few ductile failures to justify such an analysis. The values of  $\sigma_y$  obtained from this data fitting procedure are listed in Table 6; the  $\sigma_y$  parameters from this fit decrease with increasing amount of EPR-g-MA in the blend which corresponds to smaller particles, higher levels of grafting, and reduced crystallinity. The absolute values of  $\sigma_y$ , obtained by the fit, are quite large compared to those obtained from simple tensile tests; of course, the yield strength is expected to be larger at higher strain rates but there are no data available for direct comparison at the strain rates ( $\sim 10^3 \text{ s}^{-1}$ ) of this type of test. High-speed tensile data by Dijkstra et al. [32] indicate a rapid increase in yield stress as the strain rate approaches the levels estimated for the current test; thus, the estimates in Table 6 may be plausible.

The dotted lines in Fig. 12 represent the best fit of Eqs. (8) and (9) to the brittle failure stresses (limited to conditions where plane-strain is expected). Table 6 lists the values of  $K_{IC}$  obtained by this fitting procedure. Since brittle fracture was not observed in Fig. 12 a-c, no values of  $K_{IC}$  were deduced for these compositions. The values of the  $K_{IC}$  parameter obtained in this way increase with increasing EPR-g-MA content in the blend. Adams reported a  $K_{IC}$  value of  $3.0 \text{ MPa m}^{1/2}$  for Zytel 101 (nylon 6,6) tested in an impact mode (1 m/s) similar to the method reported here [33]. The values reported in Table 6 are in the same range.

80% Nylon 6 + 20% rubber  
 Dynatup, Sharp Notch  
 Thickness = 6.35 mm

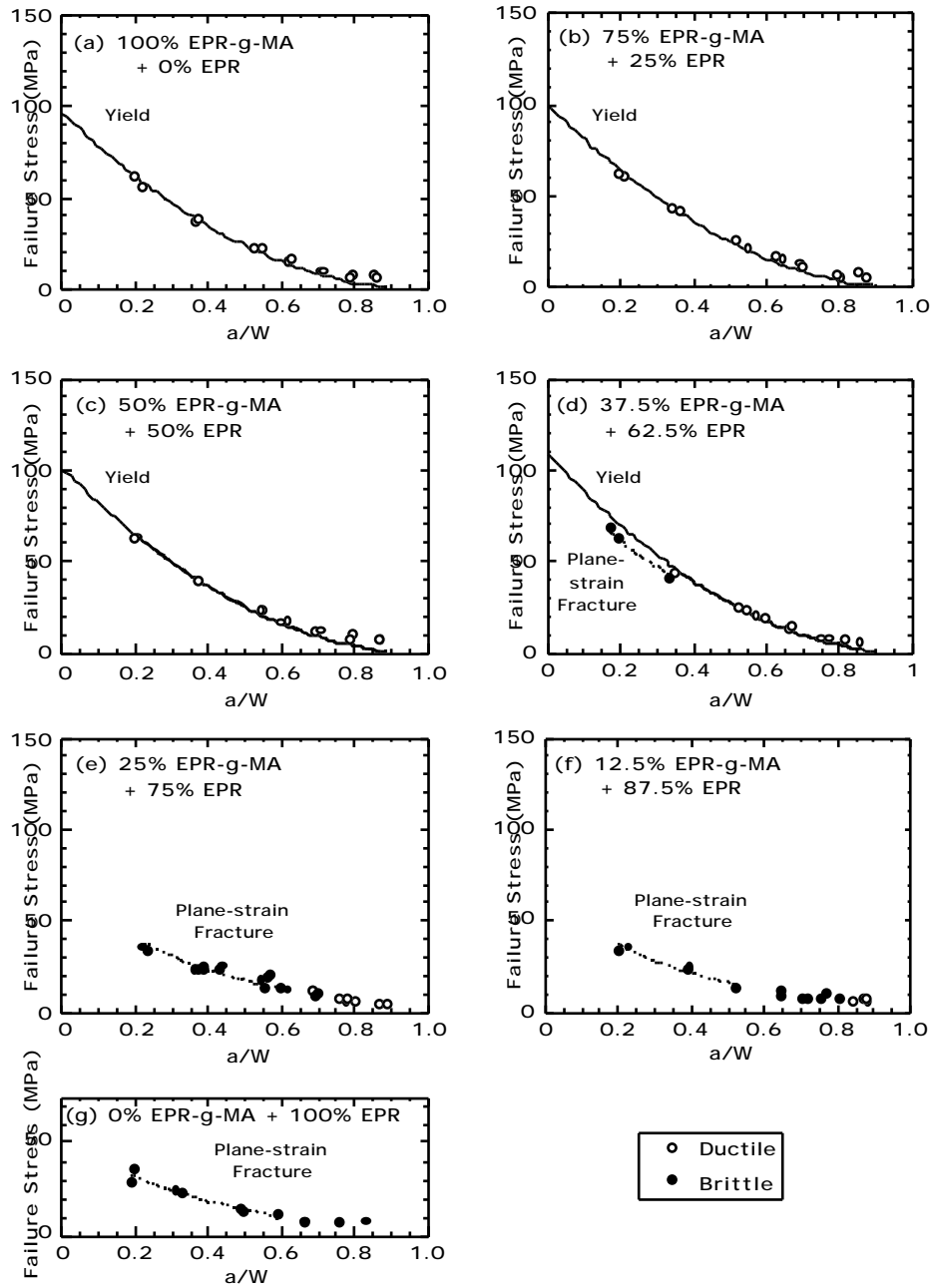


Fig. 12. Failure stress as a function of crack length ( $a/W$ ) from Dynatup measurements on thick specimens with a sharp notch for blends of 80% nylon 6 and 20% maleated EPR mixture. (O) ductile break, (●) brittle break.

## 2. 5 Conclusions

Fracture behavior of toughened nylon 6 blends of varying rubber particle size was examined by Izod and SEN3PB type tests using injection molded specimens of two thickness with sharp notches and varying ligament lengths. Plots of specific fracture energy vs ligament length were linear when ductile failure occurred; values of the limiting specific fracture energy ( $u_o$ ) and the dissipative energy density ( $u_d$ ) were obtained and discussed.

When there is 50% or more of the reactive EPR-g-MA in the rubber phase ( $\bar{d}_w = 0.24$  to  $0.61 \mu\text{m}$ ), super tough blends were obtained under all testing conditions; the specific fracture energy showed a linear relationship vs ligament length with very little scatter. The impact strength of these specimens was generally insensitive to which end of the bar that was tested. The same range of impact fracture energies was obtained with thick and thin specimens and by using either the Izod or Dynatup tests.

Blends that contained 37.5% or less of EPR-g-MA and where the rubber particle size was  $0.75 \mu\text{m}$  or higher were more sensitive to sample dimensions, location along the bar, and test configuration. A dual mode of fracture was observed, depending on ligament length, for blends which had a ductile-to-brittle transition temperature near room temperature or higher; the specimens with short ligaments fractured in a ductile manner and gave high values of the specific fracture energy, while the specimens with long ligaments showed brittle fracture and gave lower values of energy. A dual mode of fracture was observed for both Izod and SEN3PB tests. The critical ligament length at which the ductile-to-brittle transition occurred increased with increasing amount of EPR-g-MA in the blend, i.e. with decreasing rubber particle size. The change from ductile failure at short ligament length to brittle failure at longer ligaments for these transitional materials was rationalized in terms of classical equations for ductile yielding and brittle crack propagation. Values of the yield stress and critical stress intensity factor were estimated from the data using these model equations.

The parameter  $u_d$  was found to be more sensitive to rubber particle size, sample thickness and location in the molded bar than  $u_o$ . A good correlation between the standard Dynatup impact strength and the parameter  $u_d$  was observed for the gate end specimens.

## REFERENCES

- [1] Wu S. *Polym Engng Sci* 1987;27:335.
- [2] Wu S. *J Appl Polym Sci* 1988;35:549.
- [3] Lawson DF, Hergenrother WL, Matlock MG. *J Appl Polym Sci* 1990;39:2331.
- [4] Gilmore DW. *Plastics Engng* 1989;45:51.
- [5] Hobbs SY, Bopp RC, Watkins VH. *Polym Engng Sci* 1983;23:380.
- [6] Oshinski AJ, Keskkula H, Paul DR. *J Appl Polym Sci* 1996;61:623.
- [7] Oshinski AJ, Keskkula H, Paul DR. *Polymer* 1996;37:4909.
- [8] Oshinski AJ, Keskkula H, Paul DR. *Polymer* 1996;37:4919.
- [9] Kayano Y, Keskkula H, Paul DR. *Polymer* 1997;38:1885.
- [10] Kayano Y, Keskkula H, Paul DR. *Polymer* 1998;39:2835.
- [11] Borggreve RJM, Gaymans RJ, Schuijjer J. *Housz JFI. Polymer* 1987;28:1489.
- [12] Borggreve RJM, Gaymans RJ. *Polymer* 1988;29:1441.
- [13] Borggreve RJM, Gaymans RJ. *Polymer* 1989;30:63.
- [14] Oshinski AJ, Keskkula H. Paul DR. *Polymer* 1996;37:4891.
- [15] Chung I, Throckmorton E, Chunury D. *Soc Plast Engng. ANTEC* 1979;25:681.
- [16] Broberg KB. *Int J Fract* 1968;4:11.
- [17] Mai Y, Powell P. *J Polym Sci Part B: Polym Phys* 1991;29:785.
- [18] Mai Y. *Int J Mech Sci* 1993;35:995.
- [19] Mai Y. *Polymer Commun* 1989;30:330.
- [20] Vu-Khanh T. *Polymer* 1988;29:1979.
- [21] Wildes G. Keskkula H, Paul DR. *Polymer* 1999;40:7089.
- [22] Kudva RA. Keskkula H. Paul DR. *Polymer* 2000;41:335.
- [23] Flexman EA. *International conference: toughening of plastics. London: The Plastics and Rubber Inst, 1978 (p. 14).*
- [24] Flexman EA. *Polym Mater Sci Engng* 1990;63:112.
- [25] Flexman EA. *Soc Plast Engng. ANTEC* 1984;30:558.
- [26] Vu-Khanh T. *Theor Appl Fracture Mech* 1994;21:83.
- [27] Mamat A, Vu-Khanh T, Cigana P, Favis BD. *J Polym Sci Part B: Polym Phys* 1997;35:2583.
- [28] Wu J, Mai Y. *Polym Engng Sci* 1996;36:2275.
- [29] McCrum NG. Buckley CP, Bucknall CB. *Principles of polymer engineering. Oxford University Press, Oxford. 1988, pp. 194-200.*

- [30] Gross B, Srawley JE. Stress-intensity factors for single-edge-notch specimens in bending or combined bending and tension by boundary collocation of a stress function. Technical Note. D-2603, NASA, 1965. p. 8.
- [31] Brown WF, Srawley JE. ASTM 410, 1996. p. 13.
- [32] Dijkstra K, Wevers HH. Gaymans RJ. Polymer 1994;35:323.
- [33] Adams GC. Soc Plast Engng ANTEC 1988;34:1517.

## Chapter 3

### Fracture toughness of blends of nylon 6 with maleated styrene/hydrogenated butadiene/styrene tri block copolymer

#### 3. 1 Introduction

Super tough blends of nylon 6 with maleated elastomers such as maleic anhydride grafted ethylene-propylene rubber, EPR-g-MA, have become commercially important materials of considerable and scientific interest [1-12]. An essential feature of these materials is the graft copolymer generated from the reaction of the grafted maleic anhydride with the polyamide amine end groups during the melt blending process. The grafted copolymer strengthens the interface between phases, reduces interfacial tension, and provides steric stabilization that retards coalescence of the dispersed phase. The latter allows formation of stable, finely dispersed rubber particles. Super tough blends result when the rubber particle size is within the optimum range where the rubber particles can cavitate during the fracture process and permit shear yielding of the polyamide matrix [6][7][8]. A critical interparticle distance, according to the percolation model, defines an upper limit on particle size of about 1  $\mu\text{m}$  [35]. A lower limit on particle size of about 0.1  $\mu\text{m}$  is believed to be associated with difficulty in cavitation of rubber particles [7][10][12].

These observations of an optimum range of rubber particles are based on the standard notched Izod impact test which is commonly used because it is convenient and provides easy comparison among several materials. However, the Izod test provides limited information about fracture behavior, i.e., the energy absorbed under fixed conditions of notch depth, notch radius, and ligament length. Previous papers from this laboratory have reported more detailed characterization of fracture behavior based on the essential work of fracture (EWF) model using instrumented Dynatup test in a single-edge notched three-point bend (SEN3PB) configuration [20][21][28][29][32].

In a previous chapter, it was shown that a ductile-to-brittle transition occurs in both rubber particle size and ligament length for SEN3PB specimens,  $\ell$ , for blends of 80% nylon 6 and 20% rubber based on mixtures of EPR-g-MA and unmaleated rubber, i.e., EPR [28]. For marginally tough blends with rubber particles on the edge of the optimal size range, brittle fracture was found to occur for the specimens with long ligament lengths while ductile fracture was seen at short ligament lengths. It was demonstrated that the ductile fracture can be well-described by the EWF model, while the brittle fracture can be rationalized by linear elastic fracture mechanics (LEFM), e.g., by the critical stress intensity factor,  $K_{IC}$ , model [28]. Such a ductile-to-brittle transition in ligament length has also been observed for blends of nylon 6 with ABS materials compatibilized with an imidized acrylic polymer (IA) [21][29]. It has been shown that the LEFM parameters can be calculated from such brittle behavior and that they provide more in-depth information about the optimum rubber particle

size limit although the rigorous requirements for application of this model may not always be satisfied for such blends which have low yield strength and high toughness [29].

The purpose of this chapter is to expand on the previous chapter [28] by comparison of blends of nylon 6 with maleic anhydride grafted styrene/hydrogenated butadiene/styrene triblock copolymer, SEBS-g-MA, with the prior blends based on EPR-g-MA. Ductile behavior is analyzed by the EWF method while brittle fracture is analyzed in terms of the critical stress intensity factor ( $K_{IC}$ ) and the critical strain energy release rate ( $G_{IC}$ ) methods. A detailed characterization of the ductile-to-brittle transition in rubber particle size and ligament length using LEFM methods is presented.

### **3. 2 Experimental**

Table 1 shows the materials used in this work. The nylon 6 is a commercial product of Honeywell (formerly AlliedSignal) designated as B73WP (formerly Capron 8207F) which was a medium molecular weight grade ( $\bar{M}_n = 22,000$ ) with nearly equivalent amounts of acid and amine end groups. Blends of nylon 6 containing 20% total rubber based on various mixtures of maleated and non-maleated rubbers were prepared. The size of dispersed rubber particles in the polyamide matrix was varied by adjusting the ratio of non-maleated rubber to maleated rubber. Table 2 shows the compositions of the blends and their characteristics.

Table 1 Materials used in this work

Polymer	Commercial designation	Characterization <sup>a</sup>	Molecular weight <sup>a</sup>	Source
Nylon 6	Capron 8207F <sup>b</sup>	End-group content: [NH <sub>2</sub> ] = 47.9 μeq g <sup>-1</sup> [COOH] = 43.0 μeq g <sup>-1</sup>	$\overline{M}_n = 22,000$	AlliedSignal Inc.
EPR-g-MA	Exxelor 1803	43 wt.% ethylene 53 wt.% propylene 1.14 wt.% MA	Not available	Exxon Chemical Co.
EPR	Vistalon 457	43 wt.% ethylene 53 wt.% propylene	$\overline{M}_n = 54,000$ $\overline{M}_w / \overline{M}_n = 2$	Exxon Chemical Co.
SEBS-g-MA	Kraton FG-1901X	29 wt.% styrene 1.84 wt.% MA	Not available	Shell Chemical Co.
SEBS	Kraton G 1652	29 wt.% styrene	Styrene block = 7,000 EB block = 37,500	Shell Chemical Co.

<sup>a</sup> Reference [6].

<sup>b</sup> The designation of this material has been changed to B73WP.

The materials were dried for a minimum of 16 h in a vacuum oven at 80°C prior to any processing steps. The blends were melt mixed using a Killion single screw extruder ( $L/D = 30$ ,  $D = 2.54$  cm), outfitted with an intensive mixing head, operated at 240°C and 40 rpm. The desired proportion of polymer components were vigorously mixed before feeding to the extruder hopper. Each blend was extruded twice to assure adequate mixing. The masterbatch process was additionally used for preparation of blends of nylon 6 with maleated EPR. A masterbatch of 50% EPR and 50% nylon 6 was formed by melt blending in a 250 ml Brabender Plasticorder using the bale form of non-maleated EPR which was cut into strips ( $2 \times 4 \times 5$  cm<sup>3</sup>) and blended with additional nylon 6 and EPR-g-MA [13]. The blends were formed into Izod bars (ASTM D256), either 3.18 mm or 6.35 mm thick, using an Arburg Allrounder injection molding machine at 240°C. Molded specimens without defects were selected and kept in a dessicator under vacuum to avoid water sorption.

The morphology of the blends were observed by a JEOL 200 CX transmission electron microscope using ultra thin sections at an accelerating voltage of 120 kV. The thin sections (10 to 20 nm thick) were cryogenically microtomed at -50°C in the plane parallel to the injection flow direction at the center of thick (6.35 mm) samples in the region of fracture near the gate end of an Izod bar. Thin sections were exposed to a 2% aqueous solution of phosphotungstic acid for 30 min at room temperature and the nylon 6 phase was stained. Rubber particle size was determined by a semi-automated digital analysis technique using IMAGE<sup>®</sup> software from the National Institutes of Health.

Impact tests were made by the standard Izod procedure (ASTM D256) and by an instrumented Dynatup Drop Tower Model 8200; the latter employs a single-edge notched, three-point bend (SEN3PB) specimen geometry [8] [14]. The specimens were prepared by cutting injection molded bars (6.35 mm thick and 12.5 mm wide) into two pieces (one half gate-end and far-end specimens) whose lengths were exactly 54 mm. The original ligament length of the specimens ranged typically from 2 to 10 mm. A sharp notch was made by a fresh razor blade cooled in liquid nitrogen. The Dynatup test was made by dropping a 10 kg weight at a speed of 3.5 m/s, the same as in the standard Izod test, onto the center of a specimen with a span,  $S$ , of 48 mm between supports. The number of the SEN3PB specimen used was between 14 and 31. The size of the ligament length was determined by measuring the potential length of the ligament (from the original crack tip to the edge of the test specimen) from which the potential fracture area can be calculated. The fracture energy was calculated from the load-deflection curve, which was signal-conditioned using a digital low pass filter to reduce vibration noise. Drift in the baseline was corrected for all measurements. The fracture energy was obtained by excluding energy losses due to friction and contact between the specimen and the instrument. Other details of the testing procedure are described elsewhere [8][14][28].

### 3. 3 Fracture analysis

Broberg introduced the idea that the region around the crack consists of an elastic zone where fracture initiation and extension occur and a plastic zone where additional energy is absorbed during crack propagation [15]. Based on this model, Mai and coworkers [16][17][18] proposed that the total work of fracture  $W_f$  or  $U$  is divided into two parts, i.e.

$$W_f = W_e + W_p \quad (1)$$

where  $W_e$  is the "essential" work of fracture while  $W_p$  is the "non-essential" work [16][17][22][33]. It is assumed that  $W_e$  represents the energy required to create two new surfaces from yielded material and is proportional to the fracture area, while  $W_p$  is a volume energy term and is proportional to  $\ell^2$  ( $\ell$  = ligament length). Accordingly, the total fracture work is rewritten as the specific total fracture work,  $w_f$ , as follows

$$w_f = \frac{W_f}{t\ell} = w_e + w_p \ell \quad (2)$$

where  $w_e$  is the specific essential work of fracture,  $\alpha$  is a plastic zone shape factor, and  $w_p$  is the specific non-essential work of fracture. This model requires that a ligament must be fully yielded before fracture and ligament length has the limitation as follows:

$$5t < \ell \quad (3)$$

where  $t$  is the thickness.

Vu-Khanh [19] proposed an analogous relationship

$$\frac{U}{A} = G_i + \frac{1}{2} T_a A \quad (4)$$

where  $A$  is the area of the ligament to be broken,  $A = \ell t$ . The term  $G_i$  is the fracture energy at crack initiation and  $T_a$  is the tearing modulus. Prior work indicates that the approach by Mai is more appropriate because the ligament length describes the second term more accurately than the ligament area [21].

Testing conditions and sample geometries in this study may not always satisfy the criteria proposed by Mai for the yielding and ligament length. Therefore, we adopt a different nomenclature for the intercept and slope of plots of  $w_f$  versus  $\ell$ , i.e.

$$\frac{U}{A} = u_o + u_d \ell \quad (5)$$

where  $U/A$  is the total specific fracture energy,  $u_o$  is called the limiting specific fracture energy and  $u_d$  is the dissipative energy density [20][21]. In ideal cases,  $u_o = w_e$  and  $u_d = w_p$ ; these relations may not always be satisfied, therefore a different nomenclature seems appropriate.

The maximum tensile stress at the bottom of a bar (without a crack) is expressed by the following relation from linear elastic theory [23]:

$$\sigma_{\max} = \frac{3SF}{2tW^2} \quad (6)$$

where  $S$  is the span. This equation gives the failure stress when the peak load from the Dynatup load-deflection curve is substituted for  $F$ . The failure stress for ductile fracture can be expressed using unnotched tensile stress at the same conditions as the fracture,  $\sigma_y$ , as a function of normalized crack length,  $a/W$ , as follows [24]:

$$\sigma_{\max} = \sigma_y \frac{W - a}{W} \quad (7)$$

On the other hand, the failure stress for brittle fracture is expressed by  $K_{IC}$  under plane-strain conditions as follows [25]:

$$\sigma_{\max} = \frac{K_{IC}}{Y\sqrt{a}} \quad (8)$$

where  $K_{IC}$  is the critical stress intensity factor and  $Y$  is a geometrical factor which is expressed by

$$Y = 1.93 - 3.07(a/W) + 14.53(a/W)^2 - 25.11(a/W)^3 + 25.80(a/W)^4 \quad (9)$$

Plane-strain conditions are expected when  $a/W \geq 0.6$ . The yield stress or the critical stress intensity factor can be calculated by fitting plots of failure stress versus normalized crack length,  $a/W$ , to the applicable model using non-linear regression analysis. The failure mode, i.e., ductile or brittle, depends on the relative stress level for brittle fracture given in terms of  $K_{IC}$  and for ductile fracture given in terms of  $\sigma_y$  at a certain ligament length for a given material. Either ductile or brittle fracture can occur depending on which is smaller, the stress for brittle or for ductile fracture.

The size criterion to ensure plane-strain conditions, according to the ASTM testing standards, is given by [31]:

$$t, a \text{ or } \ell > 2.5 \frac{K_{IC}^2}{\sigma_y} \quad (10)$$

where  $(K_{IC}/\sigma_y)^2$  is proportional to the plastic zone size around the crack tip. The thickness and ligament length always satisfy this criterion, but the crack length may not, in this work.

The critical strain energy release rate,  $G_{IC}$ , model can also be used to analyze brittle fracture [30][31];  $G_{IC}$  is expressed by the fracture energy at peak load as follows [29]:

$$U_{\text{peakload}} = U_K + G_{IC}tW \quad (11)$$

where  $U_K$  is the kinetic energy required to accelerate a sample to the testing speed and  $\beta$  is the energy calibration factor. The term  $\beta$  is given by the following function of the crack length,  $a$ :

$$\frac{A + 18.64}{dA/dx} \quad (12)$$

where  $x = a/W$  and  $A$  is

$$A = \frac{16x^2}{(1-x^2)} (8.9 - 33.7x + 79.6x^2 - 113.0x^3 + 84.8x^4 - 25.7x^5) \quad (13)$$

for the specimen geometry used in this test [31]. Plane-strain conditions are assumed in this model and are expected only if the ratio of the crack length to the width is less than or equal to 0.6. The value of  $G_{IC}$  is deduced from the slope of a plot of total fracture energy versus  $tW$  for the specimens which fracture in a brittle manner and are in the range of  $a/W = 0.6$ .

Table 2

Morphology and impact strength for blends of 80% nylon 6 and 20% total rubber

Rubber phase composition	% Maleated rubber	$\bar{d}_w$ ( $\mu\text{m}$ )	$\bar{d}_w/\bar{d}_n$	Izod (J/m)	Ductile-to-brittle transition temperature ( $^{\circ}\text{C}$ )
x% EPR-g-MA + (100-x)% EPR	0	1.50	3.49	153	40
	12.5	1.39	1.67	142	40
	25	1.10	1.95	334	35
	37.5	0.75	1.61	405	20
	50	0.61	1.89	672	-5
	75	0.36	1.58	678	-20
	100	0.24	1.75	552	-25
x% SEBS-g-MA + (100-x)% SEBS	5	1.94	6.83	123	40
	10	1.04	3.51	264	30
	25	0.23	2.28	974	-5
	75	0.10	1.16	476	-10

According to linear elastic fracture mechanics,  $K_{IC}$  and  $G_{IC}$  should be related by the following [38]:

$$G_{IC} = \frac{(1 - \nu^2)K_{IC}^2}{E} \quad (14)$$

where  $\nu$  is Poisson's ratio and  $E$  is the tensile modulus at the same testing conditions as the fracture test.

### 3. 4 Results and discussion

#### 3. 4. 1 Morphology and notched Izod impact strength

Table 2 shows some characteristics of the blends investigated in this chapter. The weight average rubber particle size,  $\bar{d}_w$ , decreases as the amount of maleated rubber in the rubber phase increases. The particle size ranged from 0.24 to 1.50  $\mu\text{m}$  for EPR-based blends, while for the SEBS-based blends the particle size ranged from 0.10 to 1.94  $\mu\text{m}$ . The polydispersity for EPR-based blends is essentially constant as the amount of EPR-g-MA is increased; however, for SEBS-based blends the polydispersity decreased with increasing amount of SEBS-g-MA. The blends containing either 100% EPR-g-MA or 25% SEBS-g-MA lead to small particles of similar size, about 0.23 – 0.24  $\mu\text{m}$  in diameter, and have high fracture toughness. However, blends containing 25% EPR-g-MA or 10% SEBS-g-MA have large rubber particles, about 1.04 – 1.1  $\mu\text{m}$ , and are marginally tough. The fracture characteristics of these blends with similar particle sizes are compared in a later section.

Fig. 1 shows standard notched, room temperature Izod impact strength for 3.15-mm thick specimens made from the various blends as a function of their rubber particle size. The two blend systems are similar in that the notched Izod strength is at a maximum for  $\bar{d}_w$  between about 0.2 to 0.6  $\mu\text{m}$ . However, the maximum Izod strength for the SEBS blends is about 1.5 times larger than that for the EPR blends. These results are in accord with prior observations from this laboratory [6][9]. At large values of  $\bar{d}_w$ , both blend systems fractured in a brittle manner and showed similar Izod strength values.

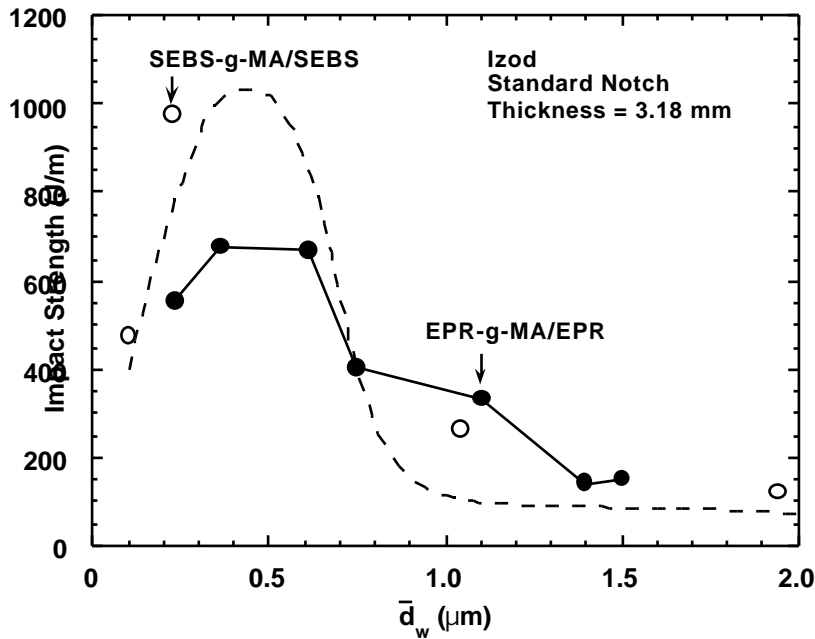


Fig. 1. Izod impact strength as a function of average rubber particle diameter for blends of 80% nylon 6 and 20% total rubber based on EPR-g-MA/EPR and SEBS-g-MA/SEBS mixtures. The broken curve is drawn from prior data for blends of SEBS/SEBS-g-MA-2% with nylon 6 ( $\bar{M}_n = 22,000$ ) [6].

Fig. 2 shows the ductile-to-brittle transition temperature (DBT) as a function of rubber particle size. Both blend systems show an increase in DBT with increasing rubber particle size. For  $\bar{d}_w > 1 \mu\text{m}$ , the DBT is near room temperature or higher for both blend systems. For  $\bar{d}_w < 1 \mu\text{m}$ , the DBT becomes much lower than room temperature; however, below  $0.4 \mu\text{m}$  the EPR-based blends show substantially lower DBT than the SEBS-based blends. This is also consistent with the results in a previous report [7]; the better low-temperature toughness of EPR-based blends is related to the lower modulus of EPR than SEBS in this temperature range.

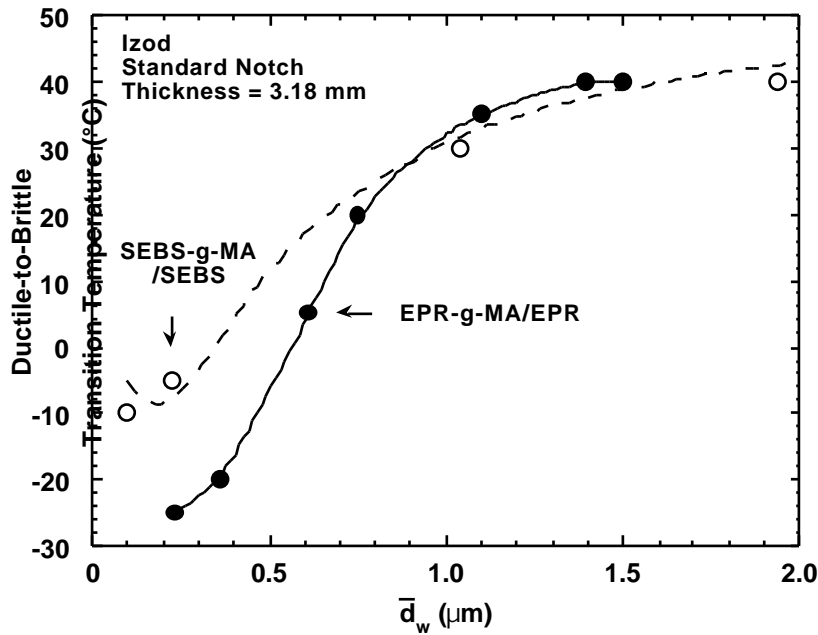


Fig. 2. Ductile-to-brittle transition temperature as a function of average rubber particle diameter for blends of 80% nylon 6 and 20% total rubber based on EPR-g-MA/EPR and SEBS-g-MA/SEBS mixtures. The broken curve is drawn from prior data for blends of SEBS/SEBS-g-MA-2% with nylon 6 ( $\bar{M}_n = 22,000$ ) [7].

### 3. 4. 2 Failure mode map for Dynatup impact test

The failure mode observed by Dynatup for 6.35-mm thick specimens in the SEN3PB configuration is summarized in Fig. 3 as a function of the rubber particle size and the ligament length. Specimens showing a partial break with relatively high specific fracture energy were classified as ductile. A stress-whitened zone surrounding the fracture surface is characteristic of a ductile fracture. Specimens exhibiting a complete break with low specific fracture energy were classified as brittle. Hinged breaks observed for four specimens containing 25% EPR-g-MA and one specimen containing 10% SEBS-g-MA, see Fig. 7, were not classified as either ductile or brittle in this paper because specimens exhibiting this type of failure may not be fully loaded in the Izod test: the pendulum either stops or the specimen deflects out of the path of the pendulum for hinged breaks in the Izod test [6].

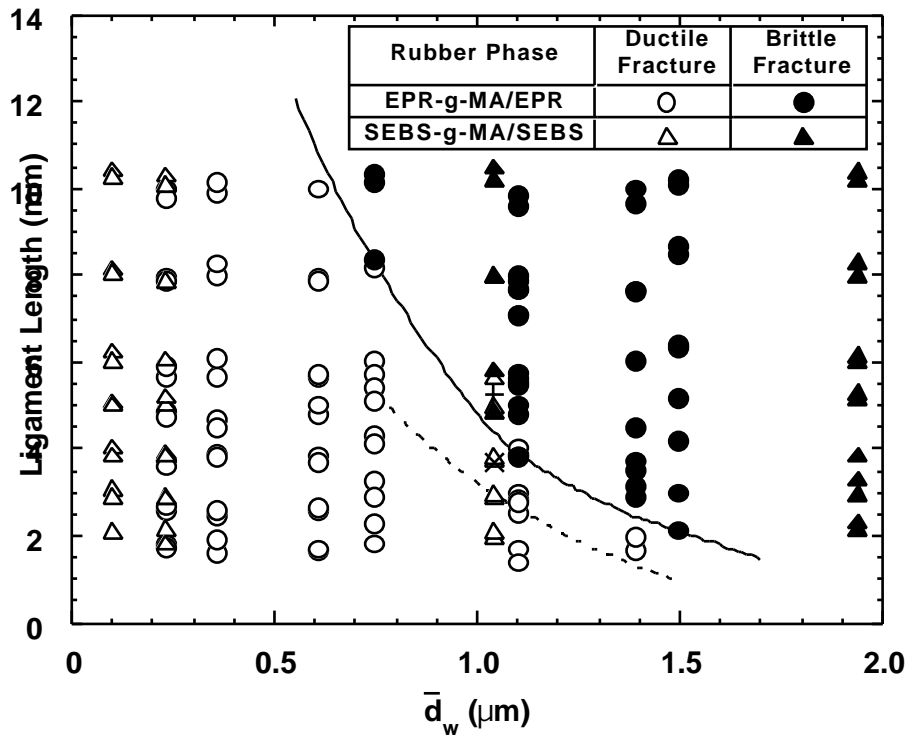


Fig. 3. Failure mode as a function of ligament length and average rubber particle diameter for blends of 80% nylon 6 and 20% total rubber measured by Dynatup for thick specimens with sharp notches. The measured ductile-to-brittle transition ligament lengths for the EPR-based blends (solid line) and for SEBS-based blends (+) are compared to the ligament length criterion which is calculated by Eq. (15) for EPR-based blends (broken line) and for SEBS-based blends (x).

Both blend systems generally exhibit similar fracture modes depending on the rubber particle size and the ligament length. Ductile fracture was observed for all ligament lengths when  $\bar{d}_w$  is less than 0.7  $\mu\text{m}$ ; whereas, brittle fracture was observed for all ligament lengths when  $\bar{d}_w$  is larger than 1.4  $\mu\text{m}$  as seen in Fig. 3. A ductile-to-brittle transition with respect to ligament length was observed for the marginally tough blends having rubber particles in the size range from 0.7 to 1.4  $\mu\text{m}$  for both blends.

The measured critical ligament lengths for the ductile-to-brittle transition are indicated as a solid line for EPR-based blends and as a plus mark for SEBS-based blends in Fig. 3. The transition ligament length increases from 2.45 to 8.25 mm as  $\bar{d}_w$  is decreased from 1.39 to 0.75  $\mu\text{m}$  for EPR-based blends. For the two blend systems with  $\bar{d}_w$  of about 1  $\mu\text{m}$ , the critical ligament length is 5.28 mm for the 10% SEBS-g-MA blend ( $\bar{d}_w = 1.04 \mu\text{m}$ ) and 3.85

mm for the 25% EPR-g-MA blend ( $\bar{d}_w = 1.1 \mu\text{m}$ ). The failure mode clearly depends on  $\bar{d}_w$  and the ligament length but seems rather independent of the rubber type.

The measured ductile-to-brittle transition ligament lengths for the EPR-based (solid line) and for the SEBS-based blends (+) are compared to the ligament length criterion given by the following equation, i.e., the right-hand side of Eq. 10 for EPR-based blends (broken line) and for SEBS-based blends (x),

$$\ell = 2.5 \frac{K_{IC}^2}{\sigma_y} \quad (15)$$

using measured  $K_{IC}$  and  $\sigma_y$  values from the stress analysis results in a later section. The calculation shows similar trends as the experimental results: the calculated critical ligament length from this criterion increases as  $\bar{d}_w$  is decreased for EPR-based blends but is slightly less than the experimentally observed length. Thus, the thickness (6.35 mm) and ligament length of specimens which fractured in a brittle manner are larger than the calculated criterion and satisfy the criterion for plane-strain conditions expressed by Eq. 10. On the other hand, the crack lengths for the EPR-based blends with  $\bar{d}_w > 1.2 \mu\text{m}$  were larger than the criterion, but those for the EPR-based blends with  $\bar{d}_w < 1.2 \mu\text{m}$  were not always larger than the criterion: the crack length did not always satisfy the criterion for plane-strain conditions, as described in detail later. Pressly reported similar trends for the transition ligament length in blends of nylon 6/ABS/IA; the transition occurs at a ligament length of about 7.7 mm for 25% ABS blend (70/25/5) at room temperature where the calculated ligament criterion also describes the measured transition ligament length reasonably well [29].

Fracture surfaces of the marginally tough blends were observed by scanning electron microscopy to further identify the deformation mechanism. Fig. 4 compares fracture surfaces for both ductile and brittle specimens for the blend based on 10% SEBS-g-MA in the rubber phase ( $\bar{d}_w = 1 \mu\text{m}$ ). This blend exhibits brittle fracture with relatively low fracture energy at a ligament length of about 4.9 mm; whereas, ductile fracture with high energy is seen at a ligament length of about 5.1 mm in Fig. 7. No matrix yielding was observed at a distance of 4 mm from the crack initiation for the brittle specimen as seen in Fig. 4(a). On the other hand, extensive yielding and matrix deformation was shown at 4 mm from the crack initiation for the sample breaking in a ductile manner as seen in Fig. 4(b). Similar trends were reported for the EPR-based blends in the previous chapter [28]. From these observations, it is suggested that higher fracture energy for ductile specimens stems from the extensive matrix deformation and yielding in the stress-whitened zone surrounding the fracture surface.

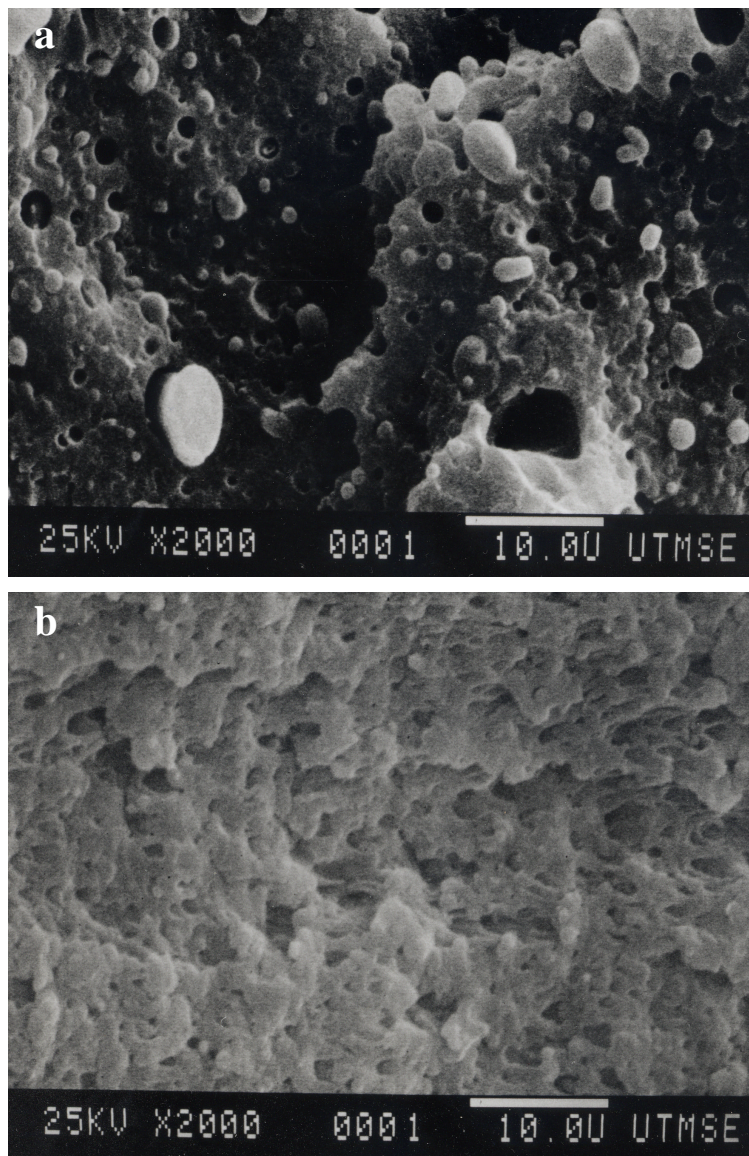


Fig. 4. SEM photomicrographs of the fracture surface at a distance of 4 mm from the crack initiation for blends based on 10% SEBS-g-MA in rubber phase: (a) brittle fracture, (b) ductile fracture.

### 3. 4. 3 Fracture analysis

In this section the load-deflection curve measured by the Dynatup impact test is analyzed in terms of both the energy and stress at fracture. The fracture energy for ductile failure is analyzed using the EWF model while that for brittle fracture is rationalized with the  $G_{IC}$  model. The fracture stress is analyzed using the yield stress or the  $K_{IC}$  models.

### 3. 4. 3. 1 Energy analysis

Ductile fracture was observed over the entire range of ligament lengths for the blends with small rubber particles ( $\bar{d}_w = 0.2 \mu\text{m}$ ), which was based on 100% EPR-g-MA and 25% SEBS-g-MA in the rubber phase, as seen in Fig. 3. Fig. 5 shows the relationship between the specific fracture energy,  $U/A$ , and the ligament length for the blends with small rubber particles. In the previous chapter [28], gate and far end specimens were analyzed separately in order to show the effect of crack position in the molded bar on the fracture behavior. It was shown that the difference in the fracture energy between crack positions is very small for the tough blends where  $\bar{d}_w$  is less than  $0.7 \mu\text{m}$ . On the other hand, scatter in the fracture energy based on the different crack positions was observed for the marginally tough blends, where  $\bar{d}_w$  is larger than  $0.7 \mu\text{m}$ ;  $u_d$  for the far end side was larger than that for the gate end side for blends with 25% and 37.5% EPR-g-MA while  $u_o$  is similar at the two crack positions. However, the fracture mode seems to be independent of the crack position and the gate and far ends showed similar trends with respect to the ductile-to-brittle transition as demonstrated in the previous chapter. Therefore, in this chapter those specimens were analyzed together, although fracture position seems to cause some scatter in fracture energy for marginally tough blends.

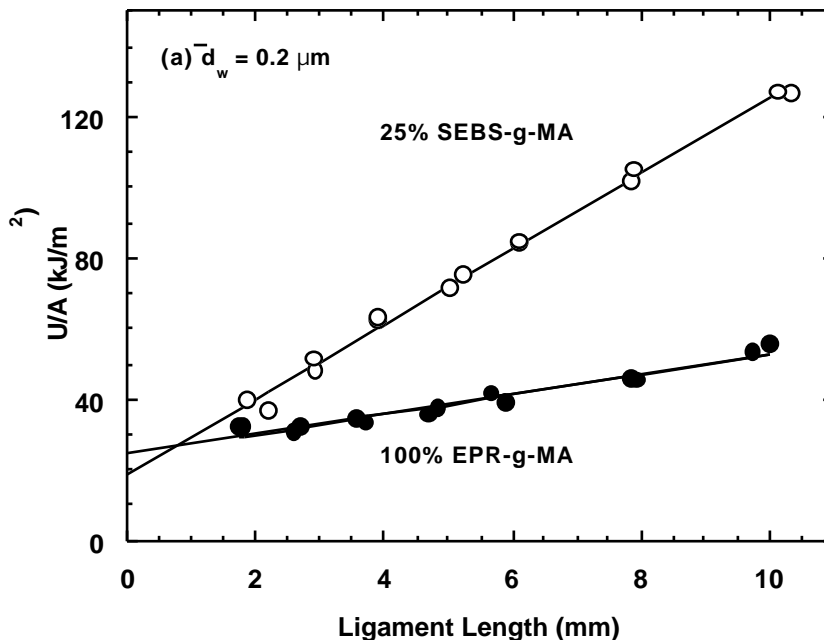


Fig. 5. Specific fracture energy as a function of ligament length for blends of 80% nylon 6 and 20% total rubber containing 100% EPR-g-MA and 25% SEBS-g-MA in the rubber phase where the average rubber particle diameter is about  $0.2 \mu\text{m}$ . The solid line for ductile data points is calculated by the EWF model.

The EWF model provides a good fit of the measured ductile fracture energy as shown in Fig. 5, and, thus, appears to be an appropriate method to analyze such behavior. The essential fracture parameters,  $u_o$  and  $u_d$ , are summarized in Table 3. The intercept,  $u_o$ , for SEBS-based blends is smaller than that for the EPR-based blends; however, the slope,  $u_d$ , is larger for the SEBS-based blends. Similar trends were reported for nylon 6 blends with maleated SEBS and maleated EPR [32]. The parameter  $u_o$  is the energy per unit area for crack initiation and propagation, while  $u_d$  is the energy per unit volume for plastic deformation near the crack tip. It is suggested that SEBS-based blends show more extensive plastic deformation than EPR-based blends in ductile fracture, while the energy for crack propagation for the former is smaller than that for the latter. These results would explain the superior toughness of SEBS-based blends compared to EPR-based blends in Izod tests and are consistent with the previous observation that SEBS-based blends exhibit larger plastic deformation zones than EPR-based blends [9].

Table 3

Fracture parameters for essential fracture work analysis for blends of 80% nylon 6 and 20% rubber

Rubber phase composition	x (%)	$u_o$ (kJ/m <sup>2</sup> )	$u_d$ (MJ/m <sup>3</sup> )
x% EPR-g-MA + (100-x)% EPR	0	-	-
	12.5	27.8	0.0
	25	20.5	3.0
	37.5	31.8	1.9
	50	28.9	3.2
	75	25.0	4.0
	100	24.4	2.8
x% SEBS-g-MA + (100-x)% SEBS	5	-	-
	10	22.4	4.6
	25	18.8	10.6
	75	17.2	0.9

Both ductile and brittle fracture modes were observed for the blends with large rubber particles ( $\bar{d}_w = 1 \mu\text{m}$ ), which contains 25% EPR-g-MA and 10% SEBS-g-MA in the rubber phase, as seen in Fig. 3. Ductile fracture occurred for the specimens with short ligament lengths and the results were analyzed by the EWF method; however, brittle fracture was observed for specimens with long ligament lengths. Thus, the EWF methodology is not applicable over the entire range of ligament lengths for these materials. As shown earlier, either the  $K_{IC}$  or  $G_{IC}$  analysis of linear elastic fracture mechanics is more appropriate than the EWF approach for these brittle fractures.

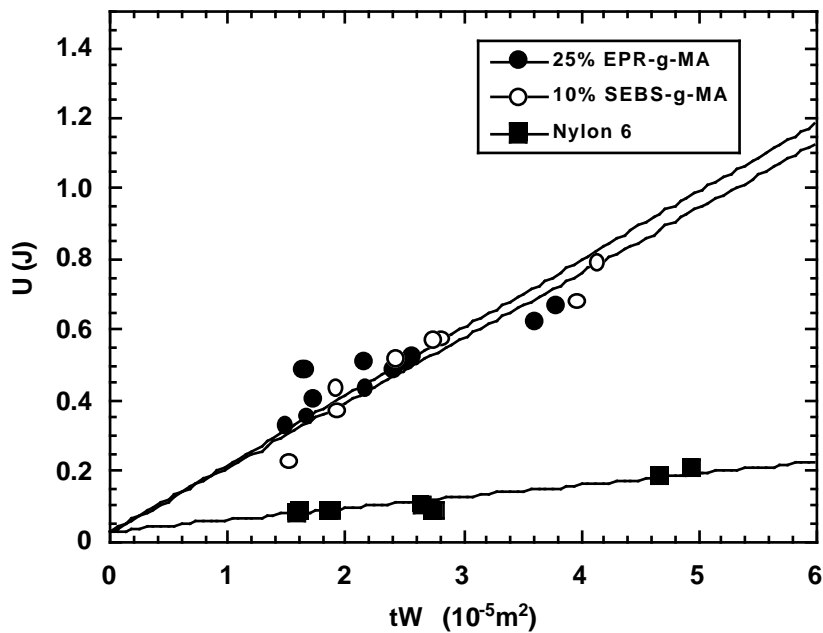


Fig. 6. Fracture energy at peak load as a function of  $tW$  based on the critical strain energy release rate model for neat nylon 6 and blends of 80% nylon 6 and 20% total rubber containing 25% EPR-g-MA and 10% SEBS-g-MA in the rubber phase where average rubber particle diameter is about  $1 \mu\text{m}$ .

Table 4

Fracture parameters for nylon 6 and blends of 80% nylon 6 and 20% rubber

Composition	% Maleated rubber	$\sigma_y$ (MPa)	$K_{IC}$ (MPa m <sup>1/2</sup> )	$G_{IC}$ (kJ/m <sup>2</sup> )
Nylon 6	0	-	1.7	3.3
80% nylon 6 + 20%(x% EPR-g-MA + (100-x)% EPR)	0	-	2.7	8.7
	12.5	-	3.2	14.4
	25	124.2	3.5	19.3
	37.5	109.3	5.3	38.4
	50	101.0	-	-
	75	100.3	-	-
	100	96.5	-	-
80% nylon 6 + 20%(x% SEBS-g-MA + (100-x)% SEBS)	5	-	1.6	6.9
	10	114.7	4.4	18.3
	25	111.9	-	-
	75	72.9	-	-

Brittle fracture energy was analyzed by the critical strain energy release rate,  $G_{IC}$ , model for the blends based on 25% EPR-g-MA and 10% SEBS-g-MA in the rubber phase. Fig. 6 shows the fracture energy at peak load as a function of  $tW$  for brittle specimens for two blend systems and neat nylon 6 based on Eq. (6). Specimens of pure nylon 6 fractured in a brittle manner for all ligament lengths; however, the only data where  $a/W$  is less than 0.6 were plotted in Fig. 6 according to the requirement of plane-strain conditions as mentioned before. The intercept in Fig. 6 was set equal to the kinetic energy [36],  $U_K$ , calculated from  $1/2mv^2$  was 0.028 to 0.030 J, where  $m$  is the weight of the specimen and  $v$  is the tup velocity of 3.5 m/s. The  $G_{IC}$  values were derived from the slope of same plots and are summarized in Table 4. The  $G_{IC}$  value for neat nylon 6 is 3.3 kJ/m<sup>2</sup> and is similar to that given by Laura (4.7 kJ/m<sup>2</sup>) [36]. The values of  $G_{IC}$  for both blend systems with rubber particles of  $\bar{d}_w = 1 \mu\text{m}$  approximately coincide with each other as shown in Table 4. The values of  $G_{IC}$  for both blends are about 5.5 times larger than that of pure nylon 6. This suggests that inclusion of rubber particles in the nylon 6 matrix increases  $G_{IC}$  values. Although the blends break in a brittle manner, toughness of the blends is considerable larger than that of neat nylon 6. It appears that the  $G_{IC}$  obtained from the brittle fracture energy for the blends is independent of the rubber type but depends on the rubber particle size.

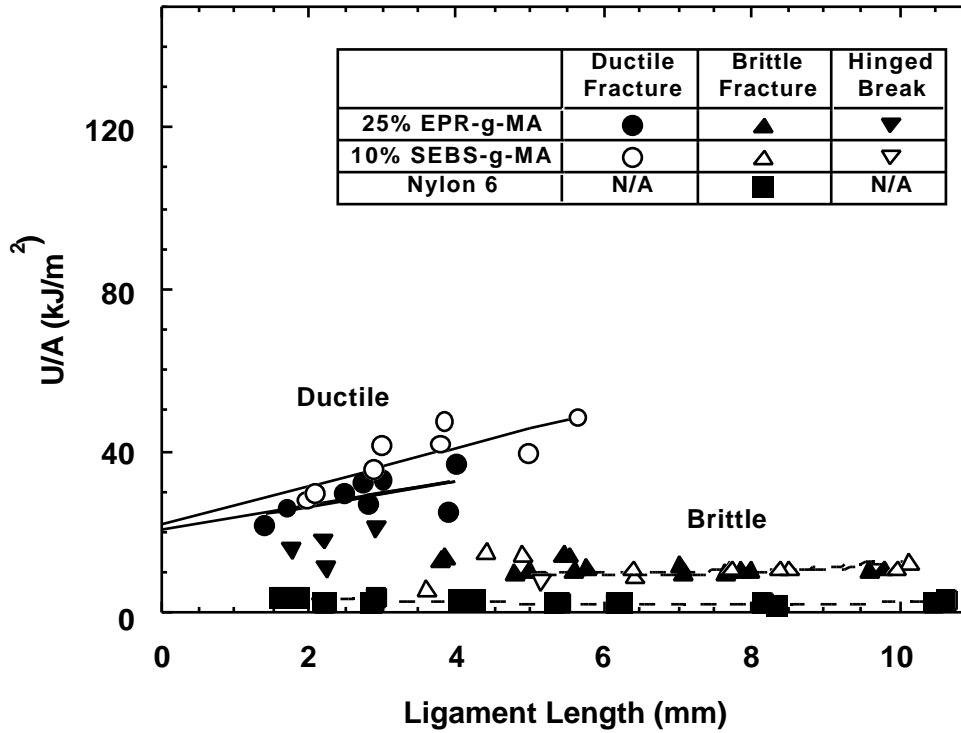


Fig. 7. Specific fracture energy as a function of ligament length for the materials described in Fig. 6. The solid line is calculated for ductile fracture by the EWF model and the broken line is drawn using energy values calculated from the  $G_{IC}$  analysis in Fig. 6.

Fig. 7 shows the specific fracture energy as a function of ligament length for neat nylon 6 and both blend systems based on 25% EPR-g-MA and 10% SEBS-g-MA in the rubber phase where  $\bar{d}_w$  is about  $1 \mu\text{m}$ . The fracture energy for specimens which broke in a brittle manner is in good agreement with the energy value calculated from  $G_{IC}$  analysis as shown by broken lines in the range of  $a/W \leq 0.6$ , i.e.,  $\ell > 5 \text{ mm}$  in Fig. 7. For neat nylon 6, the data from specimens with ligament lengths less than 5 mm ( $a/W > 0.6$ ) were not used to determine the  $G_{IC}$  values; however, the calculated values are in good accord with experimental data over the entire range of ligament lengths as seen in Fig. 7. The EWF model predicts constant specific fracture energy, i.e.  $u_d = 0$  and  $u_o = \text{constant}$ , for brittle fracture. The values for neat nylon 6 were estimated as  $u_d = 0$ ,  $u_o = 2.9 \text{ kJ/m}^2$ . Kudva showed the same order but larger values ( $u_d = 0$ ,  $u_o = 7.2 \text{ kJ/m}^2$ ) for neat nylon 6 [21]. For brittle fracture, the specific fracture energy increases slightly at long ligament lengths. Pressly observed similar trends for brittle fracture of nylon 6/ABS blends; this increase can be explained by the non-linearity of the factor  $\gamma$  with ligament length [29].

Fig. 7 also shows fracture energies for ductile specimens as a function of ligament length. Ductile fracture was observed for the specimens with ligament lengths less than about 4 mm for EPR-based blends and about 6 mm for SEBS-based blends. Both ductile and brittle fractures were observed in the range of ligament lengths from 3.5 to 6 mm for 10% SEBS-g-MA blend. These ductile fracture energies were analyzed by the EWF model as shown by solid lines in Fig. 7. Both blend systems show similar values of  $u_0$ . The value of  $u_d$  for the blend based on 10% SEBS-g-MA was slightly larger than that for the blend based on 25% EPR-g-MA. Scatter for blends with large rubber particles was greater than that for blends with small rubber particles ( $\bar{d}_w = 0.2 \mu\text{m}$ ); the former is marginally tough and unstable in the transition state and affected by crack position as described above.

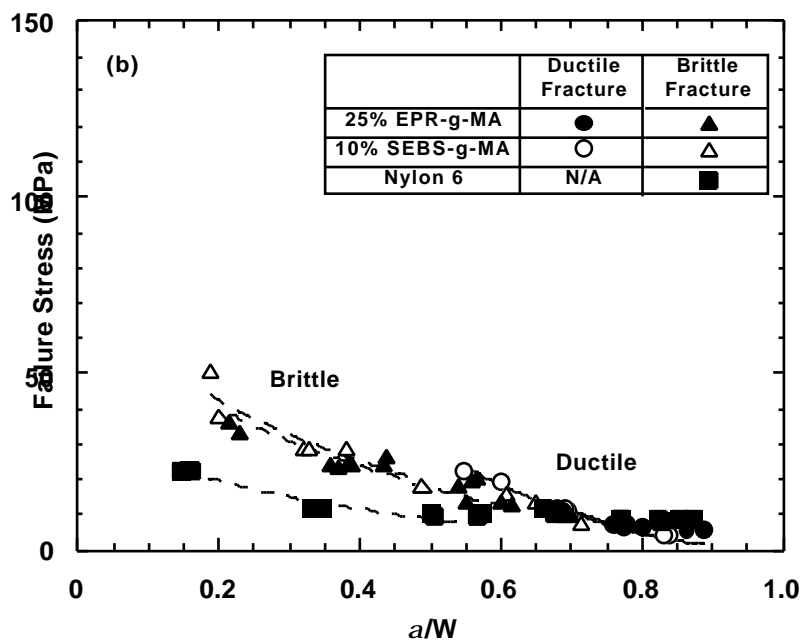
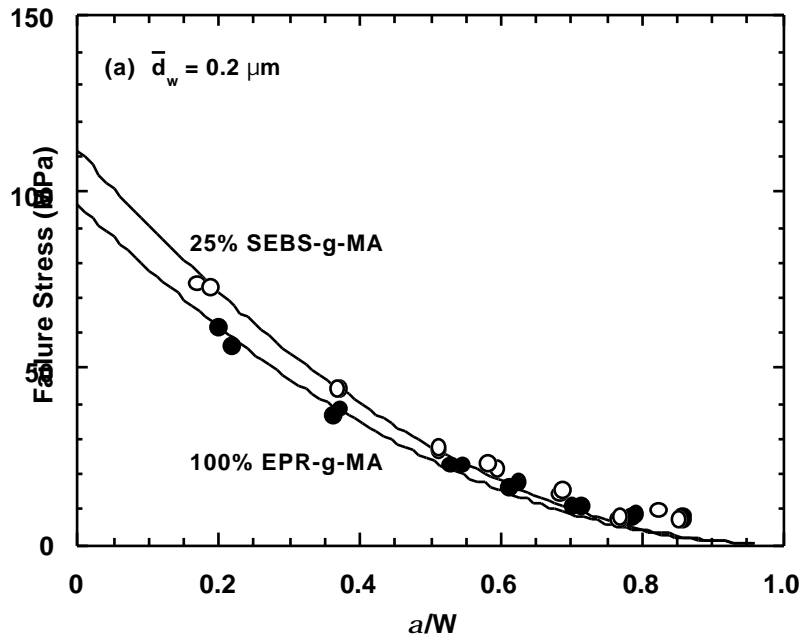


Fig. 8. Failure stress as a function of normalized crack length ( $a/W$ ) for neat nylon 6 and blends of 80% nylon 6 and 20% total rubber: (a) blends where the average rubber particle diameter is about  $0.2 \mu\text{m}$  and (b) neat nylon 6 and blends where the rubber particle size is  $1 \mu\text{m}$ . The solid line is calculated from the yield stress model, while the broken line is calculated using the  $K_{IC}$  model.

### 3. 4. 3. 2 Stress analysis

The failure stress, calculated from the peak load of the load-deflection data, is analyzed by either the yield stress,  $\sigma_y$ , model or plane-strain critical stress intensity factor,  $K_{IC}$ , model according to the fracture mode as described above. The models for  $\sigma_y$  and  $K_{IC}$  are fitted to the failure stress measurements using non-linear regression.

Figs. 8(a) and 8(b) show the failure stress as a function of  $a/W$  for the blends with small and large rubber particles, respectively. All samples for both blend systems with  $\bar{d}_w = 0.2 \mu\text{m}$  (based on 100% EPR-g-MA and 25% SEBS-g-MA in the rubber phase) failed in a ductile manner and were analyzed via the yield stress model using Eq. (7) as seen in Fig. 8(a). The yield stress model represents the ductile stress well. The values of yield stress were derived from the intercept in Fig. 8(a) and are summarized in Table 4. The value of  $\sigma_y$  for the 25% SEBS-based blends is 112 MPa which is larger than that for the 100% EPR-based blends (96.5 MPa) at  $\bar{d}_w = 0.2 \mu\text{m}$ . Pressly reported similar  $\sigma_y$  values for the compatibilized nylon 6/ABS blends:  $\sigma_y$  for nylon 6/ABS/IA (55/40/5) blends is 86 MPa and that for nylon 6/ABS/IA (70/25/5) blends is 88 MPa at room temperature [29]. Oshinski showed similar trends in Instron measurements of the yield stress for nylon 6/SEBS-g-MA and nylon 6/EPR-g-MA blends: the  $\sigma_y$  from Instron measurements for 25% SEBS-g-MA blend is 50.3 MPa and is higher than that for 100% EPR-g-MA blend which is about 44.0 MPa [37]. These values are half of the dynamic values observed in this paper. The yield stress in this study is expected to be larger than that in a simple tensile test at low speeds based on tensile data reported at high-speeds [26].

Fig. 8(b) shows failure stress as a function of  $a/W$  for neat nylon 6 and the blends containing large rubber particles ( $\bar{d}_w = 1 \mu\text{m}$ ), which is based on 10% SEBS-g-MA and 25% EPR-g-MA in the rubber phase. The ductile specimens ranged in  $a/W$  from about 0.55 to 0.85 for the 10% SEBS-g-MA blends and from about 0.65 to 0.90 for the 25% EPR-g-MA blends. The ductile behavior was analyzed using the yield stress model. Unexpectedly, the  $\sigma_y$  for the latter blends is larger than that for the former blends as seen in Table 4, although the values of failure stress for both blends are not clearly different as seen in Fig. 8(b). In this case, the higher range of  $a/W$  would result in higher  $\sigma_y$  in the 25% EPR-gMA blends, while the failure stress at  $a/W = 1$  should be zero.

The  $K_{IC}$  model was fitted to brittle fracture stress when  $a/W = 0.6$  for pure nylon 6, 10% SEBS-g-MA blend and 25% EPR-g-MA blend as indicated by the broken line in Fig. 8(b). The  $K_{IC}$  model well represents the brittle stress data with the  $K_{IC}$  values from this analysis summarized in Table 4. The  $K_{IC}$  for neat nylon 6 in this study is  $1.7 \text{ MPa m}^{1/2}$ . Typical  $K_{IC}$  values for polyamides are between 2.5 and  $3.0 \text{ MPa m}^{1/2}$  [27][34]. Note that the  $K_{IC}$  values for the both blend systems are larger than that for pure nylon 6. However, both blend systems give similar  $K_{IC}$  indicating, again, an independence of rubber type.

It is suggested that brittle fracture occurs at long ligaments, i.e., short cracks, because the failure stress determined by  $K_{IC}$  is smaller than the ductile failure stress controlled by  $\sigma_y$  in this ligament length range. On the other hand, the ductile fracture occurs at long ligament length because the ductile failure stress given by  $\sigma_y$  is smaller than the brittle failure stress expressed by  $K_{IC}$ .

#### 3. 4. 4 Effect of rubber particle size on fracture parameters

The effects of rubber particle size on fracture parameters are discussed below. Fig. 9(a) shows the effect of rubber particle size on  $K_{IC}$  for the blends based on both maleated EPR and SEBS rubbers which have rubber particles with  $\bar{d}_w > 0.7 \text{ }\mu\text{m}$ ; the blends with  $\bar{d}_w < 0.7 \text{ }\mu\text{m}$  did not show brittle fracture at any ligament lengths, so  $K_{IC}$  values could not be obtained. The data for neat nylon 6 is shown by the dotted line. For large rubber particles,  $K_{IC}$  for the blends is similar to that for pure nylon 6 ( $1.7 \text{ MPa m}^{1/2}$ ). For the EPR-based blends,  $K_{IC}$  increases from 2.7 to  $5.3 \text{ MPa m}^{1/2}$  as the rubber particle size is reduced from 1.5 to  $0.75 \text{ }\mu\text{m}$ . For EPR-based blends having  $\bar{d}_w = 0.75 \text{ }\mu\text{m}$ ,  $K_{IC}$  is about three times larger than that for neat nylon 6. Both EPR-based blends and SEBS-based blends show similar trends. This increase in  $K_{IC}$  indicates an increase of toughness as the rubber particle size is reduced.

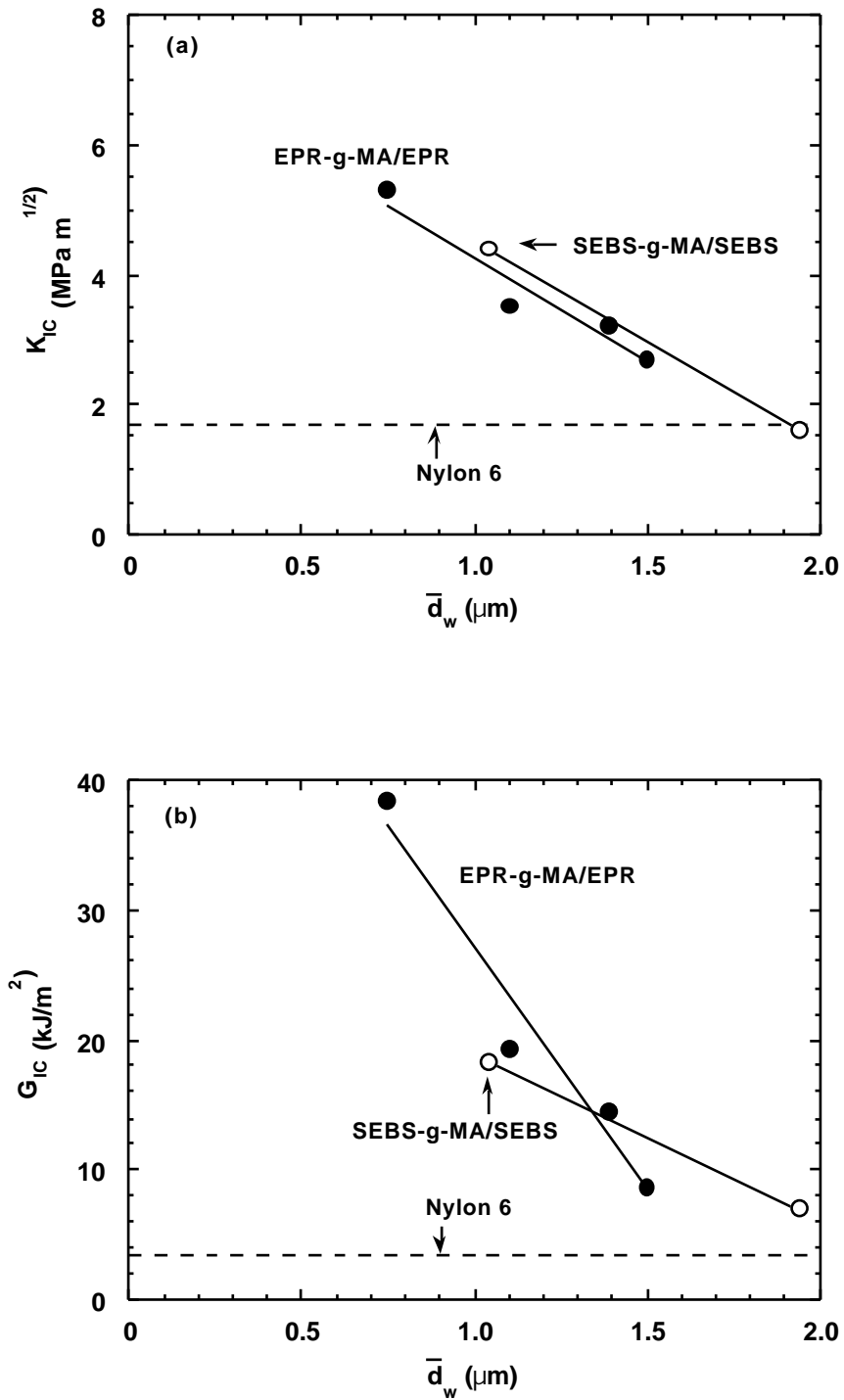


Fig. 9. Fracture parameters as a function of rubber particle diameter for neat nylon 6 and blends of 80% nylon 6 and 20% total rubber: (a)  $K_{IC}$  and (b)  $G_{IC}$ .

Table 4 shows yield stress values obtained from analysis of fracture stress data for ductile fracture as described above. The yield stresses for both blend systems decrease with increasing amount of maleated rubber. This trend corresponds to smaller particles, higher amounts of grafting and reduced crystallinity [37]. The number of data points exhibiting ductile failure for the blends containing less than 12.5% EPR-g-MA in the rubber phase is

not enough to justify the yield stress analysis shown in Fig. 3, so that the yield stress for such brittle blends was estimated by linear extrapolation of the relation between  $r_y$  and  $\bar{d}_w$ ; the estimated  $r_y$  values for EPR-based blends are 131 and 134 MPa for 12.5 and 0% EPR-g-MA blends, respectively.

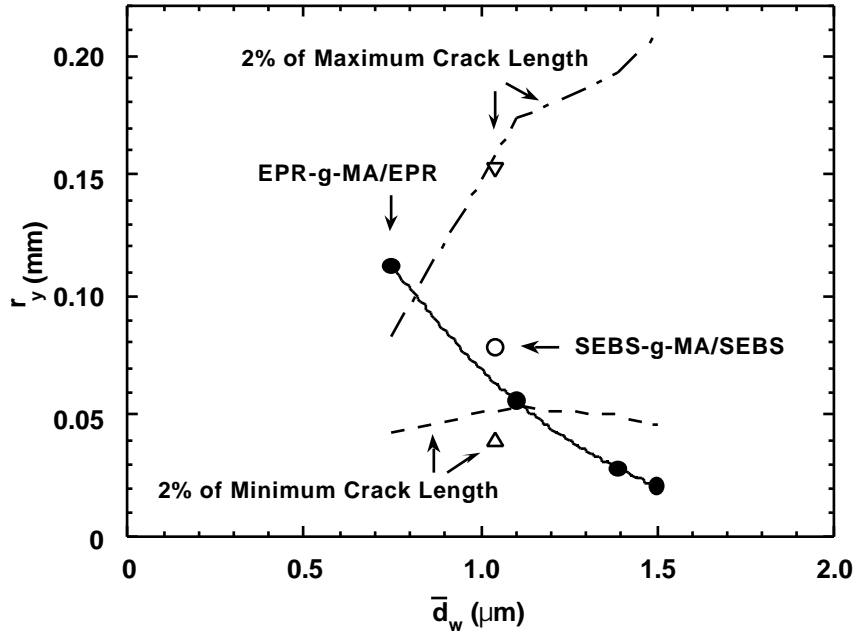


Fig. 10. Plastic-zone size for plane-strain conditions as a function of rubber particle diameter for the EPR-based blends (●) and the SEBS-based blends (○). The values of 2% of minimum and maximum crack lengths of the specimens which fracture in a brittle manner for the EPR-based blends (— — — and — . — .) and for the SEBS-based blends ( and ) are indicated.

From the relationship for  $K_{IC}$  and  $r_y$  with rubber particle size described above, it is clear that the size criterion for plane-strain conditions, expressed by Eq. (15) increases with decreasing  $\bar{d}_w$ , i.e., increasing  $K_{IC}$  and decreasing  $r_y$  as seen in Fig. 3. Both thickness and ligament length for the brittle fracture specimens are greater than the required size for plane-strain conditions. The right-hand side of Eq. (15) suggests that the required size is related to the plastic-zone size for plane-strain conditions,  $r_y$ , given by the following equation [39]:

$$r_y = \frac{1}{6} \frac{K_{IC}^2}{\sigma_y} \quad (16)$$

Fig. 10 shows  $r_y$  as a function of  $\bar{d}_w$  for both blend systems. The  $r_y$  increases from 0.025 to 0.12 mm as  $\bar{d}_w$  decreases from 1.5 to 0.75  $\mu\text{m}$  for the EPR-based blends. Fig. 10 also

indicates the values of 2% of minimum and maximum crack lengths of the specimens which fracture in a brittle manner. If plane-strain conditions are met, the plastic zone size should be less than 2% of the minimum crack length [40]. The 2% of minimum crack lengths for the EPR-based blends at  $\bar{d}_w = 1.39$  and  $1.5 \mu\text{m}$  are larger than the  $r_y$  values; therefore, the specimens fracture in plane-strain conditions and the measured  $K_{IC}$  values are considered to be valid material properties. However, the 2% of crack lengths for the EPR-based blends and the SEBS-based blends at  $\bar{d}_w = 1 \mu\text{m}$  are partially larger than the  $r_y$  values: some specimens in this regime did not fracture under plane-strain conditions. Whereas, the  $r_y$  value for the EPR-based blends at  $\bar{d}_w = 0.75 \mu\text{m}$  is larger than the 2% of maximum crack length; the brittle fracture for the EPR-based blends at  $\bar{d}_w = 0.75 \mu\text{m}$  does not clearly occur under plane-strain conditions. However, it is suggested that the ductile-to-brittle transition with respect to the ligament length corresponds to the size criterion for plane-strain conditions.

Fig. 9 (b) shows the  $G_{IC}$  values as a function of  $\bar{d}_w$ . Similar trends are seen between  $G_{IC}$  and  $\bar{d}_w$  as observed for  $K_{IC}$ . For large rubber particles, the blends have similar  $G_{IC}$  as pure nylon 6. For EPR-based blends,  $G_{IC}$  increases from 8.7 to 38.4  $\text{kJ/m}^2$  as  $\bar{d}_w$  decreases from 1.50 to 0.75  $\mu\text{m}$ . Values of  $G_{IC}$  for EPR-based blends at  $\bar{d}_w = 0.75 \mu\text{m}$  are about ten times larger than that for pure nylon 6. SEBS-based blends show a similar trend of  $G_{IC}$  increasing with decreasing  $\bar{d}_w$ . Both blend systems indicate similar  $G_{IC}$  values when  $\bar{d}_w$  is about 1  $\mu\text{m}$  as described above.

From the relation between the fracture parameters ( $K_{IC}$  and  $G_{IC}$ ) and  $\bar{d}_w$ , it is suggested that as the rubber particles become smaller, there is more deformation around the crack tip before the initiation of crack extension can occur, so that the fracture energy increases. However, there seems no difference in the fracture parameters between both blend systems.

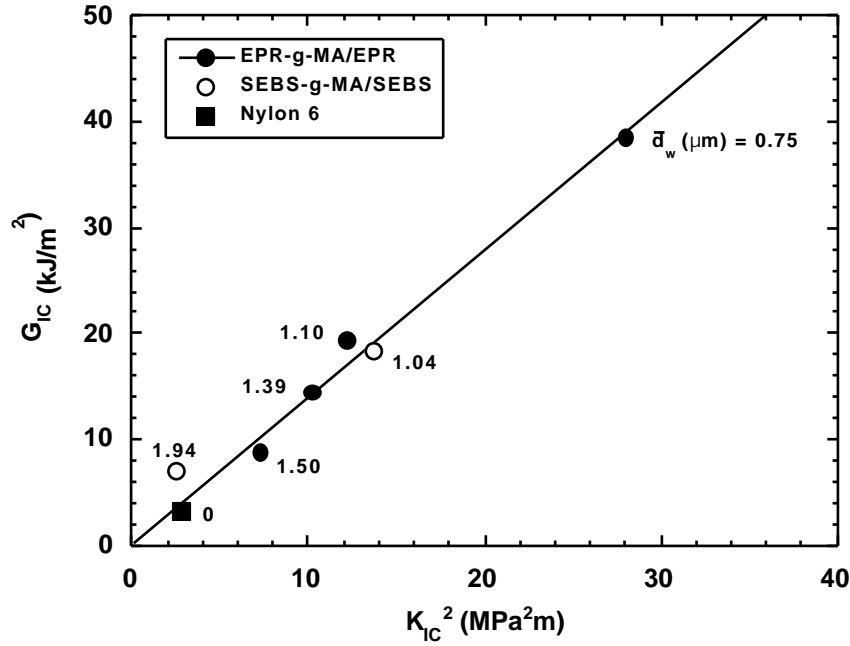


Fig. 11. Relation between  $G_{IC}$  and  $K_{IC}^2$  for neat nylon 6 and the blends of 80% nylon 6 and 20% total rubber based on EPR-g-MA/EPR and SEBS-g-MA/SEBS mixtures.

Fig. 11 shows a linear relation between  $G_{IC}$  and  $K_{IC}^2$  as expected from Eq. (14) with all materials studied more or less conforming to the same relationship. The linear relation between  $G_{IC}$  and  $K_{IC}^2$  was observed for the EPR-based blends where  $\bar{d}_w$  is less than 0.75  $\mu$ m. This linear relation implies that the tensile modulus is constant for the EPR-based blends. It is also noted that the plots for SEBS-based blends and neat nylon 6 are close to the line for the EPR-based blends. The tensile modulus estimated from the slope of the line assuming  $\nu = 0.3$  is 0.65 GPa. It is difficult to measure the tensile modulus under the testing conditions in this work, however, the tensile modulus measured by Instron at slow speed (5.08 cm/min) is 1.75 GPa for blends of nylon 6/EPR-g-MA (80/20) [37]. The modulus from the slope of Fig. 11 is about 30% of the Instron modulus. This discrepancy cannot be explained by rate effects but might be related to deviations from pure linear elastic behavior and specimen compliance [29][38].

The effects of rubber particle size on the EWF parameters ( $u_o$  and  $u_d$ ) are shown in Fig. 12. As seen in Fig. 12(a), for EPR-based blends,  $u_o$  generally increases with increasing  $\bar{d}_w$  in the range of  $\bar{d}_w < 1 \mu$ m. The trend is similar for SEBS-based blends but the absolute values of  $u_o$  are generally smaller than those for EPR-based blends by about 5 to 10 kJ/m<sup>2</sup>. Fig. 12(b) shows  $u_d$  as a function of  $\bar{d}_w$ , and somewhat similar trends are seen for the EPR-based blends and SEBS-based blends. There seems to be a maximum in  $u_d$  in

the range of  $\bar{d}_w$  between about 0.2 to 0.4  $\mu\text{m}$ . This maximum in  $u_d$  corresponds to the maximum in Izod impact strength seen in Fig. 1. The maximum value of  $u_d$  for SEBS-based blends is 2.5 times larger than that for EPR-based blends. Laura showed similar trends for the relation between the EWF parameters and  $\bar{d}_w$  [32].

The limiting specific fracture energy,  $u_o$ , for EPR-based blends was higher than that for SEBS-based blends, while the dissipative energy density,  $u_d$ , for the latter was larger than that for the former. The parameter  $u_o$  is the energy per unit area for crack initiation and propagation, while  $u_d$  is the energy per unit volume for plastic deformation. It is suggested that SEBS-based blends show more extensive plastic deformation than EPR-based blends in ductile fracture, while the energy for crack propagation for the former is smaller than that for the latter. It is suggested that the superior toughness of SEBS-based blends compared to EPR-based blends is caused from larger amount of plastic deformation.

The difference in EWF parameters between two blend systems could be explained by structure-property relations for the rubber phase. A possible explanation is as follows. Bucknall showed that the critical volume strain at cavitation decreases with decreasing modulus of rubber particle at fixed rubber particle diameter [41]. Therefore, the EPR-based blends would indicate lower critical volume strain at cavitation than the SEBS-based blends, because the modulus of EPR-based rubber particle is lower than that of SEBS particle and the latter are effectively crosslinked by the polystyrene microdomains. As a result, cavitation and shear yielding in the vicinity of crack tip would occur more easily for the EPR-based blends than the SEBS-based blends, so that  $u_o$  for EPR-based blends is higher than that for SEBS-based blends.

On the other hand, it is suggested that the yield zone expands outwards more for the SEBS-based blends than for the EPR-based blends based on comparison of the  $u_d$  values. This could be explained by load bearing structures of rubber particle which has been reported for high-impact polystyrene (HIPS) [42]. SEBS-based rubber particles should show strain-hardening based on its phase structure composed of rigid polystyrene and soft elastomer phases, which are similar to subinclusion structures (rigid core, inner rubbery phase, outer shell) observed in the salami rubber particles of HIPS. It is suggested that rubber fibrils connected between the core (polystyrene phase) and the outer shell (interface) would be able to stretch, expand and stabilize the SEBS-based rubber particle as seen in the fracture process of HIPS. The EPR-based rubber would be easy to cavitate because of lower modulus; however, the cavity in the EPR-based rubber particle is easy to break up compared to the SEBS-based rubber. Thus, shear yield zone would not expand as much for the EPR-based blends compared to the SEBS-based blends.

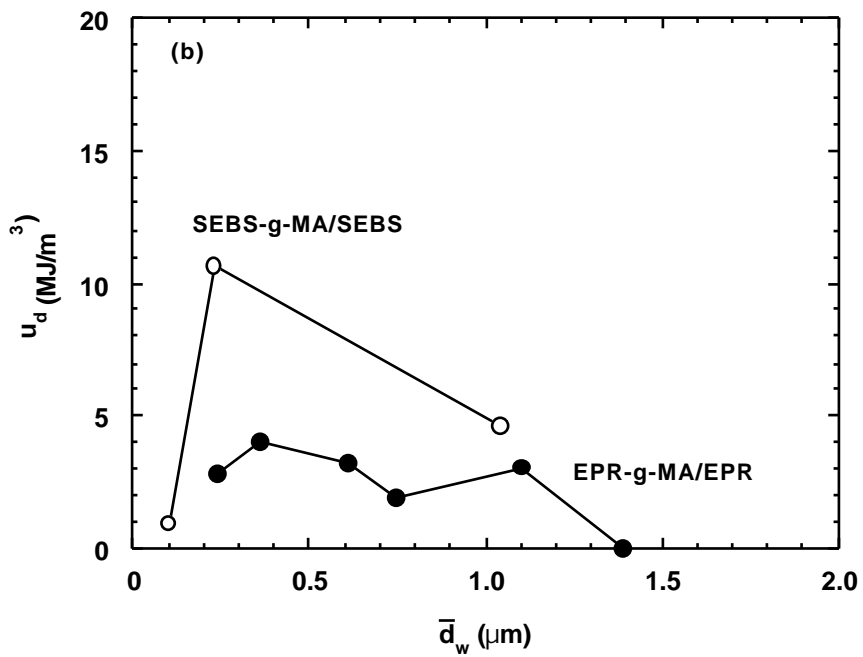
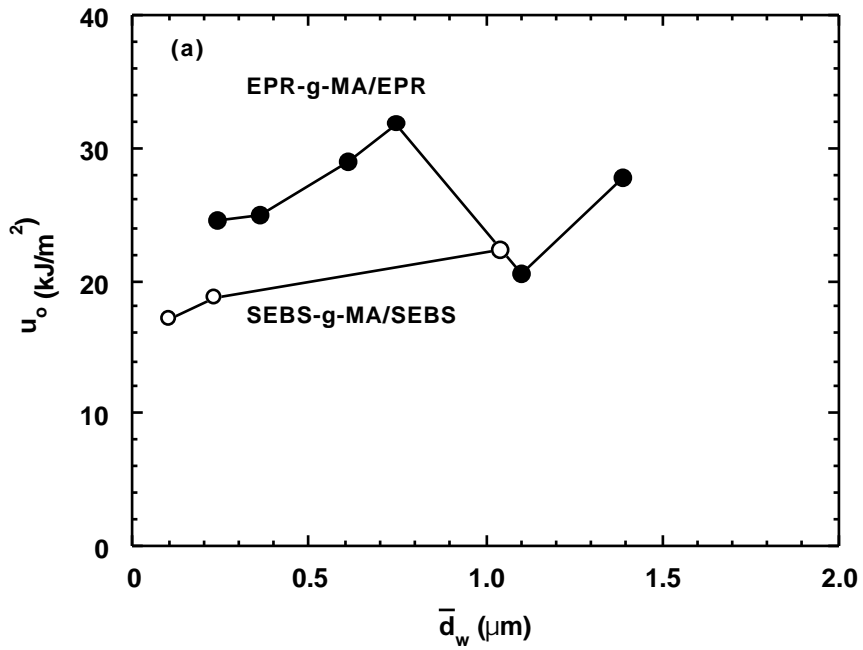


Fig. 12. Fracture parameters, (a)  $u_o$  and (b)  $u_d$ , as a function of rubber particle diameter for blends of 80% nylon 6 and 20% total rubber based on EPR-g-MA/EPR and SEBS-g-MA/SEBS mixtures.

### 3. 5 Conclusions

The effects of rubber type, rubber particle size and ligament length on the fracture behavior for blends of nylon 6 with maleated rubber were examined using instrumented Dynatup test in a SEN3PB configuration. It was found that for blends where the rubber particles are smaller than 0.7  $\mu\text{m}$  fracture in a ductile manner over the whole range of ligament lengths while blends with particles larger than 0.7  $\mu\text{m}$  show a ductile-to-brittle transition with ligament length. In this regime, ductile fracture was observed for specimens with short ligaments while brittle fracture was seen for those with long ligaments. The transition ligament length seems to be independent of rubber type but depends on rubber particle size.

The ductile fracture behavior was analyzed using the essential work of fracture (EWF) model. The limiting specific fracture energy,  $u_0$ , for EPR-based blends was higher than that for SEBS-based blends, while the dissipative energy density,  $u_d$ , for the latter was larger than that for the former. The energy required for crack initiation for ductile fracture is lower for the EPR-based blends than the SEBS-based blends, while the energy for crack propagation is larger than the SEBS-based blends. Larger fracture energies for the SEBS-based blends than the EPR-based blends can be explained by larger  $u_d$  of the SEBS-based blends.

The critical strain energy release rate,  $G_{IC}$ , and the plane-strain critical stress intensity factor,  $K_{IC}$ , were obtained from the brittle fracture behavior. Both fracture parameters increase with decreasing the rubber particle size for either blend systems. The  $G_{IC}$  and  $K_{IC}$  parameters have similar values regardless of rubber type when the rubber particle size is fixed. It was shown that fracture mode is governed by the relative levels of failure stresses given by either  $K_{IC}$  or  $\sigma_y$ . On the other hand, the transition ligament length, which increases with decreasing rubber particle size, was found to be near the size criterion for plane-strain conditions for both blend systems. These results suggest that the brittle fracture would

occur when plane-strain conditions are developed and the fracture stress is governed by  $K_{IC}$ . It is also suggested that the ductile-to-brittle transition with respect to the ligament length corresponds to the size criterion for plane-strain conditions based on the fracture mechanics parameters.

## References

- [1] Wu S. *Polym Engng Sci* 1987;27:335.
- [2] Wu S. *J Appl Polym Sci* 1988;35:549.
- [3] Lawson DF, Hergenrother WL, Matlock MG. *J Appl Polym Sci* 1990;39:2331.
- [4] Hobbs SY, Bopp RC, Watkins VH. *Polym Engng Sci* 1983;23:380.
- [6] Oshinski AJ, Keskkula H, Paul DR. *J Appl Polym Sci* 1996;61:623.
- [6] Oshinski AJ, Keskkula H, Paul DR. *Polymer* 1996;37:4909.
- [7] Oshinski AJ, Keskkula H, Paul DR. *Polymer* 1996;37:4919.
- [8] Kayano Y, Keskkula H, Paul DR. *Polymer* 1997;38:1885.
- [9] Kayano Y, Keskkula H, Paul DR. *Polymer* 1998;39:2835.
- [10] Borggreve RJM, Gaymans RJ, Schuijjer J, Housz JFI. *Polymer* 1987;28:1489.
- [11] Borggreve RJM, Gaymans RJ. *Polymer* 1988;29:1441.
- [12] Borggreve RJM, Gaymans RJ. *Polymer* 1989;30:63.
- [13] Oshinski AJ, Keskkula H, Paul DR. *Polymer* 1996;37:4891.
- [14] Chung I, Throckmorton E, Chunury D. *Soc Plast Engng. ANTEC* 1979;25:681.
- [15] Broberg KB. *Int J Fract* 1968;4:11.
- [16] Mai Y, Powell P. *J Polym Sci Part B: Polym Phys* 1991;29:785.
- [17] Mai Y. *Int J Mech Sci* 1993;35:995.
- [18] Mai Y. *Polymer Commun* 1989;30:330.
- [19] Vu-Khanh T. *Polymer* 1988;29:1979.
- [20] Wildes G, Keskkula H, Paul DR. *Polymer* 1999;40:7089.
- [21] Kudva RA, Keskkula H, Paul DR. *Polymer* 2000;41:335.
- [22] Wu J, Mai Y. *Polym Engng Sci* 1996;36:2275.
- [23] McCrum NG, Buckley CP, Bucknall CB. *Principles of polymer engineering*. Oxford University Press, Oxford. 1988, pp. 194-200.
- [24] Gross B, Srawley JE. Stress-intensity factors for single-edge-notch specimens in bending or combined bending and tension by boundary collocation of a stress function. Technical Note. D-2603, NASA, 1965. p. 8.
- [25] Brown WF, Srawley JE. *ASTM* 410, 1996. p. 13.
- [26] Dijkstra K, Wevers HH, Gaymans RJ. *Polymer* 1994;35:323.
- [27] Adams GC. *Soc Plast Engng ANTEC* 1988;34:1517.
- [28] Okada O, Keskkula H, Paul DR. *Polymer* 2000;41:8061.
- [29] Pressly TG, Keskkula H, Paul DR. *Polymer* 2001;42:3043.
- [30] Santana OO, MasPOCH ML, Martinez AB. *Polym Bull* 1997;39:511.
- [31] Standard test method for plane-strain fracture toughness and strain energy release rate of plastic materials. D5045, ASTM, 1999.
- [32] Laura DM, Keskkula H, Paul DR. *Polymer*
- [33] Wong S-C, Mai Y-W. *Polym Engng Sci* 1999;39:356.
- [34] Williams JG. *Fracture mechanics of polymers*, Wiley, New York, 1984.
- [35] Margolina A, Wu S. *Polymer* 1988;29:2170.

- [36] Laura DM, Keskkula H, Paul DR. *Polymer* 2001;42:6161.
- [37] Oshinski AJ, Keskkula H, Paul DR. *Polymer* 1992;33:268.
- [38] A linear elastic fracture mechanics (LEFM) standard for determining  $K_{IC}$  and  $G_{IC}$  for plastics at high loading rates. FR177,ESIS, 1996.
- [39] McClintock FA, Irwin GR. ASTM 381, 1965, p. 84.
- [40] Hertzberg RW. *Deformation and fracture mechanics of engineering materials*, New York: Wiley, 1996, p. 346.
- [41] Bucknall CB. In: Haward RN, Young RJ, editors. *The physics of glassy polymers*, 2nd ed. London: Chapman & Hall, 1997.
- [42] Bucknall CB. In: Paul DR, Bucknall CB, editors. *Polymer blends*, vol. 2. New York: Wiley, 2000. p. 83-117.

## Chapter 4

### Nylon 6 as a modifier for maleated ethylene-propylene elastomers

#### 4.1 Introduction

A wide range of polymeric materials with elastomeric properties that can be fabricated by melt processing procedures used for thermoplastics, known as thermoplastic elastomers (TPE), have achieved significant commercial importance over the last 20 years or more<sup>1</sup>. One approach to formation of such materials is block copolymerization, where soft and hard segments are appropriately arranged to obtain desirable mechanical behavior; important examples of this type include triblock structures containing styrene/diene<sup>2, 3</sup> segments formed by anionic polymerization and segmented copolymers based on polyester<sup>4-6</sup> or polyurethane<sup>7-13</sup> condensation polymerizations. Another approach involves melt blending of rubbery materials with rigid thermoplastics<sup>5, 6, 8, 13-18</sup>. Thermoplastic elastomers, whether based block copolymers or blends, must contain two polymeric phases that have widely different softening temperatures so that at use temperatures, one phase is rubbery and the other is either glassy or crystalline<sup>3, 9, 10, 14-16, 19, 20</sup>.

In a melt blending approach, it is feasible to use chemical reactivity of the component polymers to achieve TPE materials with controlled morphology and chemical bonding between the matrix and the dispersed phases. Rubber toughening of polyamides with maleated elastomers may serve as a model for this approach<sup>21-23</sup>. In such blends, reaction of the polyamide amine end groups with the grafted maleic anhydride leads to polyamide-rubber graft copolymer via imide linkages which enable the formation of rubber particles of about 0.1 to 0.5  $\mu\text{m}$  in diameter dispersed in the polyamide matrix<sup>24-29</sup>. Control of morphology (particle size or interparticle distance) is key to super tough, rigid materials. By varying the ratio of maleated rubber to polyamide, it should be possible to make fine polyamide particles dispersed in a rubbery matrix. When stressed, the rigid particles should provide some degree of resistance to flow or creep of the elastomer matrix (or physical crosslinking) due to the chemical bonding of these particles to the matrix; such mixtures should approximate TPE behavior since above the polyamide melting point melt processing should also be possible. Within the limits of phase inversion it should be possible to control the stiffness or hardness of such blends by the elastomer/polyamide ratio.

Table 1 Materials used in this work

Polymer	Commercial designation	Characterization <sup>a</sup>	Molecular weight <sup>a</sup>	Brabender torque <sup>b</sup> (N•m)	Source
Nylon 6	Capron 8207F	End-group content: [NH <sub>2</sub> ] = 47.9 μeq g <sup>-1</sup> [COOH] = 43.0 μeq g <sup>-1</sup>	$\bar{M}_n = 22,000$	5.4	AlliedSignal Inc.
Nylon 6	Ultramide B0	End-group content: [NH <sub>2</sub> ] = 74.2 μeq g <sup>-1</sup> [COOH] = 77.0 μeq g <sup>-1</sup>	$\bar{M}_n = 13,200$	2.0	BASF Corp.
EPR-g-MA	Exxelor 1803	43 wt% ethylene 53 wt% propylene 1.14 wt% MA	Not available	8.2	Exxon Chemical Co.

<sup>a</sup> Ref. [27].

<sup>b</sup> Torque value taken after 10 minutes at 240 °C and 60 rpm.

Table 2 The physical properties and particle size of EPR-g-MA/nylon 6 blends

% Nylon 6	Hardness (Shore A)	Modulus at 50% elongation (MPa)	Tensile strength <sup>a</sup> (MPa)	Elongation at break <sup>a</sup> (%)	Set after break <sup>a</sup> (%)	$T_g$ (°C)	$\bar{d}_w$ ( $\mu\text{m}$ )	$\bar{d}_w/\bar{d}_n$
0	48	0.27	0.28	380	42.3	-38.5	-	-
5	49	0.33	0.36	260	24.3	-36.4	0.14	1.27
10	50	0.37	0.41	260	21.2	-35.7	0.17	1.28
15	53	0.47	0.53	220	19.8	-35.3	0.19	1.30
20	55	0.57	0.69	200	18.5	-35.1	0.23	1.43
30	68	1.07	1.20	130	7.2	-35.1	0.23	1.42
40	83	N/A	6.23	30	4.5	-34.3	0.30	1.50

<sup>a</sup> Extension rate = 12.7 cm/min

The morphology and structure-property relationships for thermoplastic elastomers prepared by this approach have been reported by R. C. Thamm et al.<sup>30</sup>, based on graft copolymers of poly(pivalolactone and ethylene/propylene/diene monomer, EPDM, terpolymers. Burlett et al.<sup>31-33</sup> have also reported on elastomer-based alloys with thermoplastic polymers formed via reactive processing. This chapter explores the use of the amine-anhydride reaction to produce TPE materials by melt blending nylon 6 with ethylene-propylene rubber grafted with maleic anhydride, EPR-g-MA. The morphology and the mechanical properties of such blends where nylon 6 is the dispersed phase are described here.

## 4.2 Experimental

Table 1 describes materials used in this study. The rubber type is a commercially available random ethylene/propylene copolymer grafted with maleic anhydride (EPR-g-MA) from Exxon Chemicals designated as Exxelor 1803. This rubber was blended with the nylon 6, Capron 8207F from AlliedSignal, with a medium molecular weight ( $\overline{M}_n=22000$ ) having balanced acid and amine end groups. A low molecular weight nylon 6 ( $\overline{M}_n=13200$ ) with equal acid and amine end groups, Ultramid B0, an experimental material from BASF, was hydrolyzed by two extrusion passes through the single screw extruder at 300°C and 10 rpm without prior drying to reduce its molecular weight and to increase its reactivity. An antioxidant, Irganox 1076, at the level of 0.2 wt% in the EPR-g-MA rubber was used in the blends.

Rheological properties were measured using a Brabender Plasticorder with a 50 cm<sup>3</sup> mixing head and standard rotors operated at 240°C and 60 rpm. Torque was recorded continuously, as a function of mixing time.

The materials were dried before melt blending in a vacuum oven for a minimum of 16 h at 60°C for EPR-g-MA and at 80°C for nylon 6. Blends were prepared by vigorously mixing all components together and extruding twice at 240°C and 40 rpm in a Killion single screw extruder ( $L/D = 30$ ,  $D = 2.54$  cm) outfitted with an intensive mixing head. The blends were injection molded into tensile bars (ASTM D638 Type ) by an Arburg Allrounder injection molding machine.

Shore A hardness was measured with a Pacific Transducer durometer according to ASTM D2240. Stress-strain properties were measured at room temperature by an Instron Testing Machine according to ASTM D412 (1980) using a cross-head speed of from 5.08 cm/min to 50.8 cm/min. The permanent set after break was determined at 10 min after failure of tensile specimens. The hysteresis ratio was calculated from the area between the loading and unloading curve at a cross-head speed of 12.7 cm/min. The Young's modulus was measured from the initial slope of the stress-strain curve at a cross-head speed of 5.08 cm/min.

The dynamic mechanical properties were determined by a Polymer Laboratories DMTA at a frequency of 30 Hz. The temperature range of those measurements was from -100 to 100°C at a heating rate of 3 °C/min.

The morphology of the blends was observed by a JEOL 200 CX transmission electron microscope (TEM) using ultra-thin sections (10 to 20 nm) cryogenically microtomed at -50°C perpendicular to the flow direction of injection molded bars. The nylon 6 phase was stained by exposure of the thin sections to a 2% aqueous solution of phosphotungstic acid, PTA, for 30 min at room temperature. The TEM was operated at an accelerating voltage of 120 kV. Nylon 6 particle size was determined by a semi-automatic digital analysis technique using IMAGE® software from the National Institutes of Health.

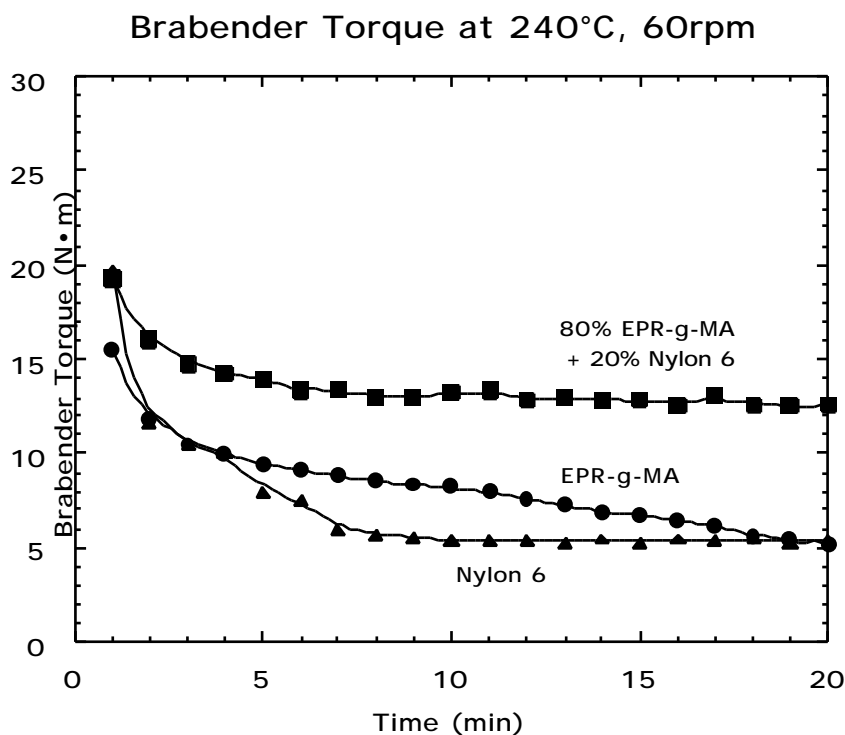


Fig. 1. Brabender torque response at 240°C and 60 rpm for nylon 6, EPR-g-MA and 80% EPR-g-MA / 20% nylon 6 blend.

### 4.3 Morphology

The grafting of nylon 6 to EPR-g-MA causes changes in rheological behavior which can be monitored during melt blending in a Brabender mixer. Fig. 1 shows that while nylon 6 and EPR-g-MA have relatively similar melt viscosities at 240°C, the 80/20 blend of EPR-g-MA/nylon 6 develops a torque of more than twice that of the individual blend components. It is apparent that the reaction between the two components is very rapid, since the high torque of the blend is established early in the experiment while the charge to the Brabender begins to be heated and fluxed.

The graft copolymer formed in situ by the reaction of the nylon 6 amine end groups with maleic anhydride in EPR-g-MA acts as a compatibilizer that leads to a very fine dispersion of the nylon 6 phase in the rubber matrix largely by limiting the frequency of particle-particle coalescence. In addition, the presence of the rubber/polyamide graft copolymer at the domain interfaces results in chemical bonding of the nylon 6 particles to the rubber matrix. The result should be a material with stable morphology and good adhesion between the hard and soft phases<sup>34-36</sup>.

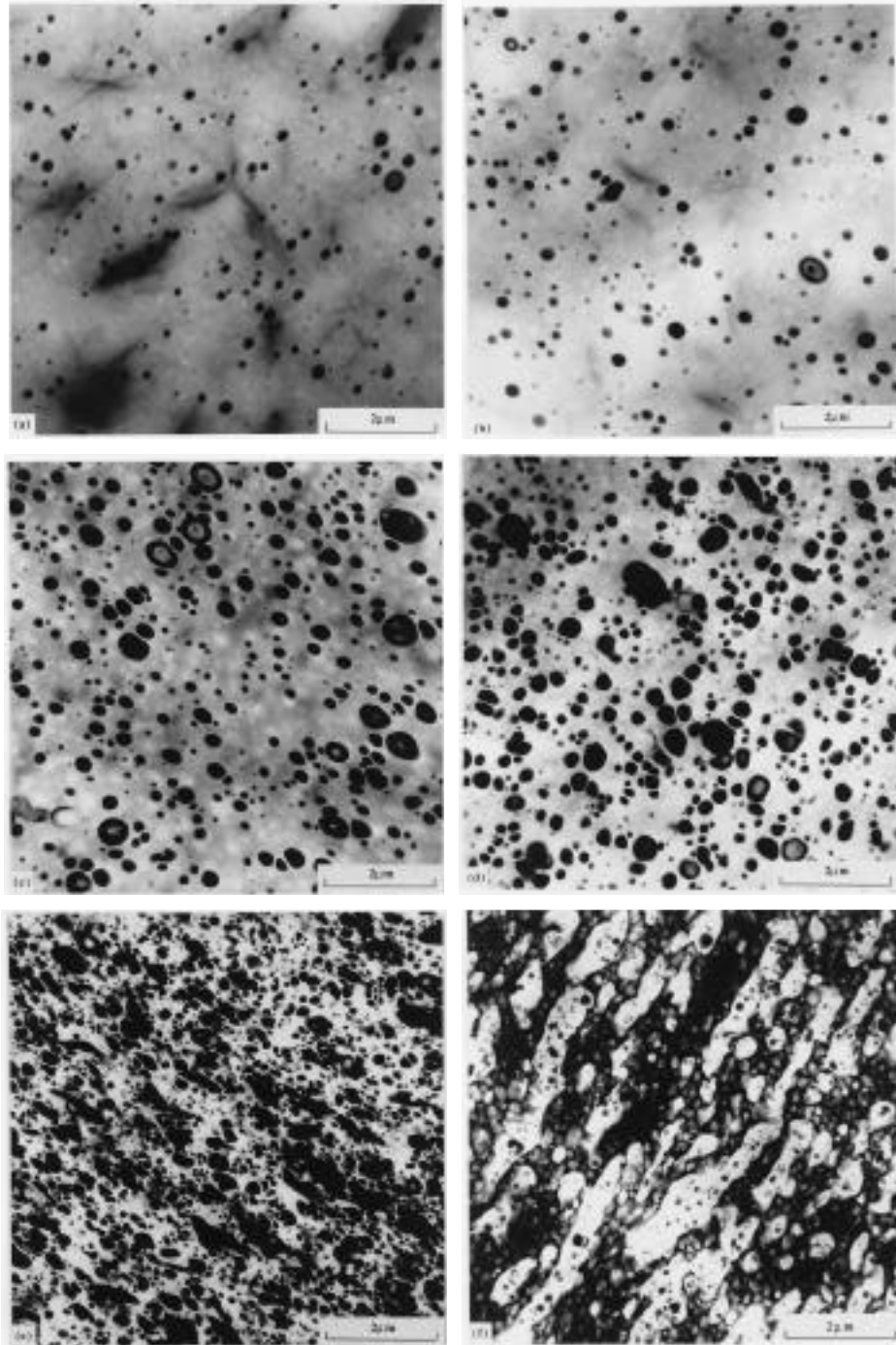


Fig. 2. TEM photomicrographs of blends of x% nylon 6 and (100-x)% EPR-g-MA: (a) x = 5, (b) x = 10, (c) x = 20, (d) x = 30, (e) x = 40, and (f) x = 50%.

Fig. 2 shows the morphology of blends containing 5 to 50% nylon 6 in EPR-g-MA. The samples for microscopy were taken from the center of injection molded test bars across the flow direction. The nylon 6 particle size and size distribution are shown in Table 2 and Fig. 3. Some increase in particle size is noted as the nylon 6 content is increased from 5 to 30%. At 40% nylon 6, the polyamide particles are elongated with evidence of co-continuity of the phases; at 50% nylon 6 this is more obvious. At 60% nylon 6, the phase inversion is complete and EPR-g-MA is now the dispersed phase within the nylon 6 matrix.

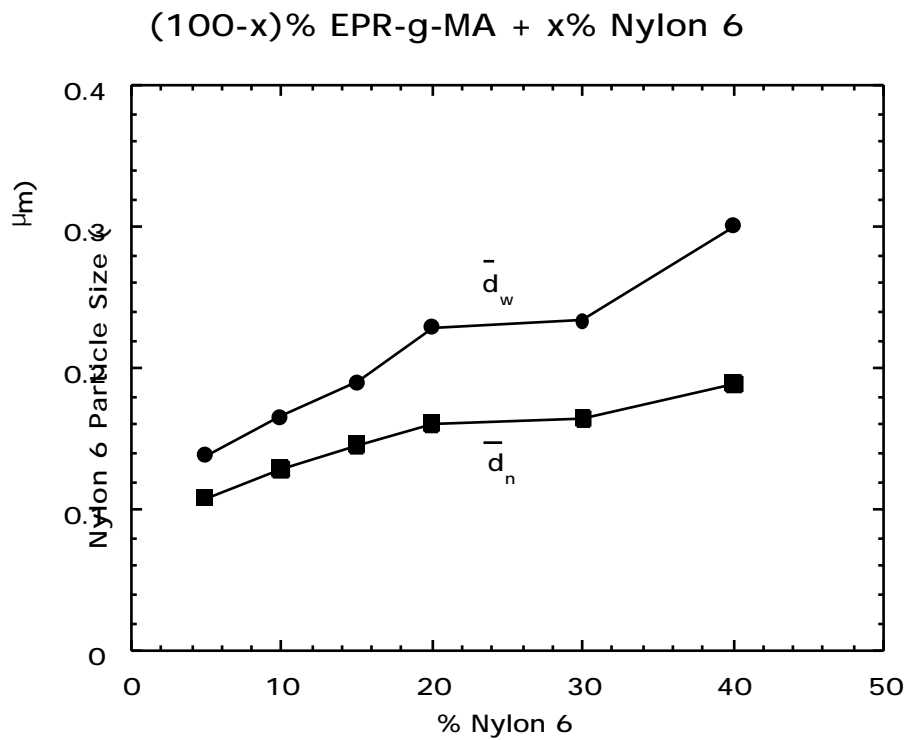


Fig. 3. Effect of nylon 6 content on weight and number average nylon 6 particle diameter for blends of (100-x)% EPR-g-MA and x% nylon 6.

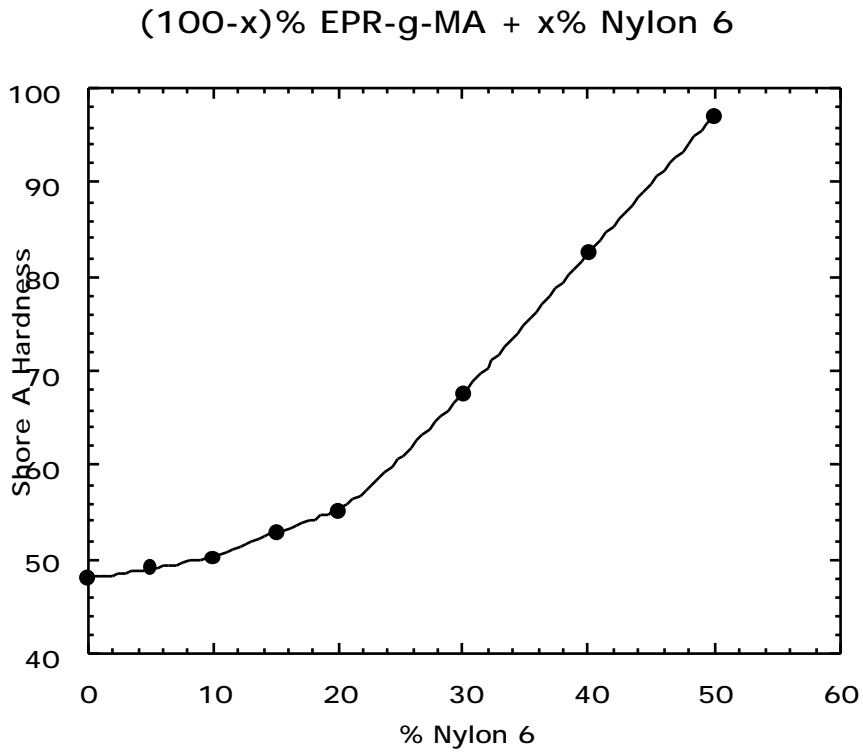


Fig. 4. Effect of nylon 6 content on Shore A hardness for blends of (100-x)% EPR-g-MA and x% nylon 6.

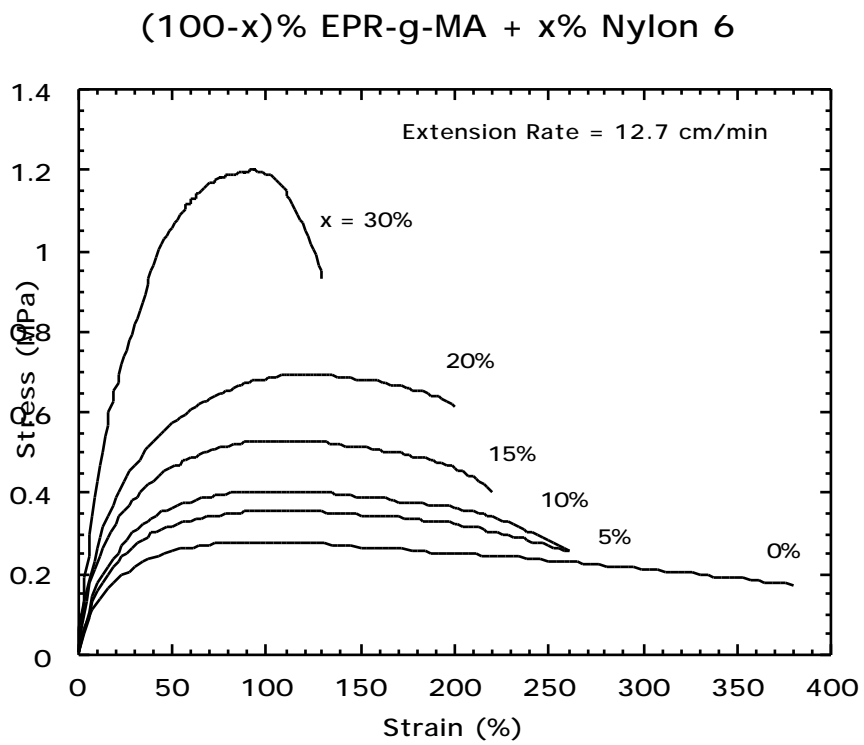


Fig. 5. Stress-strain properties for blends of (100-x)% EPR-g-MA and x% nylon 6.

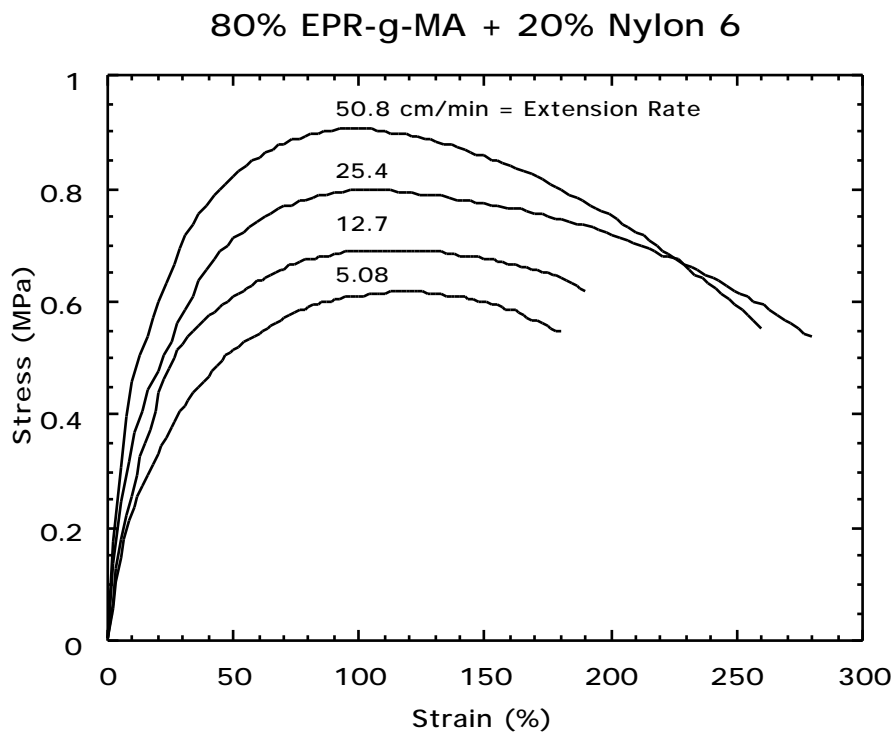


Fig. 6. Stress-strain diagrams for blends of 80% EPR-g-MA and 20% nylon 6 at various extension rates.

#### 4.4 Mechanical properties

The Shore A hardness of these blends increases steadily with nylon 6 content, as seen in Fig. 4. The increase is rather modest up to 16.5 vol% (20 wt%) of nylon 6 and then becomes more dramatic.

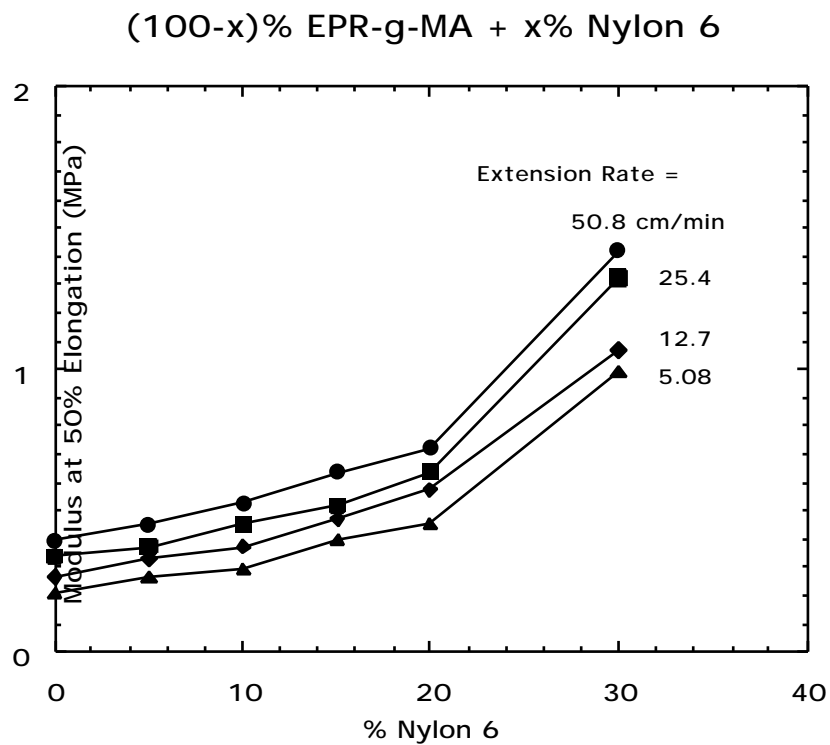


Fig. 7. Effect of nylon 6 content on the secant modulus (50% elongation) at various extension rates for blends of (100-x)% EPR-g-MA and x% nylon 6.

Typical stress-strain curves for the blends are shown in Fig. 5; selected properties are summarized in Table 2. These results were obtained at a cross-head speed of 12.7 cm/min; results for other testing speeds from 5 to 51 cm/min are shown in Fig. 6 for a blend containing 20% nylon 6. These data indicate an increase in the peak stress of about 30% and a shift in the stress peak to a slightly lower extension (from about 120 to 100%) as the rate of extension is increased from 5 to 51 cm/min. The two highest extension rates give rise to the highest failure elongations. Fig. 7 shows that for all blends the modulus increases noticeably as the testing speed increases.

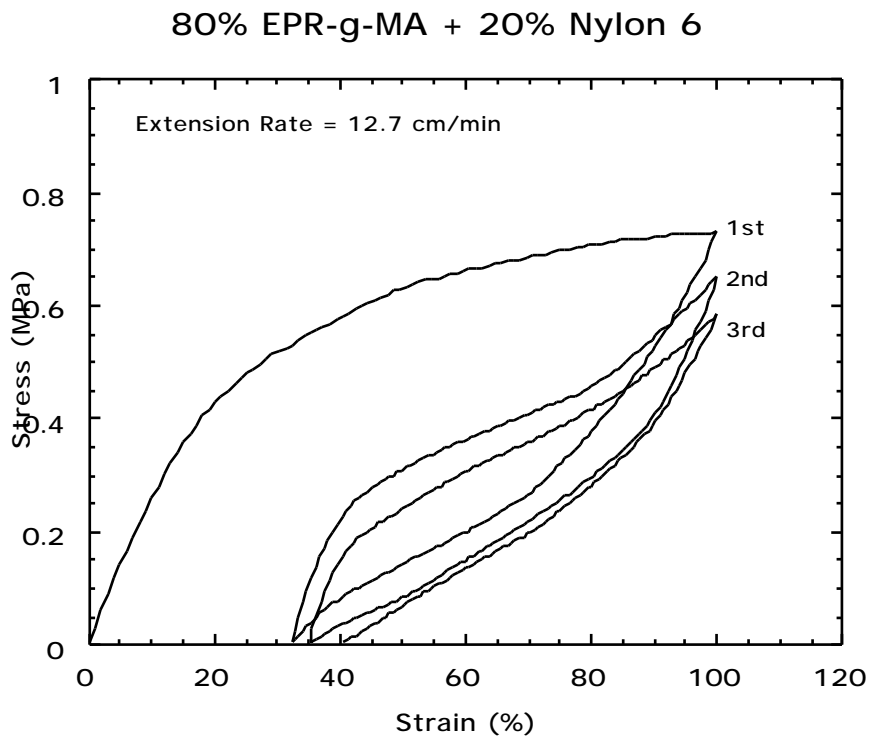


Fig. 8. Cyclic stress-strain behavior for blends of 80% EPR-g-MA and 20% nylon 6.

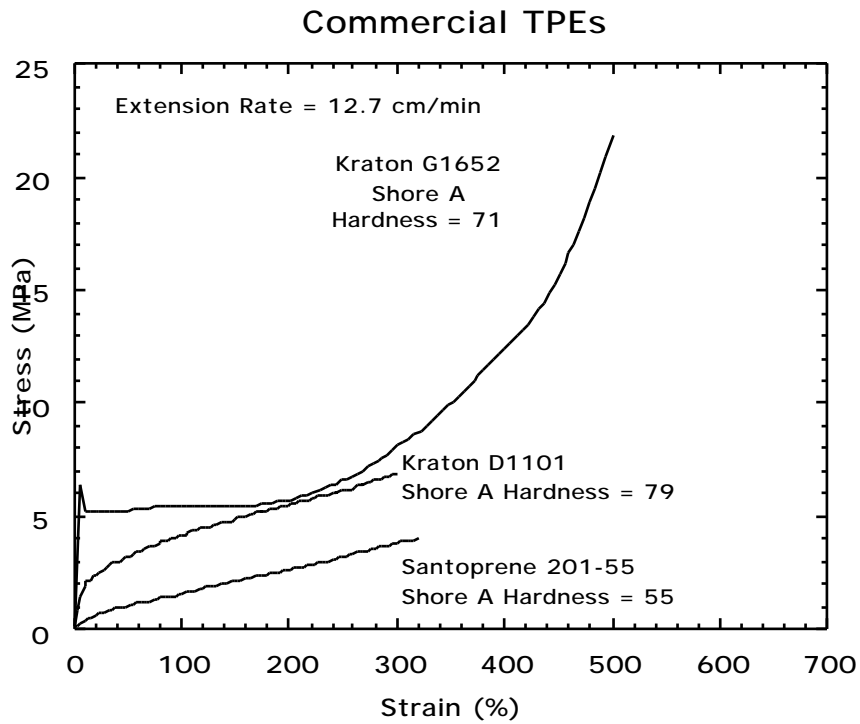


Fig. 9. Stress-strain properties for three commercial TPE materials.

Table 3 The physical properties and particle size of EPR-g-MA/nylon 6 blends

Composition	Hardness (Shore A)	Modulus at 50% elongation <sup>a</sup> (MPa)	Maximum strength <sup>a</sup> (MPa)	Elongation at break <sup>a</sup> (%)	Set after break <sup>a</sup> (%)	Hysteresis loss <sup>a</sup> (%)	$\bar{d}_w$ ( $\mu\text{m}$ )	$T_g$ ( $^{\circ}\text{C}$ )
100% EPR-g-MA	48	0.27	0.28	380	42.3	66.4	-	-38.5
80% EPR-g-MA + 20% nylon 6	55	0.57	0.69	200	18.5	65.4	0.23	-35.1
80% EPR-g-MA + 20% hydrolyzed nylon 6	55	0.63	0.84	190	17.9	66.0	0.15	-35.8
78.8% EPR-g-MA + 20% nylon 6 + 1.2% MgO	60	1.40	1.79	140	6.5	64.5	0.12	-34.5

<sup>a</sup> Extension rate = 12.7 cm/min

Table 4 Conditions for nylon 6 hydrolysis in a single screw extruder and resulting Brabender torque data

Material	Conditions of raw nylon 6 before extrusion		Extrusion temperature (°C)	Extruder (rpm)	Torque after 10 min (N•m)	$\bar{M}_n$
	Form of nylon	Drying				
Capron 8207F <sup>a</sup>	Granules	Yes	-	-	5.4	22000
Ultramide BO <sup>a</sup>	Granules	Yes	-	-	2.0	13200
Ultramide B0 <sup>b</sup>	Powder	No	300	10	1.3	11000 <sup>c</sup>

<sup>a</sup> Pellets dried before Brabender experiment.

<sup>b</sup> Water content = 4.2 wt%.

<sup>c</sup> Molecular weight value estimated from Brabender torque/molecular weight relationship [27].

The hysteresis loss,  $H$ , is given by

$$H = (W - W_r) / W$$

where  $W$  is the area under the first loading curve up to a particular strain (100%) and  $W_r$  is the corresponding area under the unloading curve<sup>37</sup>. The hysteresis behavior for a maximum strain of 100% strain is shown in Fig. 8 for an 80/20 EPR-g-MA/nylon 6 blend. The calculated hysteresis losses for this and other blends are given in Table 3. A hysteresis loss of 66% was determined for EPR-g-MA without any nylon 6 additive; incorporation of 20% nylon 6 does not significantly alter this measure of the mechanical loss process under the conditions used in this work.

Permanent set after break was found to be more or less independent of testing speed. As seen in Table 2, the addition of even small amounts of nylon 6 reduces the permanent set; it is substantially constant at about 20% for compositions containing 5-20% nylon 6 but drops to quite low levels for blends containing 30-40% nylon 6.

Fig. 9 shows typical stress-strain curves for three commercial TPE materials; a styrene-butadiene-styrene triblock, SBS (Kraton D1101), a styrene-hydrogenated butadiene-styrene triblock, SEBS (Kraton G1652) and a dynamically vulcanized polypropylene/ethylene-propylene rubber blend, Santoprene, having Shore A hardness values of 79, 71 and 55, respectively. Kraton G1652 shows a yield point at 10% elongation and a drawing process from 20% to 200% elongation. From 200% elongation to fracture, significant work hardening is observed<sup>20, 38</sup>. The other materials showed no yield point, but a steady increase in stress before fracture. Both SBS and SEBS materials exhibit higher tensile strength than the Santoprene material. As seen from Table 2, these commercial TPE materials have higher Shore A hardness values than the typical 20% nylon 6 and 80% EPR-g-MA blends examined in this study.

As seen from comparison of stress-strain properties of the commercial TPE materials with the various blends of EPR-g-MA and nylon 6 (see Figs. 5 and 9), the latter have lower strength and exhibit stress softening which was not seen for any of the commercial TPE materials. Compared to the hard phases in triblock copolymer or dynamically vulcanized TPE materials, the nylon 6 phase is much less effective for reinforcing (stiffen or strengthen) the EPR-g-MA matrix or providing effective crosslinking to retard its viscoelastic relaxation during stress-strain testing.

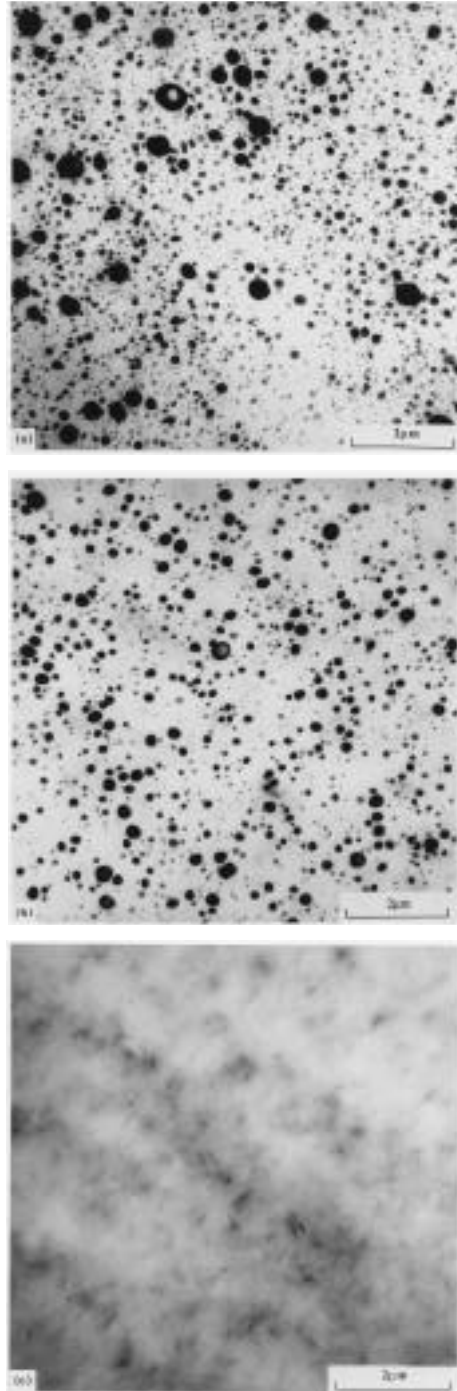


Fig. 10. TEM photomicrographs for: (a) blends of 80% EPR-g-MA and 20% hydrolyzed nylon 6; (b) blend of 78.8% EPR-g-MA and 20% nylon 6 containing 1.2% MgO, stained with phosphotungstic acid and (c) without staining.

Such behavior should be improved by having a greater number of chemical attachments between EPR-g-MA and nylon 6, and this can be achieved, in principle, by using a lower molecular weight of nylon 6<sup>39</sup>. Calculations show that two nylon 6 grafts per EPR-g-MA molecule would be theoretically possible when the  $\overline{M}_n$  of nylon 6 is less than 7000. There is no convenient source of such low molecular weight nylon 6 materials, so another approach was attempted. Ultramide B0 is a very low molecular weight nylon 6 but

its  $\overline{M}_n$  is about twice the target value; one hydrolysis reaction per chain of this polymer should produce the desired level of amine functionality. In an attempt to obtain such a low  $\overline{M}_n$  nylon 6, Ultramide B0 containing approximately 4.2% water was extruded twice at 300°C through a single screw extruder to effect hydrolysis<sup>39-44</sup>. As seen in Table 4, this procedure does lead to reduction of the nylon 6 molecular weight but not fully to the target value. Blends of this very low molecular weight nylon 6, produced by hydrolysis, with EPR-g-MA were prepared. These blends have a significantly reduced dispersed phase particle size (0.15 versus 0.23  $\mu\text{m}$  for blends based on Capron 8207F); see Fig. 10. As seen in Fig. 11, blends based on the hydrolyzed nylon 6 do have somewhat improved tensile properties; however, their properties are still far below those of the other TPE materials whose stress-strain characteristics are shown in Fig. 9.

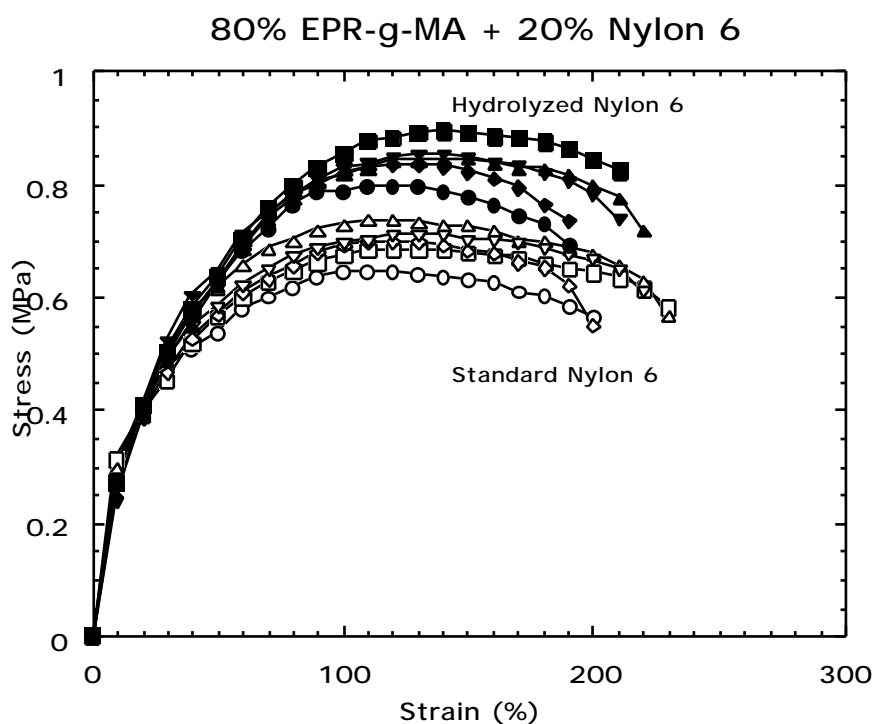


Fig. 11. Stress-strain curves for various individual samples of 80% EPR-g-MA and 20% nylon 6 blends showing difference between standard (open symbols) and hydrolyzed (solid symbols) nylon 6.

The addition of magnesium oxide to these blends was examined as another means to improve their mechanical performance. It has been reported that the addition of a small amount of MgO is effective for crosslinking in methacrylic acid containing elastomers [45, 46]. Because of the carboxylic acid end-groups in nylon 6 and possibly some free acid groups in EPR-g-MA, this approach was considered to be potentially useful for improving the tensile properties of these blends.

80% EPR-g-MA + (20-x)% Nylon 6 + x% MgO

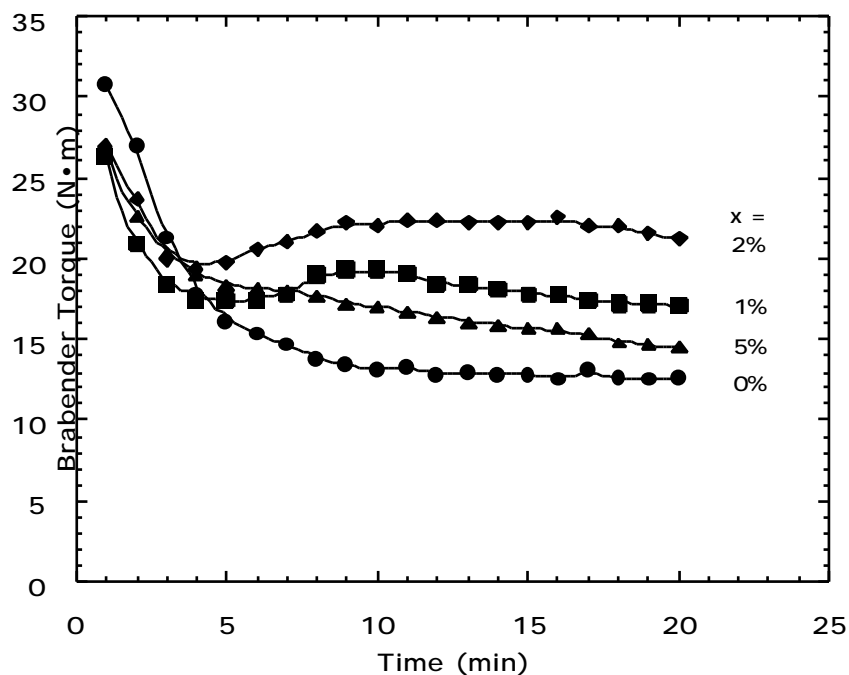


Fig. 12. Brabender torque response for blends of 80% EPR-g-MA and (20-x)% nylon 6 containing x% MgO.

Fig. 10(b) shows the effect of 1.2% MgO on the 80/20 EPR-g-MA/nylon 6 blend. Addition of MgO clearly contributes to reducing the particle size of nylon 6 domains (see Table 3) as found with the use of the hydrolyzed nylon 6. In Fig. 10(c), non-stained TEM photomicrographs show very small particles of MgO in this blend.

Fig. 12 shows that addition of MgO increases the melt viscosity of these blends as indicated by Brabender torque rheometry. A maximum effect is achieved at a loading level of 2% which gives rise to almost a two-fold increase in torque at 10 min. Torque rheometer data in Fig. 13 indicate that the addition of MgO to the other components of these blends shows no significant effect. Fig. 13(a) shows that the addition of MgO to the unmaleated EPR and its blend with nylon 6 has no effect on the torque response. Also, the effect of MgO on the blends with both of the elastomer components, i.e. EPR and EPR-g-MA is negligible (Fig. 13(b)). The lack of torque increases when MgO is added to EPR-g-MA is rather surprising in light of the data shown in Fig. 12. It implies the presence of some chemical synergism when the three principal blend components are melt blended together. No further explanation for this effect can be given at this time. As seen in Fig. 13(c), there is no effect on the torque response when MgO is melt blended with nylon 6. The fact that a torque increase is not seen on the addition of MgO to either EPR-g-MA or nylon 6 may be due to the relative absence of water in these experiments or some presence of trace of moisture in the ternary blends that do show a torque increase.

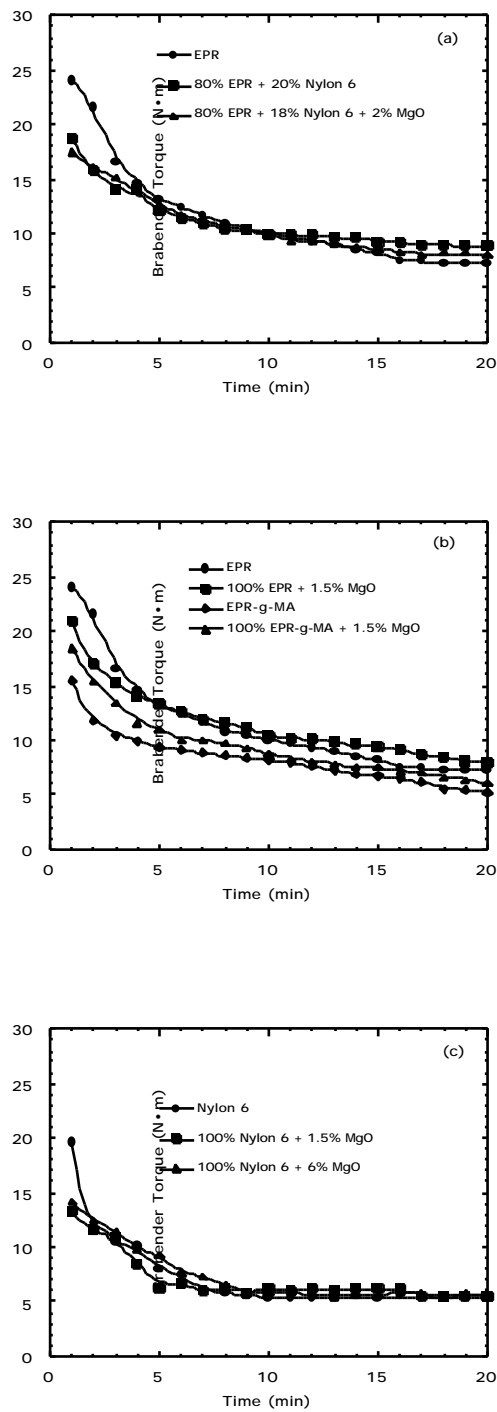


Fig. 13. Brabender torque response for: (a) blends of non-maleated EPR and nylon 6 with and without MgO; (b) mixtures of non-maleated EPR with MgO and EPR-g-MA with MgO; and (c) mixtures of nylon 6 and MgO.

The addition of small amounts of magnesium oxide to the blends causes significant improvement in tensile properties, as seen in Fig. 14. The maximum stress at 100% strain for the blend with 1.2% by weight MgO is more than twice that of the corresponding blend without MgO. However, the strength is still significantly less than that of Kraton and Santoprene materials, and there is no work hardening before ultimate fracture. It is

(100-x-y)% EPR-g-MA + x% Nylon 6 + y% MgO

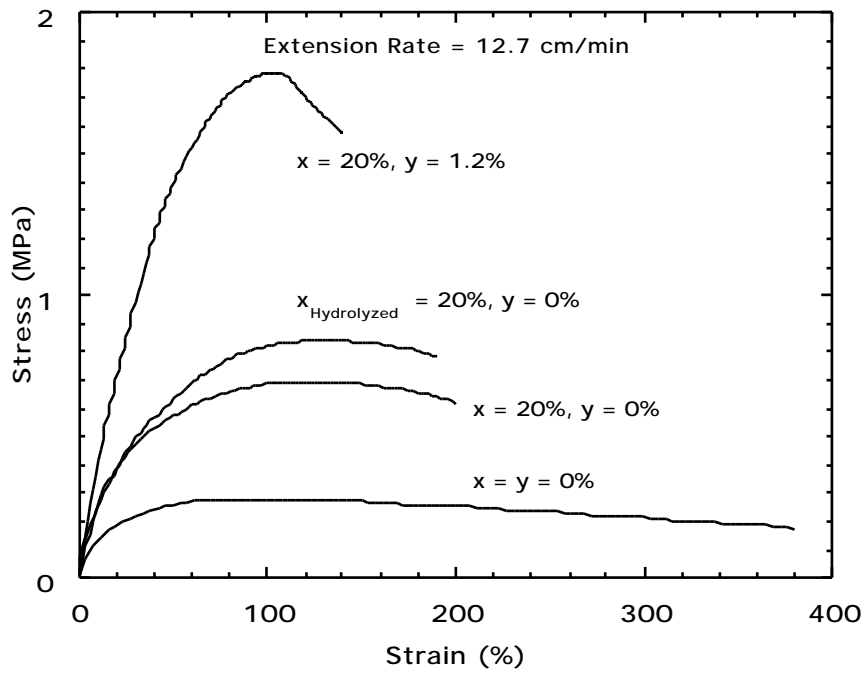


Fig. 14. Stress-strain properties for blends of (100-x-y)% EPR-g-MA/x% nylon 6/y% MgO.

78.8% EPR-g-MA + 20% Nylon 6 + 1.2% MgO

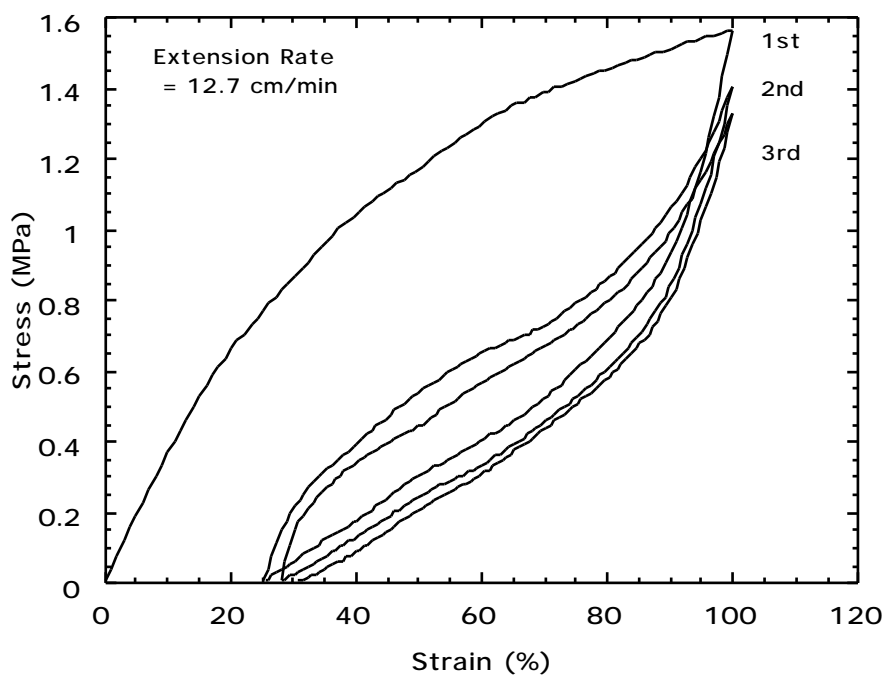


Fig. 15. Cyclic stress-strain behavior of blends of 78.8% EPR-g-MA, 20% nylon 6 and 1.2% MgO.

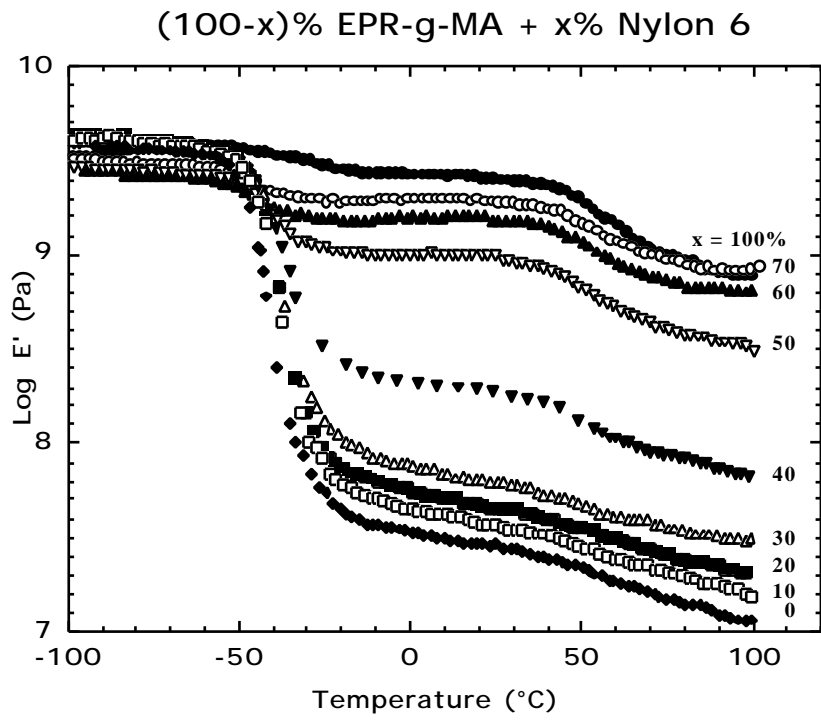


Fig. 16. Dynamic storage modulus for blends of (100-x)% EPR-g-MA and x% nylon 6.

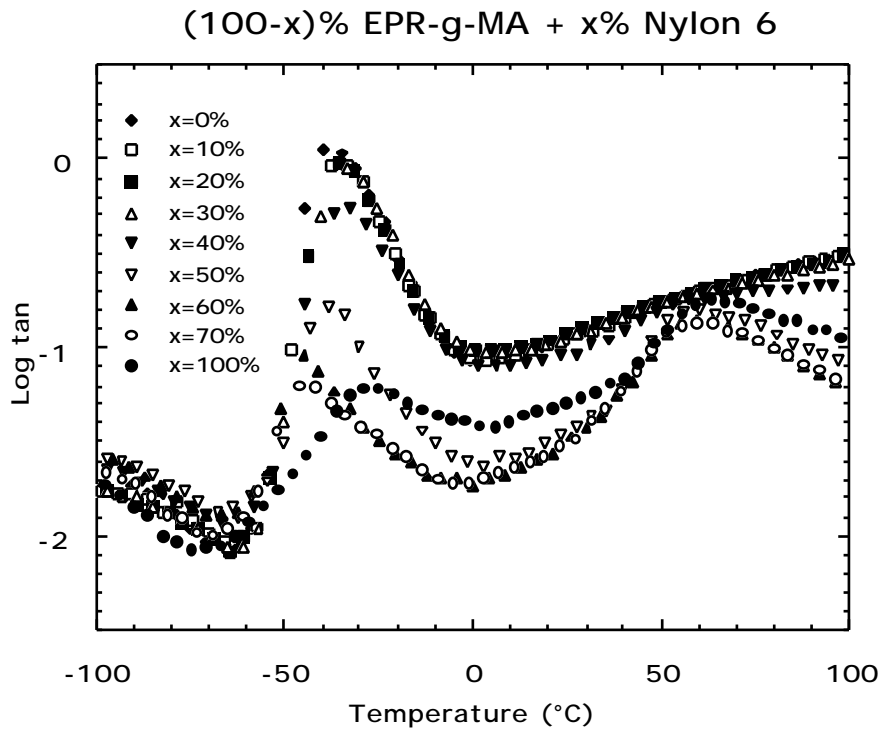


Fig. 17. Tan curves for blends of (100-x)% EPR-g-MA and x% nylon 6.

suggested that the smaller nylon 6 particle size in these blends is caused by the increase of melt viscosity resulting from the presence of MgO which may lead to more grafting of nylon 6 to the EPR-g-MA. Together, these effects give rise to the improvement of the tensile properties of the blends of EPR-g-MA and nylon 6.

The hysteresis loss at a strain of 100% for the 78.8/20/1.2 EPR-g-MA/nylon 6/MgO blends is shown in Fig. 15 and Table 3. In spite of the increased stress caused by MgO, the hysteresis loss is substantially the same at about 65% for both compositions.

#### 4.5 Dynamic mechanical properties

Blends of EPR-g-MA with nylon 6 over the entire composition range were characterized by measuring the dynamic mechanical properties at 30 Hz. The storage modulus,  $E'$ , is shown as a function of temperature in Fig. 16; results for blends based on the hydrolyzed nylon 6 and those containing MgO are substantially the same as for the standard EPR-g-MA/nylon 6 blends. Loss tangent,  $\tan \delta$ , data are shown in Fig. 17. Two interesting trends deserve mention. First, as the nylon 6 content in the EPR-g-MA matrix increases from 0 to 40%, there is a decrease in magnitude of the rubber  $\tan \delta$  peak and a small increase in the temperature where this peak occurs (see  $T_g$  column in Table 2); over this range the dispersed nylon 6 phase particle size increases from 0.14 to 0.30  $\mu\text{m}$ . Second, for compositions in the regions of phase inversion but where the rubber is the dispersed phase, the rubber phase  $\tan \delta$  peak is more typical of that for rubber toughened polymers such as ABS<sup>47-50</sup>. In styrene/acrylonitrile grafted polybutadiene rubbers the  $T_g$  of the grafted rubber is lower than that of the ungrafted rubber. In the current blends, the rubber phase  $T_g$  drops from -38 at 50% EPR-g-MA to -42°C at 30% EPR-g-MA. The rubber phase  $T_g$  peaks for the blends based on the hydrolyzed nylon 6 and the blends containing MgO are almost the same as those of the blends shown.

#### 4.6 Modeling of modulus data

Experimental values of the tensile modulus,  $E$ , from stress-strain testing at 5.08 cm/min (Fig. 18(a)) and the storage modulus,  $E'$ , from dynamic mechanical measurements (Fig. 18(b)) are shown for blends encompassing the whole composition range. These data represent compositions where there are nylon 6 particles in the EPR-g-MA matrix, continuing through the phase inversion to compositions where the EPR-g-MA particles are dispersed in the nylon 6 matrix. Equations for composite materials by Kerner<sup>51</sup>, Faucher<sup>52</sup>, and Hill<sup>53</sup> were considered for modeling these experimental results. Additional approaches for predicting elastic moduli for blends of hard and soft polymers phases have been reported [54]. The self-consistent theory proposed by Hill appears to give the best

representation of the current experimental data and is probably the most sound from a mathematical point of view<sup>54</sup>. This model has the form

$$\frac{{}_1K_1}{K_1 + \frac{4}{3}G} + \frac{{}_2K_2}{K_2 + \frac{4}{3}G} + 5 \frac{{}_1G_2}{G - G_2} + \frac{{}_2G_1}{G - G_1} + 2 = 0 \quad (1)$$

where  $K$  is the bulk modulus and  $G$  is the shear modulus of the blend, while the corresponding component elastic properties of each component have the appropriate subscript and  $v_i$  is the volume fraction of component  $i$ .

Standard relations of elastic theory are used to relate the tensile modulus,  $E_i$ , to the bulk,  $K_i$ , and shear,  $G_i$ , moduli of each component (or the blend) via Poisson's ratio,  $\nu_i$ ,

$$K_i = \frac{E_i}{3(1 - 2\nu_i)} \quad \text{and} \quad G_i = \frac{E_i}{2(1 + \nu_i)} \quad (2)$$

Poisson's ratio was assumed to be 0.49 for EPR-g-MA and 0.33 for nylon 6<sup>55</sup> and to be a linear function of composition for the blends. The solid lines shown in Fig. 18(a) and (b) were calculated using Hill's theory. As it turns out, the calculated results for the blends are quite insensitive to the assumption about the composition dependence of Poisson's ratio.

Quite similar results were calculated by assuming  $\nu = 0.49$  for all blends where the rubber is in the continuous phase and  $\nu = 0.33$  for all blends where nylon 6 is continuous phase. The values for the dynamic storage modulus  $E'$  are essentially the same as those for tensile modulus  $E$  measured in stress-strain tests when nylon 6 forms the matrix. However, the values of  $E$  are noticeably smaller than the corresponding  $E'$  value<sup>56</sup> in blends where the rubber phase is the matrix. It is interesting to note that the experimental points from the dynamic measurements agree better with the calculated curve up to about 35 vol% of nylon 6 than those of the stress-strain measurements. This range corresponds to blends where nylon 6 is dispersed as discrete particles in EPR-g-MA. Beyond phase inversion, where rubber particles are dispersed in the nylon 6 matrix, a larger deviation from the calculated values is apparent in both measurements. The largest deviation in both cases occurs for compositions in the phase inversion region. As this model does not consider the phase inversion issue, there is no appropriate way to deal with the deviations of calculated modulus values from the experimental ones in the phase inversion region.

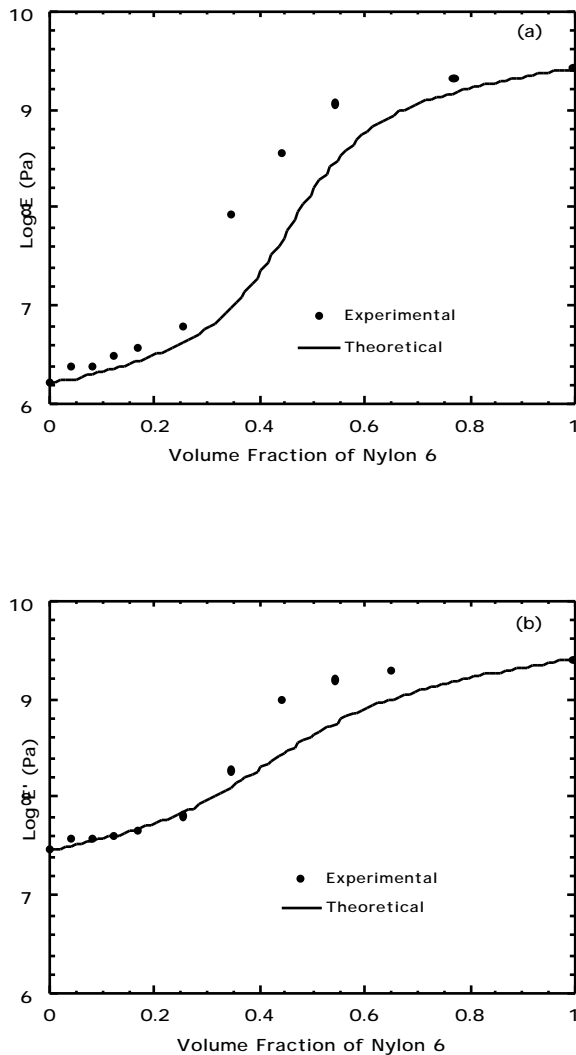


Fig. 18. Effect of nylon 6 content on: (a) Young's modulus,  $E$ , from stress-strain measurement and (b) dynamic storage modulus,  $E'$ , for blends of (100-x) vol% EPR-g-MA and x vol% nylon 6.

#### 4.7 Conclusions

The morphology and physical properties of blends of nylon 6 and EPR-g-MA have been examined. As the content of nylon 6 is increased from 5 to 30%, the average size of the dispersed nylon 6 particles in the matrix of EPR-g-MA increased from 0.14 to 0.23  $\mu\text{m}$ , while the hardness, modulus and tensile strength of the blend increased. The observed values of the modulus are in reasonable agreement with those predicted by a theoretical model. As the content of nylon 6 is increased from 30 to 50%, the physical properties of the blends change rapidly, due to phase inversion, i.e., the polyamide becomes the continuous phase with spherical, dispersed particles of EPR-g-MA.

The blends with an EPR-g-MA continuous phase have lower strength than commercial thermoplastic elastomers or TPE materials and show stress softening which indicates that the nylon 6 phase does not strongly reinforce the EPR-g-MA matrix. The blends based on a nylon 6 with reduced molecular weight made by a hydrolysis process showed somewhat improved strength and a reduced nylon particle size. The addition of magnesium oxide to these blends causes significant improvement in tensile properties. This may be the result of the reduced particle size caused by the increase in melt viscosity or the formation of ionic cluster type crosslinks.

## References

1. Legge, N. R., Holden, G. and Schroeder, H. E., Eds., 'Thermoplastic Elastomers: A Comprehensive Review' Hanser Publishers, New York, 1987
2. Holden, G. and Legge, N. R., in Ref. 1, pp. 47-65
3. Morton, M. *Rubber Chem. Techn.* 1983, **56**, 1096
4. Cella, R. J. *J. Polym. Sci. : Symp.* 1973, **42**, 727
5. Wells, S. C., Ed., 'Handbook of Thermoplastic Elastomers' Van Nostrand Reinhold, New York, 1979, pp. 103-215
6. Wood, A. S. *Modern Plastics* 1985, **62 (3)**, 42
7. Bonart, R. *Angew. Makromol. Chem.* 1977, **58/59**, 259
8. Bonk, H. W., in 'Modern Plastics Encyclopedia 1984-85', Agranoff, J., Ed., McGraw-Hill, Inc., New York, 1985, p. 100
9. Cooper, S. L., Huh, D. S. and Morris, W. J. *Ind. Eng. Chem. Prod. Res. Develop.* 1968, **7**, 248
10. Puett, D. *J. Polym. Sci., A-2* 1967, **5**, 839
11. Samuels, S. L. and Wilkes, G. L. *J. Polym. Sci. : Symp.* 1973, **43**, 149
12. Walker, B. M., Ed., 'Handbook of Thermoplastic Elastomers' Van Nostrand Reinhold, New York, 1979
13. Wolkenbreit, S., in Ref. 12, pp. 216-246
14. Puett, D., Smith, K. J. J., Ciferri, A. and Kontos, E. G. *J. Chem. Phys.* 1964, **40**, 253
15. Puett, D., Smith, K. J. and Ciferri, A. *J. Chem. Phys.* 1965, **69**, 141
16. Coran, A. Y., Patel, R. P. and Williams, D. *Rubber Chem. Techn.* 1982, **55**, 116
17. Rader, C. P., in 'Handbook of Plastics, Elastomers, and Composites', Harper, C. A., Ed, McGraw-Hill, New York, 1996, pp. 5.1
18. Jha, A. and Bhowmick, A. K. *Polymer* 1997, **38**, 4337
19. Lilaonitkul, A., West, J. C. and Cooper, S. L. *J. Macromol. Sci. Phys.* 1976, **B12**, 563
20. Beecher, J. F., Marker, L., Bradford, R. D. and Aggarwal, S. L. *Am. Chem. Soc., Polymer Preprints* 1967, **8**, 1532
21. Gaymans, R. J., in 'Rubber Toughened Engineering Plastics', Collyer, A. A., Ed., Chapman & Hall, London, 1994, pp. 210-242
22. Keskkula, H. and Paul, D. R., in Ref. 21, pp. 136-164
23. Borggreve, R. J. M., Gaymans, R. J., Schuijjer, J. and Housz, J. F. I. *Polymer* 1987, **28**, 1489
24. Oshinski, A. J., Keskkula, H. and Paul, D. R. *Polymer* 1992, **33**, 268
25. Oshinski, A. J., Keskkula, H. and Paul, D. R. *Polymer* 1992, **33**, 284
26. Oshinski, A. J., Keskkula, H. and Paul, D. R. *J. Appl. Polym. Sci.* 1996, **61**, 623

27. Oshinski, A. J., Keskkula, H. and Paul, D. R. *Polymer* 1996, **37**, 4891
28. Oshinski, A. J., Keskkula, H. and Paul, D. R. *Polymer* 1996, **37**, 4909
29. Oshinski, A. J., Keskkula, H. and Paul, D. R. *Polymer* 1996, **37**, 4919
30. Thamm, R. C. and Buck, W. H. *J. Polym. Sci., Polym. Chem. Ed.* 1978, **16**, 539
31. Burlett, D. J., Bauer, R. G. and Kelley, M. M. US Pat. 5,023,301 1991 (assigned to The Goodyear Tire & Rubber Company)
32. Burlett, D. J., Pyle, K. J., Sinsky, M. S., Bauer, R. G., Tung, D. A. and Parameswaran, V. R. US Pat. 5,268,134 1993 (assigned to The Goodyear Tire & Rubber Company)
33. Burlett, D. J. Proceedings of Intersociety Polymer Conference, 1995, Baltimore,
34. Frazer, W. J. *Chem. Ind.* 1966, **33**, 1399
35. Haward, R. N. and Mann, J. *Proc. Phys. Soc.* 1964, **A282**, 120
36. Keskkula, H. *Appl. Polym. Symp.* 1970, **15**, 51
37. Andrews, E. H. and Fukahori, Y. *J. Mater. Sci.* 1977, **12**, 1307
38. Beecher, J. F., Marker, L. and Bradford, R. D. *J. Polym. Sci., Part C* 1969, **26**, 117
39. Kohan, M. I., Ed, 'Nylon Plastics Handbook' Hanser Publishers, New York, 1995
40. Paterson, M. W. A., White, J. R. *J. Mater. Sci.* 1992, **27**, 6229
41. Paterson, M. W. A. and White, J. R. *Polym. Eng. Sci.* 1993, **33**, 1475
42. Pezzin, G. *J. Appl. Polym. Sci.* 1964, **8**, 2195
43. Russel, D. P. and Beaumont, P. W. R. *J. Mater. Sci.* 1980, **15**, 208
44. Russel, D. P. and Beaumont, P. W. R. *J. Mater. Sci.* 1980, **15**, 197
45. Keskkula, H. Ph. D. Dissertation, University of Cincinnati, 1953
46. Coran AY, Endter CK. US Patent 4,661,554, 1987 (assigned to Monsanto).
47. Morbitzer, L., Ott, K. H., Schuster, H. and Kranz, D. *Angew. Makromol. Chem.* 1972, **27**, 57
48. Morbitzer, L., Kranz, D., Humme, G. and Ott, K. H. *J. Appl. Polym. Sci.* 1976, **20**, 2691
49. Beck, R. H., Gratch, S., Newman, S. and Rusch, K. C. *J. Polym. Sci., Polym. Lett.* 1968, **6**, 707
50. Wang, T. T. and Sharpe, L. H. *J. Adhesion* 1969, **1**, 69
51. Kerner, E. H. *Proc. Phys. Soc.* 1956, **69B**, 808
52. Faucher, J. A. *J. Polym. Sci.: Polym. Phys. Ed.* 1974, **12**, 2153
53. Hill, R. *J. Mech. Phys. Solids* 1965, **13**, 213
54. Coran AY, Patel R. *J Appl Polym Sci* 1976;29:3005.
55. Bucknall, C. B. 'Toughened Plastics', Applied Science Publishers, London, 1977, p. 118

56. Brandrup, J. and Immergut, E. H., Eds., 'Polymer Handbook' 3rd Edition, John Wiley & Sons, New York, 1989, p. V/113
57. Uemura, S. and Takayanagi, M. *J. Appl. Polym. Sci.* 1966, **10**, 113

## **Chapter 5**

### **Mechanical properties of blends of maleated ethylene-propylene rubber and nylon 6**

#### **5.1 Introduction**

Thermoplastic elastomer (TPE) compositions prepared by mixing elastomers with thermoplastics are of significant commercial interest [1-8]. Two polymeric phases where one is rubbery and the other is either glassy or crystalline are an essential feature of all thermoplastic elastomers [9]. Morphology is a key factor affecting the mechanical properties of TPE blends as in the case of block copolymers [10]. Typical commercial triblock copolymers showing TPE behavior have polystyrene spheres, about 10 nm in diameter, dispersed in a matrix of polybutadiene [11]. On the other hand certain block copolymers (polyurethanes, polyesters, etc.) depend on a crystalline phase to act as thermally labile crosslinks. The crystalline regions appear to be continuous and highly interconnected. A morphology consisting of substantially continuous and interpenetrating crystalline and amorphous domains has been proposed [12].

Physical blending of two existing polymers may result in dual-phase continuity and phase inversion in the intermediate composition range [7, 8, 13-18]. An early example of a commercial product with dual-phase continuity was reported for blends of polypropylene and ethylene-propylene rubber (EPR) by Kresge et al [7]. These authors reported that crystallinity in the ethylene-propylene copolymer phase arising from long ethylene sequences can have profound effects on the mechanical behavior of the elastomer and its blends. Baldwin and Ver Strate reviewed the relationship between copolymer composition and crystallinity [19].

An attractive approach is to use chemical reactivity of the component polymers to achieve TPE materials of controlled morphology with chemical bonding between the phases. Blends of polyamides with maleated elastomers serve as a model for this approach. Blends of nylon 6 and EPR-g-MA having a continuous elastomer phase were described previously [20]. This chapter focuses on the complete composition range, including the region where interpenetrating networks may be formed, for blends of nylon 6 and EPR-g-MA. The effects of compositions and crystallinity of EPR-g-MA on the morphological, thermal and mechanical properties were investigated.

Table 1 Materials used in this work

Polymer	Commercial designation	Characterization <sup>a</sup>	Molecular weight <sup>a</sup>	Brabender torque <sup>b</sup> (N•m)	Source
Nylon 6	Capron 8207F	End-group content: [NH <sub>2</sub> ] = 47.9 µeq g <sup>-1</sup> [COOH] = 43.0 µeq g <sup>-1</sup>	$\bar{M}_n = 22,000$	5.4	AlliedSignal Inc.
H-EPR-g-MA	Exxelor 1801	43 wt% ethylene 53 wt% propylene 1.21 wt% MA Crystalline <sup>c</sup> T <sub>m</sub> = 47 °C <sup>c</sup>	Not available	13.5	Exxon Chemical Co.
EPR-g-MA	Exxelor 1803	43 wt% ethylene 53 wt% propylene 1.14 wt% MA Slightly crystalline <sup>c</sup> T <sub>m</sub> = 127 °C <sup>c</sup>	Not available	8.2	Exxon Chemical Co.

<sup>a</sup> Ref. [27].

<sup>b</sup> Torque value taken after 10 minutes at 240 °C and 60 rpm.

<sup>c</sup> Information from supplier.

Table 2 Physical properties and morphology of nylon 6/maleated EPR blends

Rubber	% Nylon 6	Young's modulus <sup>a</sup> (MPa)	Yield stress <sup>a</sup> (MPa)	Tensile strength <sup>a</sup> (MPa)	Elongation at break <sup>a</sup> (%)	Dispersed phase	$\bar{d}_w$ ( $\mu\text{m}$ )	$\bar{d}_w/\bar{d}_n$
EPR-g-MA	0	1.62	0.21	0.15	380	-	-	-
	20	3.65	0.70	0.55	180	Nylon 6	0.23	1.43
	40	83.4	4.90	7.10	50	Nylon 6	0.30	1.50
	50	361	15.7	22.7	190	-	-	-
	60	1120	24.4	31.5	240	EPR-g-MA	0.22	1.39
	80	2000	41.8	34.7	140	EPR-g-MA	0.24	1.47
	100	2600	76.3	46.4	30	-	-	-
H-EPR-g-MA	0	1.36	2.39	4.80	540	-	-	-
	20	31.0	5.70	5.70	130	Nylon 6	0.12	1.52
	40	117	9.00	13.6	60	Nylon 6	0.31	3.71
	50	407	18.9	31.3	230	-	-	-
	60	629	27.4	34.9	230	H-EPR-g-MA	0.25	1.47
	80	1280	40.2	35.8	210	H-EPR-g-MA	0.19	2.00
	100	2600	76.3	46.4	30	-	-	-

<sup>a</sup> Extension rate = 5.08 cm/min

## 5.2 Experimental

Table 1 describes the materials used in this work. Two commercially available ethylene/propylene copolymers grafted with maleic anhydride were obtained from Exxon Chemical, Exxelor 1803 and 1801; the former is nearly free of crystallinity and is designated here as EPR-g-MA while the latter has a higher level of ethylene crystallinity and is designated here as H-EPR-g-MA. These rubbers were blended with a nylon 6 from AlliedSignal, Capron 8207F, with a medium molecular weight ( $\overline{M}_n = 22,000$ ) and balanced acid and amine end groups. An antioxidant, Irganox 1076, was added to all blends at the level of 0.2 wt% of the rubber phase. The materials were dried in a vacuum oven for a minimum of 16 hours at 60°C for EPR-g-MA and H-EPR-g-MA and at 80°C for nylon 6 before melt blending.

Rheological properties were measured in a Brabender Plasticorder with a 50 cm<sup>3</sup> mixing head and standard rotors operated at 240°C and 60 rpm: torque values were recorded continuously during mixing of blends.

Blends were extruded twice at 240°C and 40 rpm using a Killion single screw extruder ( $L/D = 30$ ,  $D = 2.54$  cm) outfitted with an intensive mixing head after vigorously mixing all components together. The blends were injection molded into tensile bars (ASTM D638 Type ) using an Arburg Allrounder injection molding machine. The molded specimens were stored in a vacuum desiccator in order to prevent water sorption. Those with defects and air bubbles were discarded.

Shore A hardness was examined with a Pacific Transducer durometer according to ASTM D2240. Stress-strain properties were determined by an Instron according to ASTM D412 (1980) at room temperature: the cross-head speed was varied from 5.08 cm/min to 50.8 cm/min. The permanent set after break was measured at 10 minutes after rupture of tensile specimens. The Young's modulus was obtained from the initial slope of the stress-strain curve at a cross-head speed of 5.08 cm/min. Standard deviation for tensile measurements was typically less than 10%.

A Polymer Laboratories DMTA was used to measure dynamic mechanical properties in cantilever mode at a medium frequency of 30 Hz from -100 to 100°C at a heating rate of 3 °C/min. Heats of fusion for the blends were measured by a differential scanning calorimeter (Perkin-Elmer DSC-7) for specimens taken from injection-molded bars with a scan rate of 20 °C/min. The heat of fusion of the nylon 6 or rubber phase was defined as the area under the endothermic peak for first heating. The integration of the nylon 6 melting peak was typically run from 190 to 225°C; the temperature limits for ethylene melting were 105 to 135°C for EPR-g-MA blends and 30 to 80°C for H-EPR-g-MA blends. The baseline was subtracted for each measurement.

A JEOL 200 CX transmission electron microscope (TEM) was used for morphology observation at an accelerating voltage of 120 kV using ultra-thin sections cryogenically microtomed at  $-50^{\circ}\text{C}$  perpendicular and parallel to the flow direction of injection molded bars. The nylon 6 phase was stained by a 2% aqueous solution of phosphotungstic acid for 30 minutes at room temperature. Average particle sizes were determined using a semi-automatic digital image analysis technique by IMAGE® software from the National Institutes of Health.

### 5.3 Morphology

The morphology of blends of both EPR-g-MA and H-EPR-g-MA with nylon 6 was evaluated over the entire composition range by transmission electron microscopy. In general, the morphology showed similar trends for both blend systems, see Figure 1. Discrete particles of the minor phase in a matrix of the major phase were observed at 20 and 80% nylon 6; particle sizes are summarized in Table 2. A tendency for co-continuity was observed for the intermediate compositions as seen in the TEM photomicrographs for blends containing 40 to 60% nylon 6 in Figure 1. An elongated nylon 6 phase was observed at 40% nylon 6; at 50% nylon 6 this was more obvious. For injection molded bars of the blend containing 50% nylon 6, the rubber phase appears elongated in both perpendicular and parallel directions to the flow. At 60% nylon 6, phase inversion is complete and the rubber exists as a dispersed phase within the nylon 6 matrix. The TEM observations show that the phase inversion composition is about 50% nylon 6 for both rubber systems.

However, there are some morphological differences between EPR-g-MA and H-EPR-g-MA in these blends. First, the nylon 6 particles are smaller when the rubber matrix is H-EPR-g-MA than EPR-g-MA at 20% nylon 6. This is consistent with the higher melt viscosity [16] of H-EPR-g-MA than EPR-g-MA. Second, the EPR-g-MA phase shows a more elongated structure than H-EPR-g-MA for blends of intermediate composition: at 50% rubber, smooth elongated rubber platelets of 0.1 to 1  $\mu\text{m}$  in thickness and 6  $\mu\text{m}$  in length for EPR-g-MA were observed (Figure 1c); however, rubber phases with pointed shapes of 0.3 to 1  $\mu\text{m}$  in width and 3  $\mu\text{m}$  in length were found for H-EPR-g-MA (Figure 1d). The comparable rubber phase size that ranges from 0.1 to 4  $\mu\text{m}$  in width was observed in continuous phase structure for ethylene-propylene rubber/polypropylene (70/30) blends by Kresge [7].

For blends in the inversion region, small particles were observed in the elongated phase indicative of a bimodal particle size distribution as noted in a paper by Kudva et al [21]. This type of composite droplet morphology where the dispersed phase contains

droplets of the matrix phase was observed for polypropylene/polycarbonate blends by Favis et al [18].

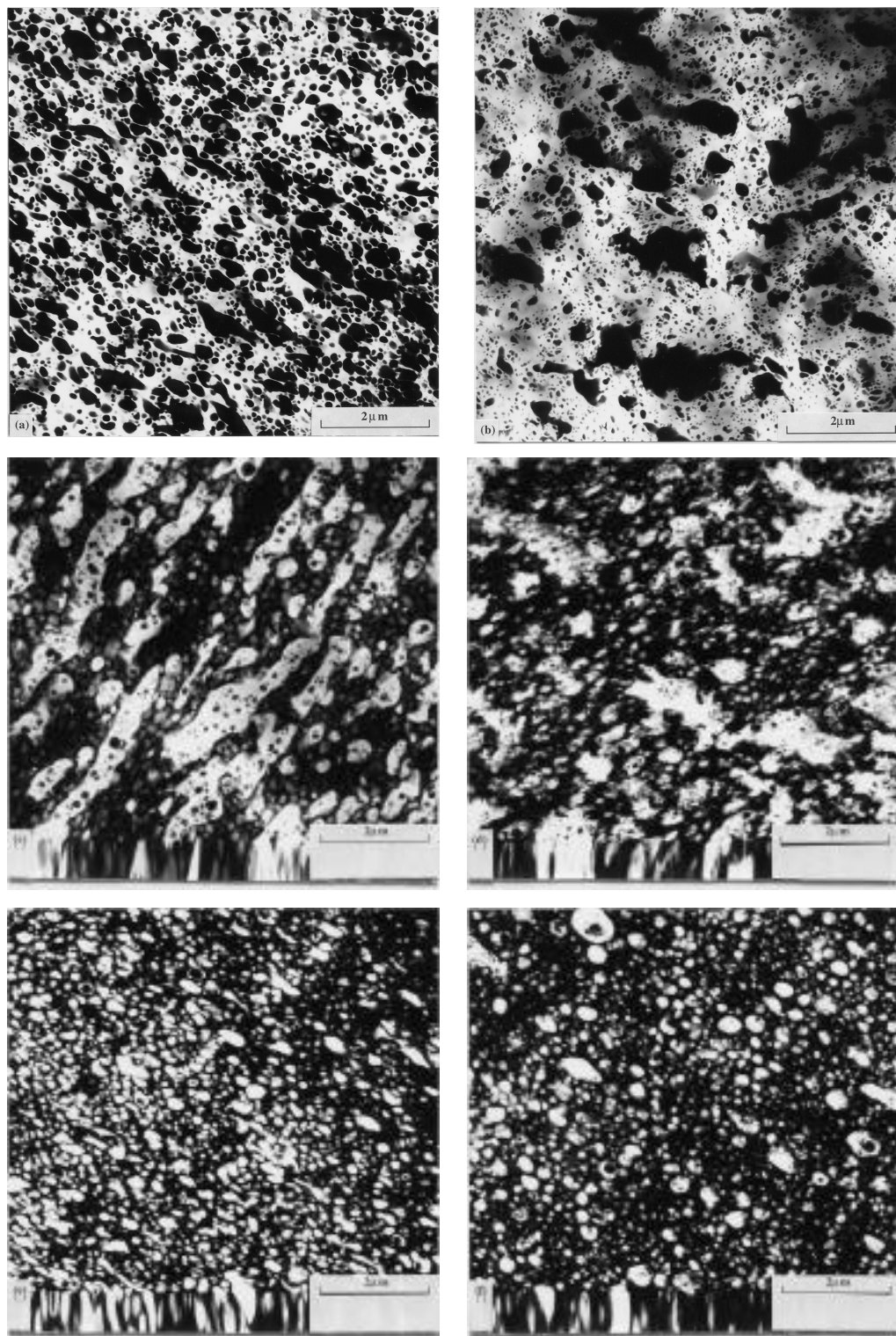


Figure 1. TEM photomicrographs of blends of (100-x)% maleated EPR and x% nylon 6: (a) and (b) x = 40, (c) and (d) x = 50, (e) and (f) x = 60; photomicrographs (a), (c) and (e) are for blends with EPR-g-MA; photomicrographs (b), (d) and (f) are for blends with H-EPR-g-MA. All views were taken in the direction perpendicular to the flow for these injection molded compositions.

Grafting of nylon 6 onto the maleated rubber during melt processing increases melt viscosity which can be monitored by the torque response during melt mixing in a Brabender [20]. While nylon 6 and EPR-g-MA have relatively similar melt viscosities at 240°C, their blends have much higher torques as illustrated by the data in Figure 2; indeed, the 40/60 blend of EPR-g-MA/nylon 6 develops a torque of more than twice that of the individual blend components. It is clear that the grafting of nylon 6 onto maleated rubber is very rapid, since the high torque of the blend is observed early in the mixing process [20]. The torque value for neat H-EPR-g-MA is higher than that for pure EPR-g-MA as seen in Table 1.

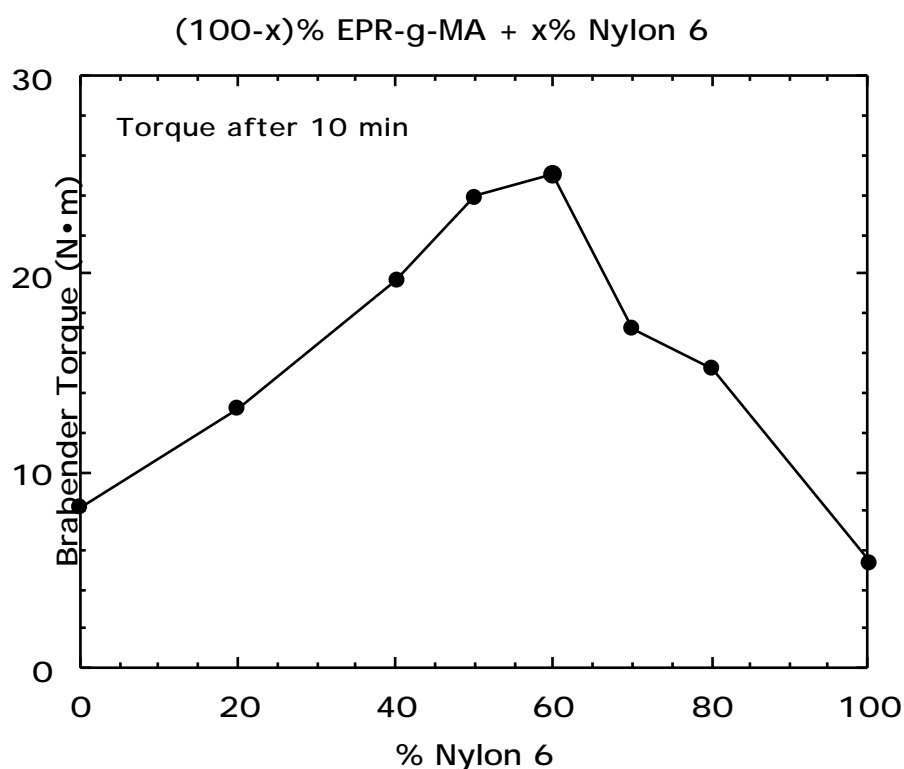


Figure 2. Brabender torque after 10 minutes at 240°C and 60 rpm as a function of nylon 6 content for blends of (100-x)% EPR-g-MA and x% nylon 6.

Table 3 Physical properties in the rubbery region of nylon 6/maleated EPR blends

Rubber	% Nylon 6	Hardness (Shore A)	Set after break <sup>a</sup> (%)	T <sub>g</sub> (°C)
EPR-g-MA	0	48	48.8	-38.5
	20	55	18.1	-35.1
	40	83	3.0	-34.3
H-EPR-g-MA	0	80	126.5	-23.0
	20	82	32.5	-19.1
	40	98	20.7	-18.1

<sup>a</sup> Extension rate = 5.08 cm/min

Table 4 Glass transition temperature and  $\tan \delta$  at peak from DMTA for nylon 6/maleated EPR blends

Rubber	% Nylon 6	Rubber phase		Nylon 6 phase	
		$T_g$ (°C)	$\tan \delta$ at peak maximum	$T_g$ (°C)	$\tan \delta$ at peak maximum
EPR-g-MA	0	-38.5	1.10	N/A	N/A
	20	-35.1	0.97	N/A	N/A
	40	-34.3	0.57	52.3 (shoulder)	N/A
	50	-38.2	0.17	59.3	0.16
	60	-45.1	0.089	59.5	0.14
	70	-45.6	0.064	60.0	0.14
	100	N/A	N/A	65.8	0.18
	H-EPR-g-MA	0	-23.0	0.21	N/A
20		-19.1	0.18	N/A	N/A
40		-18.1	0.13	61.6 (shoulder)	N/A
50		-30.0	0.068	64.6	0.15
60		-31.4	0.046	64.8	0.12
70		-32.8	0.038	64.0	0.12
80		-36.3	0.031	60.5	0.11
100		N/A	N/A	65.8	0.18

The graft copolymer formed by reaction of the nylon 6 amine end groups with maleic anhydride on EPR-g-MA is a compatibilizer that leads to a very fine dispersion between the nylon 6 phase and the rubber phase largely by limiting the frequency of particle-particle coalescence. In addition, the rubber/polyamide graft copolymers provide adhesion at the domain interfaces. Thus, blends of nylon 6 and maleated rubber should have a stable morphology and good adhesion between the hard and soft phases.

#### **5.4 Mechanical properties**

Shore A hardness values for the blends with a rubbery continuous phase, i.e., 0 to 40% nylon 6, are summarized in Table 3. The H-EPR-g-MA blends are harder than the EPR-g-MA blends; the former have values from 80 to 98, while the latter have values from 48 to 83 over this composition range. This is consistent with the higher crystallinity of H-EPR-g-MA.

Figure 3 shows stress-strain diagrams for neat EPR-g-MA and H-EPR-g-MA. The latter exhibits strain-hardening while the former does not. The tensile strength of H-EPR-g-MA is 30 times that of EPR-g-MA and the elongation at break of the former is 1.4 times larger than the latter. Strain-hardening generally results from molecular alignment in the direction of the strain or from strain-induced crystallization [22]. Crystallization during stretching has been observed by X-ray diffraction for an ethylene-propylene-diene terpolymer (EPDM) lightly crosslinked with peroxide [23].

Figure 3 also shows stress-strain diagrams for blends containing 20% nylon 6. The blend based on H-EPR-g-MA has a slightly lower elongation at break but much higher tensile strength than the blend based on EPR-g-MA. The blends do not show strain-hardening since they break just beyond the yield point. There is some evidence that the addition of the nylon 6 phase tends to inhibit crystallinity induced by deformation.

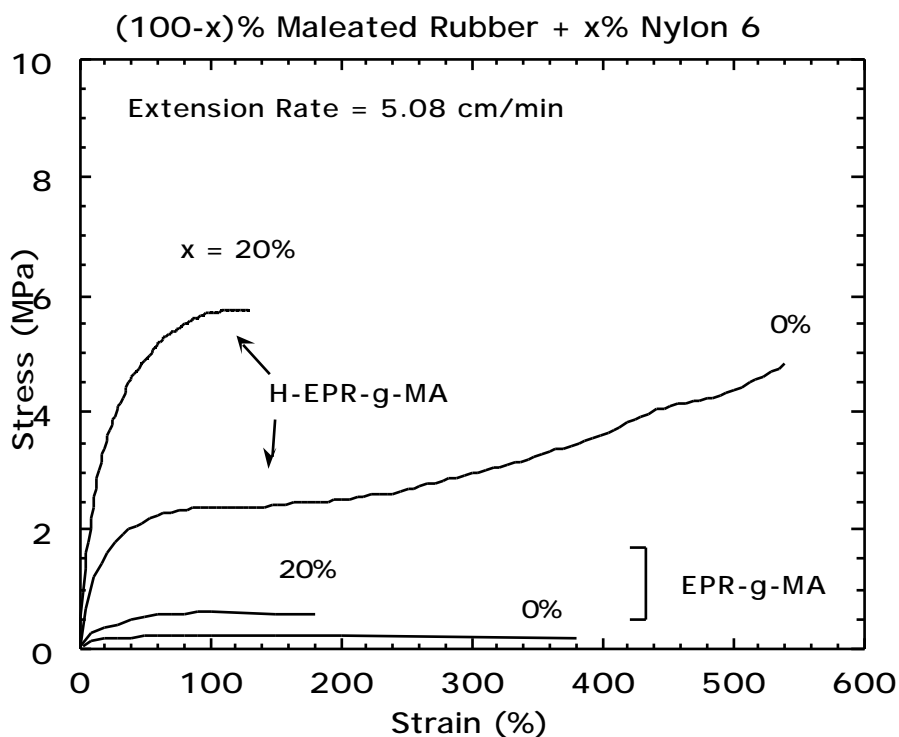


Figure 3. Stress-strain curves for blends of (100-x)% maleated EPR and x% nylon 6: x = 0 and 20%.

The non-recoverable deformation after failure, or set after break, during tensile testing at a cross-head speed of 5.08 cm/min shows similar trends for both blends; the amount of set decreases to quite low values when the nylon 6 content increases as seen in Table 3. The set values for blends based on H-EPR-g-MA are higher than those based on EPR-g-MA; this suggests that the crystalline phase of H-EPR-g-MA may undergo a typical drawing mechanism.

Figure 4 shows stress-strain curves for blends containing 40 to 100% nylon 6. Strain-hardening is apparent for both blends systems when the sample contains 40% or more nylon 6. Cold-drawing was observed and elongation at break was unexpectedly high for these intermediate blends. The blends based on H-EPR-g-MA showed a greater degree of strain-hardening than those based on EPR-g-MA.

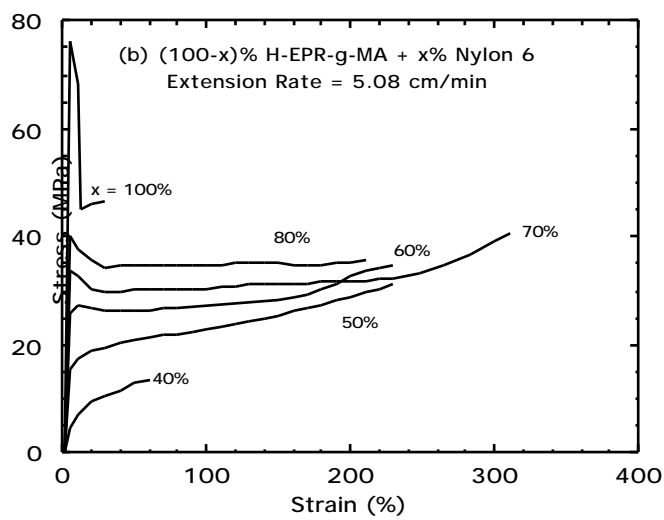
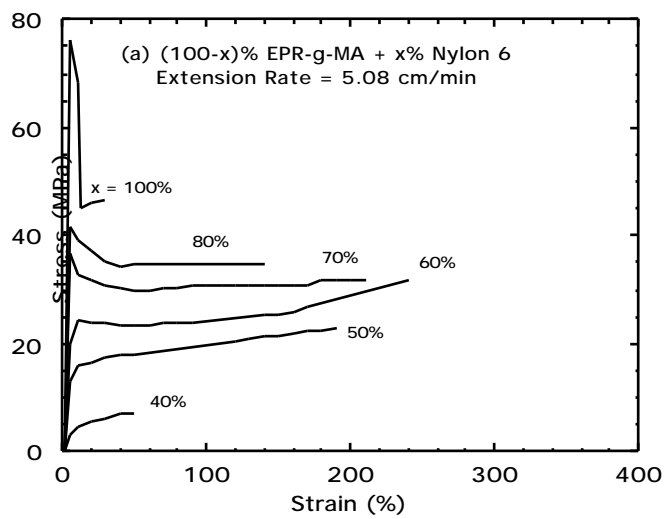


Figure 4. Stress-strain curves for blends of  $(100-x)\%$  maleated EPR and  $x\%$  nylon 6:  $x = 40$  to  $100\%$ ; (a) blends based on EPR-g-MA; (b) blends based on H-EPR-g-MA.

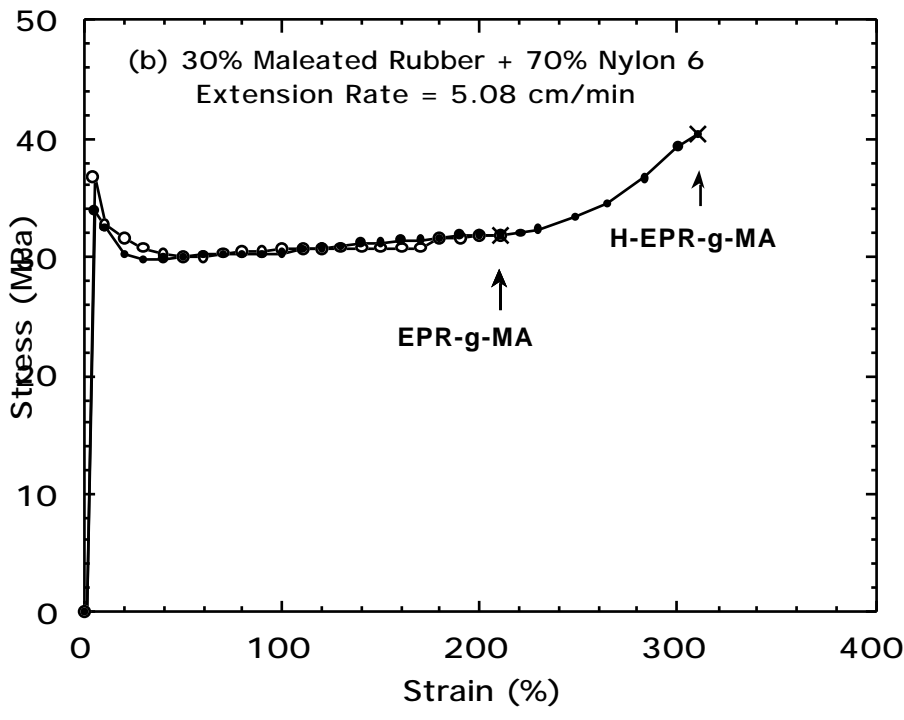
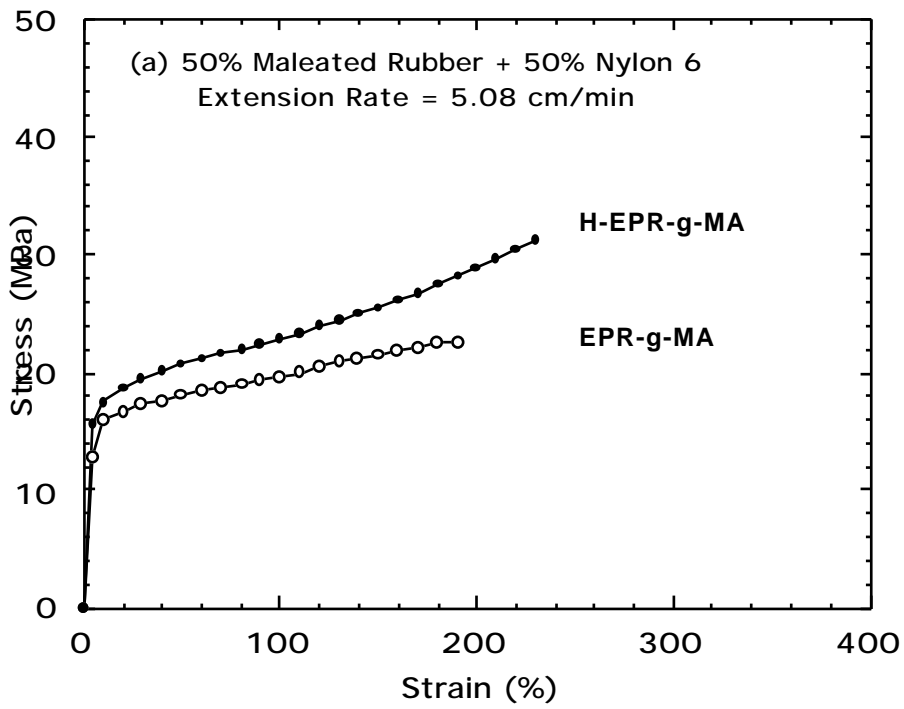


Figure 5. Stress-strain curves for blends of (100-x)% maleated EPR and x% nylon 6: (a) x = 50%; (b) x = 70%.

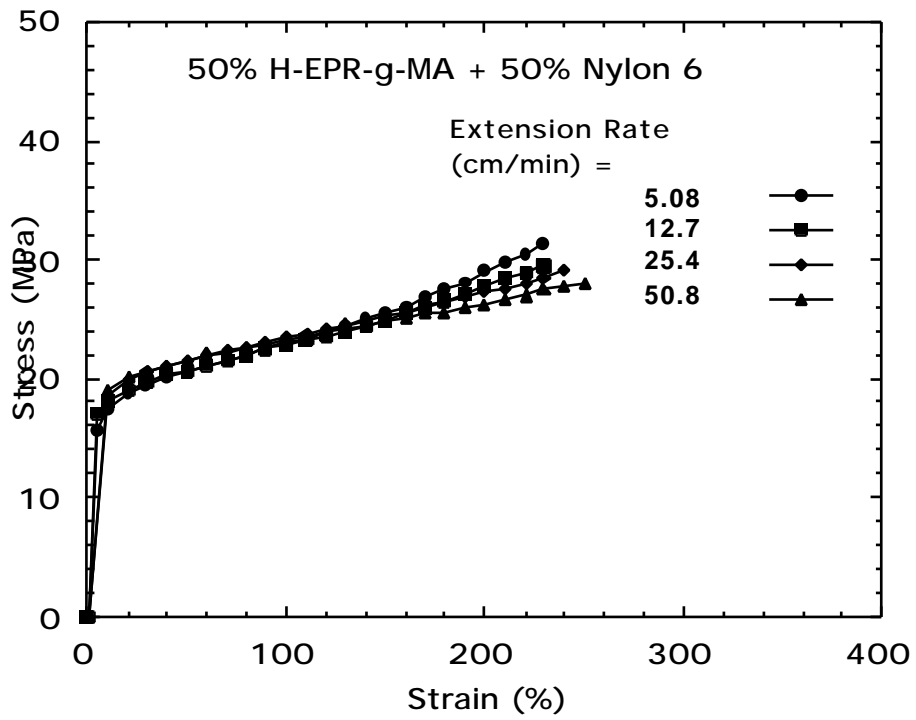


Figure 6. Stress-strain curves for blends of 50% maleated EPR and 50% nylon 6 at various extension rates.

Figure 5(a) provides a detailed comparison of blends based on the two maleated rubbers at 50% nylon 6. The blend based on H-EPR-g-MA shows higher stresses beyond the yield and a higher elongation at break. The slope in the post-yield region, i.e., degree of strain-hardening, is also higher for the H-EPR-g-MA blend. At 70% nylon 6 these differences disappear, i.e., the two stress-strain diagrams are virtually identical as seen in Figure 5(b). Both blends show the same yielding and cold-drawing behavior until 200% elongation. However, the ultimate properties, tensile strength and elongation at break, are greater for the blends based on H-EPR-g-MA.

The effect of crosshead speed on the stress-strain curve was examined. For blends containing less than 40% nylon 6, stress levels at a given strain were higher for faster test speeds [20]; however, for blends containing 50% nylon 6 or more, the effect of test speed on the stress-strain diagram was substantially less as illustrated in Figure 6.

Blends containing 60% or more of nylon 6 showed a distinct yield point, while blends containing less than 50% nylon 6 did not. In the latter case, the reported yield stress was defined as the stress where the tangents of the initial and final parts of the load-elongation curve intersect [24]. Figure 7 shows the effect of nylon 6 content on the yield stress. The blends based on H-EPR-g-MA show higher yield stress than those based on EPR-g-MA when the nylon 6 content is less than 60% as mentioned earlier (Figure 5a). This may be explained on the basis of the higher crystallinity of H-EPR-g-MA. However, for the blends containing more than 70% nylon 6, there is no distinguishable difference in the yield stress.

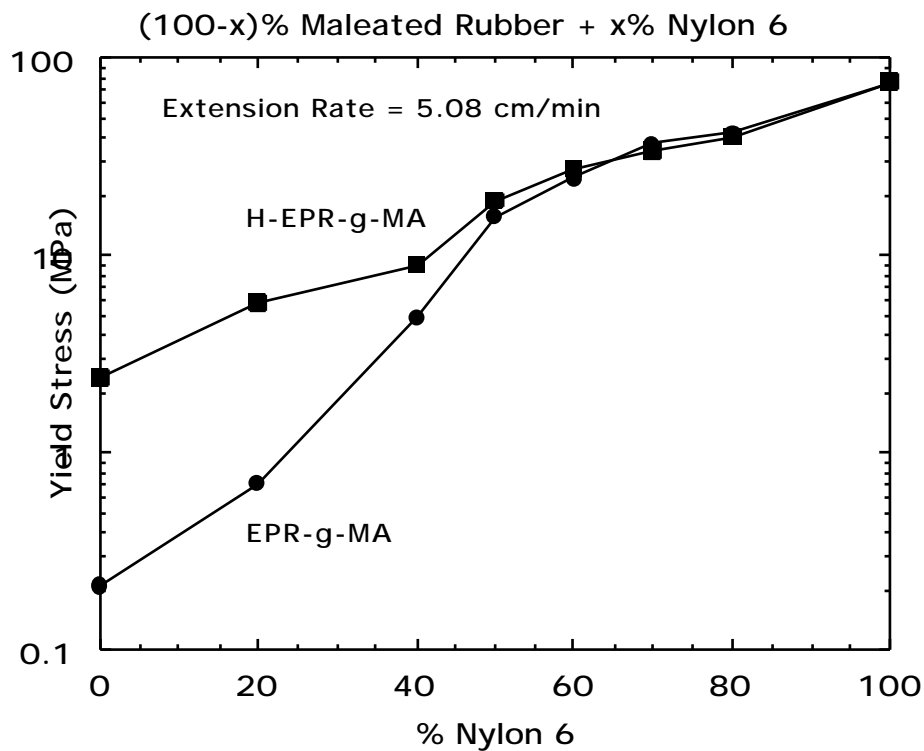


Figure 7. Yield stress as a function of nylon 6 content for blends of (100-x)% maleated EPR and x% nylon 6.

Figure 8 compares the ultimate properties of these blends to that expected from simple additivity (dotted line). The ultimate tensile strength and elongation at break show similar trends for the blends based on either rubber. When the rubber is the continuous phase, both strength and elongation are below the additive values, which suggests that the nylon 6 particles in the rubber matrix do not cause effective reinforcement [20]. When nylon 6 forms the continuous phase, the tensile strength is equal to or higher than the additive value and the elongation at break is always higher than average. The H-EPR-g-MA based blends generally have superior ultimate properties.

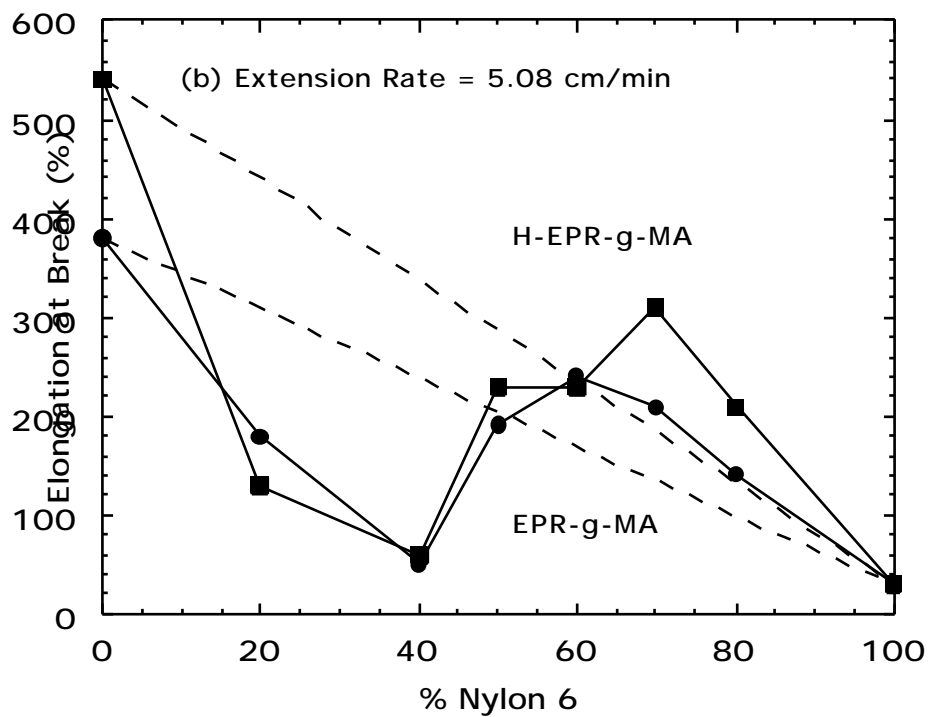
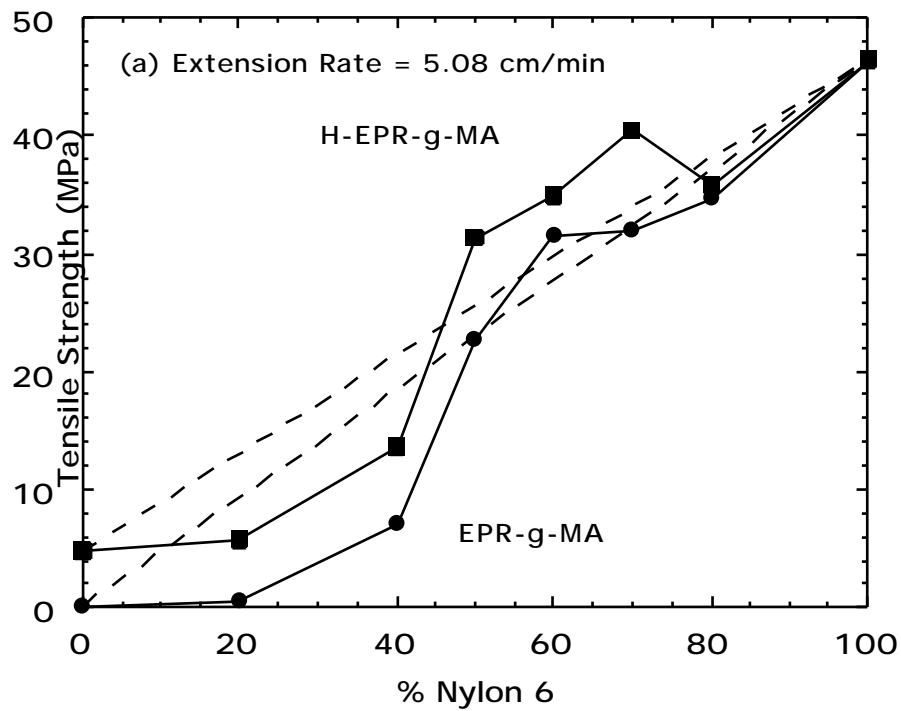


Figure 8. Ultimate properties as a function of nylon 6 content for blends of (100-x)% maleated EPR and x% nylon 6: (a) tensile strength and (b) elongation at break.

## 5.5 Thermal and dynamic mechanical analysis

Figure 9 shows DSC thermograms for blends containing 40% nylon 6 prepared from the two different maleated elastomers. Both materials show a peak at about 217°C from melting of nylon 6. However, they show distinctly different peaks at a lower temperature due to melting the crystallinity formed from sequences of ethylene units in the rubber; namely a peak at 125°C for EPR-g-MA blends and a peak at 45°C for H-EPR-g-MA blends. The heat of fusion for the latter peak is larger than that of the former. Ver Strate et al [25] have reported that major melting point depression results from addition of the comonomer in ethylene-propylene copolymers and showed two different melting points at about 120 and 50°C which are in the range observed in this study. The melting peaks for nylon 6 and the rubber do not depend significantly on blend composition; these phases are not expected to exhibit cocrystallization like that reported for blends of EPDM and low-density polyethylene (LDPE) [26].

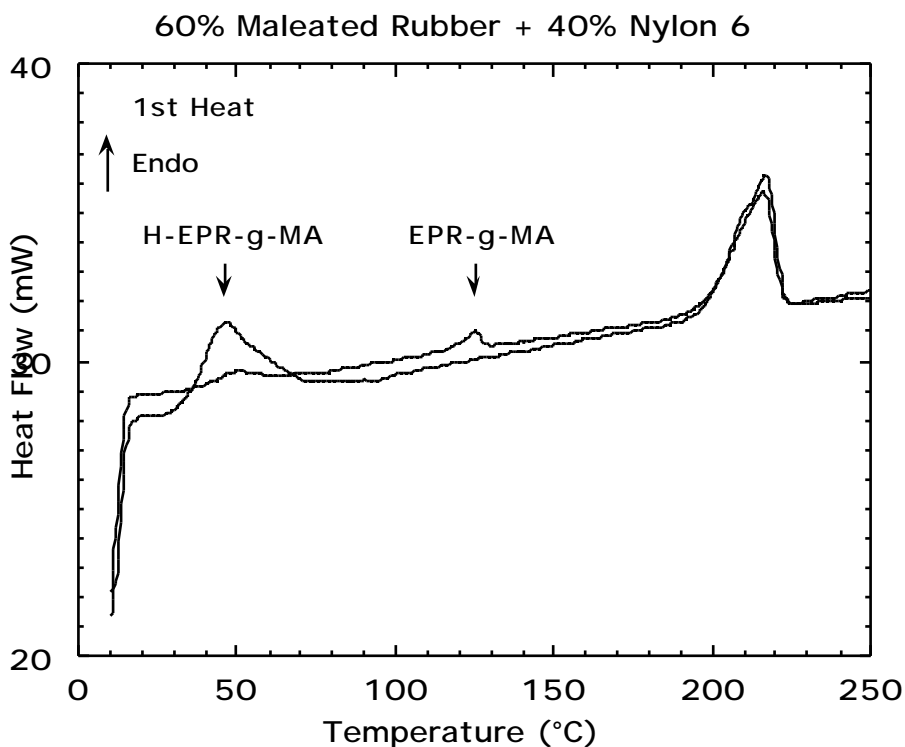


Figure 9. DSC thermograms of first heat cycle for blends of 60% maleated EPR and 40% nylon 6.

Figure 10(a) shows how the heat of melting of the ethylene sequences varies with the nylon 6 content of the blends. The blends based on H-EPR-g-MA show a much higher heat of fusion than those based on EPR-g-MA, especially for lower content of nylon 6. The larger values of the ultimate tensile properties for the H-EPR-g-MA blends can be explained by these larger heats of fusion, i.e., larger crystallinity of ethylene in the blends. For the rubbery blends in which the nylon 6 particles are dispersed in the rubber matrix phase, higher crystallinity provides more extensive tie points that act as crosslinks in the deformation field. On the other hand, for the intermediate and nonrubbery blends, larger crystallinity results in larger strain-hardening as mentioned earlier.

Figure 10(b) shows the relation between the heat of fusion of nylon 6 and the content of nylon 6 in the blend. For blends containing less than 40% nylon 6, the experimental values are very close to what is expected by additivity. However, for blends containing from 50 to 80% nylon 6 the observed heats of fusion are lower than additive. Oshinski reported that reactive blends have lower crystallinity than expected from additivity [27]. Grafting of nylon 6 onto rubber reduces the crystallization rate of nylon 6 because the melt viscosity increases as seen in Figure 2 [28].

Figure 11 shows the dynamic mechanical storage modulus ( $E'$ ) and loss tangent ( $\tan \delta$ ) for the blends based on H-EPR-g-MA as a function of temperature; similar data have been reported previously for blends based on EPR-g-MA [20]. The locations of the observed  $\tan \delta$  peaks associated with the glass transitions of the rubber and nylon 6 are given in Table 4. Both blends showed similar trends including a small increase in the  $T_g$  of about 5°C for the rubber phase as the nylon 6 content increases from 0 to 40%. As the nylon 6 content is increased further from 50 to 70 or 80%, the  $T_g$  of the dispersed rubber decreases below that of the neat rubbers. This behavior is also observed for grafted polybutadiene rubbers in ABS materials [29] and is attributed to dilatational stresses stemming from differences in the volume contraction of the phases on cooling. A  $\tan \delta$  peak associated with the  $\alpha$ -relaxation of nylon 6 occurs at -26.5°C near the glass transition for these two rubbers. The values of  $T_g$  for the rubber phase of H-EPR-g-MA blends are higher than those of EPR-g-MA blends, because of the higher crystallinity of H-EPR-g-MA. However, it should be noted that there is little difference in the elongation at break of those blends as mentioned above.

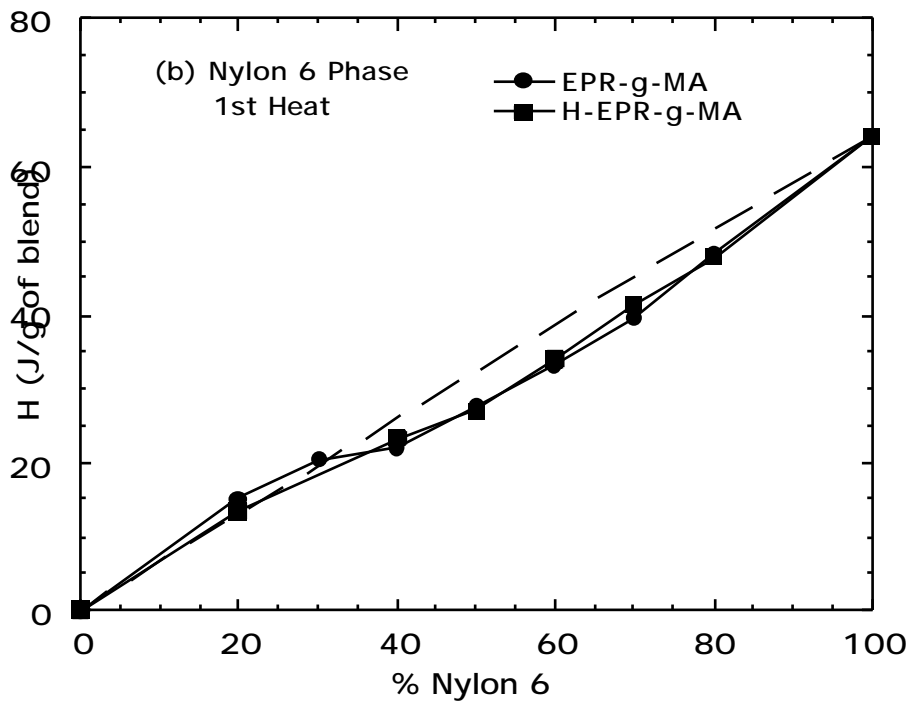
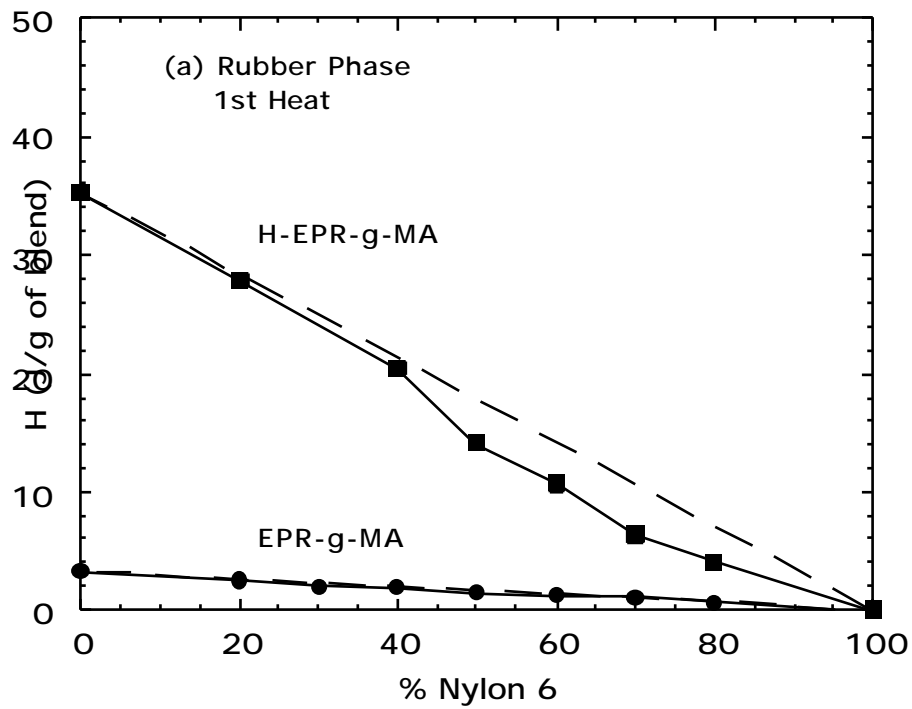


Figure 10. Heat of fusion for melting peaks of (a) rubber phase and (b) nylon 6 phase from a first heat as a function of nylon 6 content.

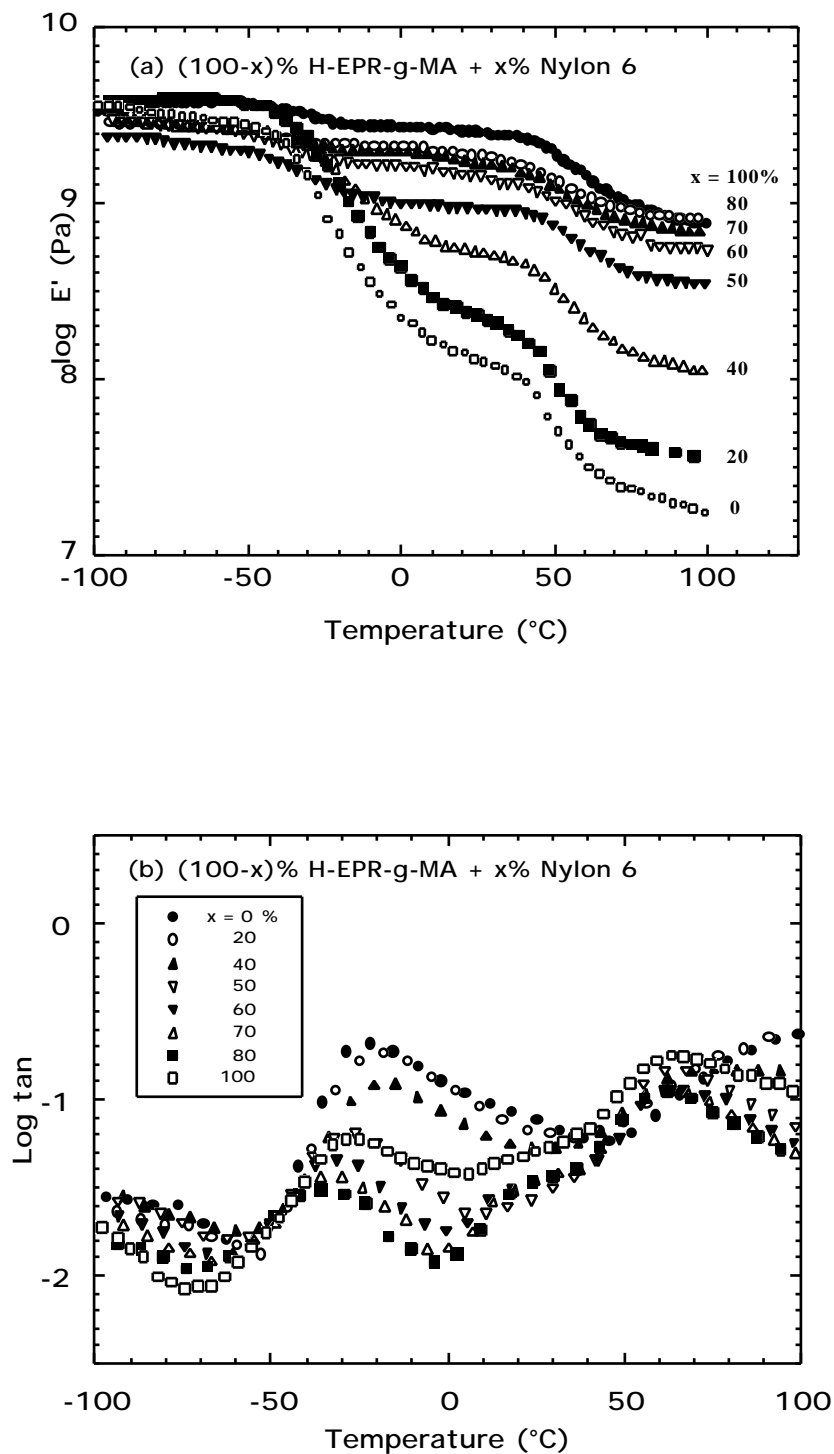


Figure 11 Viscoelastic data as a function of temperature for blends of  $(100-x)\%$  H-EPR-g-MA and  $x\%$  nylon 6: dynamic storage modulus (a) and  $\text{tan } \delta$  (b). Similar data for blends with EPR-g-MA have been reported previously [20].

The storage modulus  $E'$  of each blend shows a significant decrease at the glass transition of the rubber and the nylon 6 phase and at the melting point of nylon 6 (off the scale used in the current graphs). It is interesting to note that a significant decrease in modulus occurs at about  $50^\circ\text{C}$  for blends based on H-EPR-g-MA that contain less than 50% of nylon 6. This results from melting of the crystalline phase of H-EPR-g-MA as seen by DSC; however, no corresponding  $\tan \delta$  peak was observed.

The size of the  $\tan \delta$  peak associated with the rubber phase is shown as a function of nylon 6 content in Figure 12. When the nylon 6 phase is dispersed in a matrix of rubber, the EPR-g-MA blends have higher values of  $\tan \delta$  than the H-EPR-g-MA blends. This behavior is consistent with a lower level of crystallinity as found by DSC.

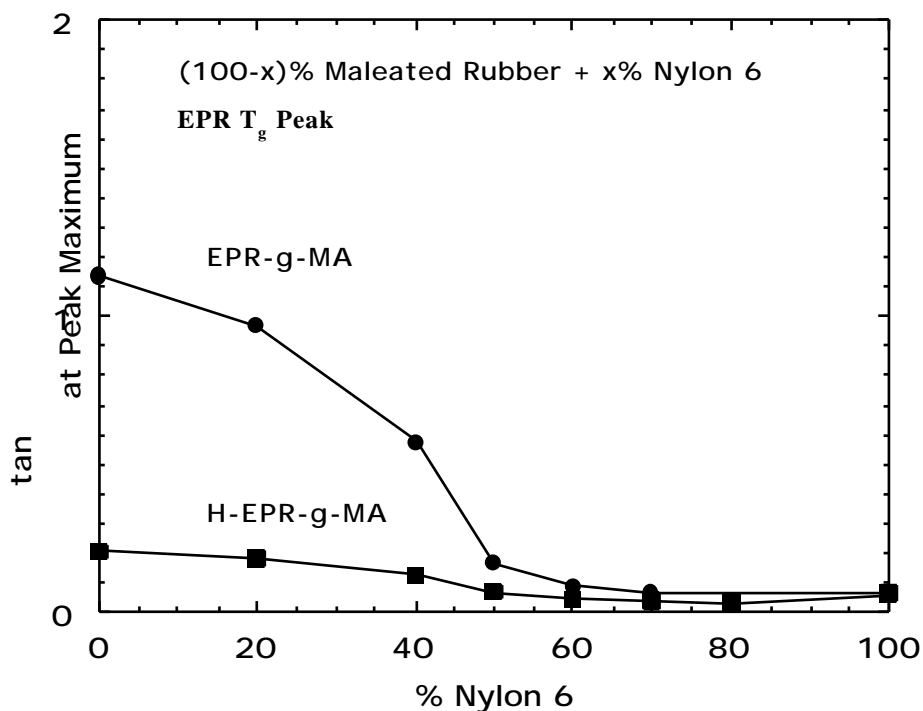


Figure 12  $\tan \delta$  at peak maximum for rubber phase  $T_g$  as a function of nylon 6 content for blends of  $(100-x)\%$  maleated EPR and  $x\%$  nylon 6.

Experimental values of the modulus from stress-strain testing at 5.08 cm/min,  $E$ , are shown for blends of nylon 6 with EPR-g-MA and with H-EPR-g-MA over the entire composition range in Figure 13. The observed values are compared to theoretical predictions (solid lines) calculated using a self-consistent theory proposed by Hill [30]. This model is expressed in the form

$$\frac{{}_1K_1}{K_1 + \frac{4}{3}G} + \frac{{}_2K_2}{K_2 + \frac{4}{3}G} + 5 \frac{{}_1G_2}{G - G_2} + \frac{{}_2G_1}{G - G_1} + 2 = 0 \quad (1)$$

where  $K$  is the bulk modulus and  $G$  is the shear modulus of the blend, the subscript indicates the corresponding component  $i$ , and  $v_i$  is the volume fraction of component  $i$ .

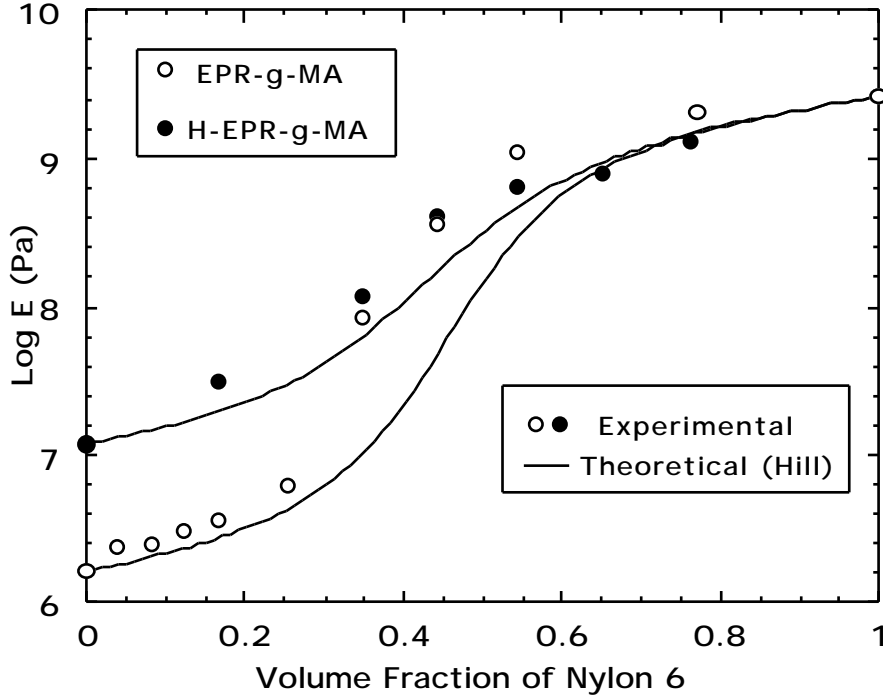


Figure 13. Effect of nylon 6 content on Young's modulus,  $E$ , from stress-strain diagrams for blends of nylon 6 and maleated EPR: (○) EPR-g-MA and (●) H-EPR-g-MA.

The tensile,  $E_i$ , bulk,  $K_i$ , and shear,  $G_i$ , moduli of each component (or blend) are interrelated via Poisson's ratio,  $\nu_i$ , by the following

$$K_i = \frac{E_i}{3(1 - 2\nu_i)} \quad \text{and} \quad G_i = \frac{E_i}{2(1 + \nu_i)} \quad (2)$$

Poisson's ratio was assumed to be 0.49 for EPR-g-MA and 0.33 for nylon 6 [31] and to be a linear function of composition for the blends.

Figure 14 shows similar comparison between calculated and experimental values of the dynamic storage modulus. The calculated values are from the Hill equation assuming that Young's modulus,  $E$ , can be replaced with the complex modulus [32],  $E^*$ , and that in turn  $E^*$  is approximately equal to the storage modulus [33],  $E'$ . There is little difference between  $E$  and  $E'$  for blends in which nylon 6 phase is continuous, while  $E'$  is larger than

$E$  for blends where nylon 6 is a discrete phase in a rubber matrix. Both  $E$  and  $E'$  are higher for the blends based on H-EPR-g-MA than those based on EPR-g-MA, because of the larger crystallinity of the former. When compared at constant values of modulus (either  $E$  or  $E'$ ), especially in the phase inversion region, the volume fraction of nylon 6 from the experimental result is lower than that from the theoretical curve as seen in Figures 13 and 14. This deviation between apparent and actual volume fractions is larger for EPR-g-MA blends than for H-EPR-g-MA blends. This may be caused by an anisotropic structure, i.e., more elongated morphology for EPR-g-MA blends than for H-EPR-g-MA as seen by TEM.

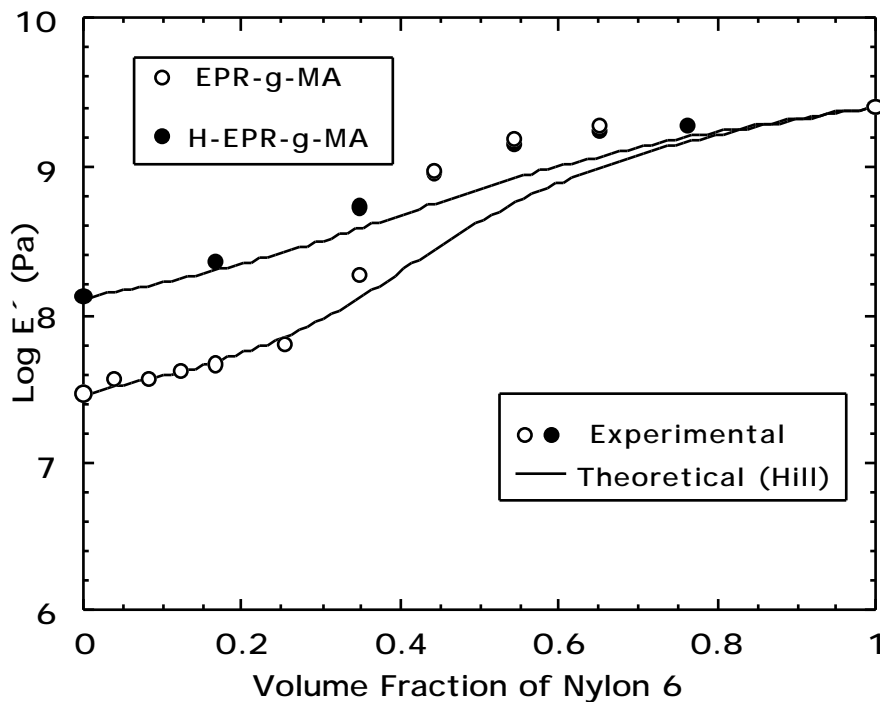


Figure 14. Effect of nylon 6 content on dynamic storage modulus,  $E'$ , from dynamic mechanical testing for blends of nylon 6 and maleated EPR: (○) EPR-g-MA and (●) H-EPR-g-MA

Table 5 Phase inversion volume fraction of nylon 6 for nylon 6/maleated EPR blends

Rubber phase	Calculated <sup>a</sup>	TEM	Young's modulus	Storage modulus
EPR-g-MA	0.40	ca 0.44	0.32	0.40
H-EPR-g-MA	0.29	ca 0.44	0.40	0.40

<sup>a</sup> Calculated by torque ratio [eq. (3)].

## 5.6 Phase inversion behavior

Dual phase continuity, i.e., phase inversion, occurs when the slope of  $\log E$  or  $\log E'$  as a function of composition is steepest [13]. The phase inversion compositions from curves calculated by the Hill equation are 44 vol% (50 wt%) for both  $E$  and  $E'$  for both rubber systems. However, the inversion points from the experimental modulus values occur at lower nylon 6 content as seen in Table 5.

There are several models to predict phase inversion composition for polymer blends [16]. Recently, Mekhilef suggested that the Avgeropoulos model, in which torque ratio is equated with the volume fraction ratio, predicts the point of phase inversion better than various semi-empirical models using the viscosity ratio [14]. In the Avgeropoulos model, the inversion point composition is expressed as [15]

$$T_1 / T_2 = v_1 / v_2 \quad (3)$$

where  $T_i$  is the torque of polymer  $i$ . The inversion point predicted by the Avgeropoulos model for EPR-g-MA blends is 40 vol% (46 wt%) and that for H-EPR-g-MA is 29 vol% (34wt%). Experimental values from TEM observations and modulus curves are compared to the predicted values in Table 5. The predicted value for the EPR-g-MA blends was found to be close to the values from TEM. In the case of H-EPR-g-MA blends, the predicted value was less than the experimental values. Favis pointed out that morphology of polymer blends is affected by various material parameters such as viscosity ratio, composition, elasticity, shear stress and interfacial modification [16]. Recently, Bourry showed that both elastic and viscous effects should be considered for blends of high-density polyethylene and polystyrene [17]. These factors other than composition no doubt account for some of the discrepancy between the predicted values and the experimental values observed in this study.

## 5.7 Conclusions

The morphology, thermal properties and mechanical behavior for blends of nylon 6 with EPR-g-MA and H-EPR-g-MA have been examined over the whole composition range. Generally, both types of rubber show similar morphological features; however, the following differences were noted. First, the rubbery blends of H-EPR-g-MA yield smaller nylon 6 particles than that of EPR-g-MA at low contents of nylon 6. Second, in the inversion range, the EPR-g-MA phase is rather smooth and elongated, while the H-EPR-g-MA phase is pointed and discrete. The size and shape of the dispersed rubber particles are similar for the two types of rubber when nylon 6 is the continuous phase.

Two typical tensile behaviors were observed for both blend systems based on EPR-g-MA and H-EPR-g-MA, viz., homogeneous deformation without a well-defined yield point and inhomogeneous deformation with necking and cold-drawing. These behaviors depend on morphology of the blends. The former is observed for the rubbery blends where nylon 6 spheres are dispersed in a rubber matrix and for the intermediate blends. The latter is observed for the polyamide-rich blends where rubber particles are dispersed in a nylon 6 matrix phase.

H-EPR-g-MA blends have superior mechanical properties compared to EPR-g-MA blends. Strain-hardening, which may be caused by strain-induced crystallization of ethylene sequences, is observed for neat H-EPR-g-MA. However, adding nylon 6 results in poor ultimate properties in the rubbery region, where tensile strength and elongation at break are lower than expected from additivity. Hardness, tensile strength, set after break, and static Young's modulus and dynamic storage modulus for H-EPR-g-MA blends indicate larger values than those for EPR-g-MA blends. These results are consistent with higher crystallinity of H-EPR-g-MA than EPR-g-MA. For the intermediate blends (40 to 60% nylon 6), strain-hardening is observed for both blend systems. Yield stress and tensile strength at break for the H-EPR-g-MA blends are higher than those based on EPR-g-MA. The former blends have steeper slopes in the post yield region than the latter blends. Both elongation at break and tensile strength increase as nylon 6 content is increased in the intermediate composition range. On the other hand, tensile strength increases but elongation at break decreases with nylon 6 content in the composition range where the rubber phase is dispersed. Stress-strain curves show cold-drawing behavior and are virtually identical for both blend systems in this composition region. However, elongation at break for EPR-g-MA blends is lower than that for H-EPR-g-MA blends at 70 and 80% nylon 6. The former blends break before the stress can increase, while the latter blends do not.

Thermal analysis shows that the H-EPR-g-MA blends have higher crystallinity based on ethylene sequences than the EPR-g-MA blends although the latter has the higher melting temperature. The rubber phase values of  $\tan \delta$  at peak maximum are higher for EPR-g-MA blends than for H-EPR-g-MA blends which is consistent with the difference in crystallinity between two rubbers. Experimental modulus values were compared to those predicted by the Hill theory. The difference between these values is small when the nylon 6 content is at either extreme for both blends. However, in the intermediate region (i.e., 20 to 80% nylon 6), H-EPR-g-MA blends show better agreement with the model than do EPR-g-MA blends.

The phase inversion compositions from TEM and modulus curves were compared to predicted values from the model of Avgeropoulos. The predicted value for the EPR-g-MA blends is close to that found by TEM but differs from that indicated by the experimental modulus curve. In the case of H-EPR-g-MA blends, the predicted value is less than the experimental value.

## References

1. Wolfe Jr JR. In: Legge NR, Holden G, Schroeder HE, editors. Thermoplastic elastomers: a comprehensive review. New York: Hanser Publishers, 1987. pp. 117-131.
2. Bohn L. Rubber Chem Technol 1968;41:495.
3. Reed MC, Harding J. Ind Eng Chem 1949;41:675.
4. Hammer CF. In Paul DR, Newman S, editors. Polymer blends, vol. 2. New York: Academic Press, 1978. pp. 219-241.
5. Hartman PF, Eddy CL, Koo GP. Rubber World 1970;163(1):59.
6. Ramos-Devalle LF, Ramirez RR. Rubber Chem Technol 1982;55:1328.
7. Kresge EN. In: Paul DR, Newman S, editors. Polymer blends, vol. 2. New York: Academic Press, 1978. pp. 293-318.
8. Ranalli R. In: Whelan A, Lee KS, editors. Developments in rubber technology. vol. 3. Thermoplastic rubbers. London: Applied Science Publishers, 1982. pp. 21-57.
9. Legge NR, Davison S, De La Mare HE, Holden G, Martin MK. In: Tess RW, Poehlein GW, editors. Applied Polymer Science, 2nd ed.: ACS Symp. Series, 1985;285:175-217.
10. Molau GE. In: Aggarwal SL. editor. Block polymers. New York: Plenum Press, 1970. p. 79.
11. Beecher JF, Marker L, Bradford RD. J. Polym Sci, Part C 1969;26:117.
12. Cella RJ. J Polym Sci: Symp Ed 1973;42:727.
13. Jordhamo GM, Manson JA, Sperling LH. Polym Eng Sci 1986;26:517.
14. Mekhilef N, Verhoogt H. Polymer 1996;37:4069.
15. Avgeropoulos GN, Weissert FC, Biddison PH, Böhm GGA. Rubber Chem Technol 1976;49:93.
16. Favis BD. In: Paul DR, Bucknall CB, editors. Polymer blends, vol. 1. New York: John Wiley & Sons, 2000. pp. 501-537.
17. Bourry D, Favis BD. J Polym Sci: Polym Phys 1998;36:1889.
18. Favis BD, Chalifoux JP. Polymer 1988;29:1761.
19. Baldwin FP, Ver Strate G. Rubber Chem Technol 1972;45:709.
20. Okada O, Keskkula H, Paul DR. Polymer 1999;40:2699.
21. Kudva RA, Keskkula H, Paul DR. Polymer 1998;39:2447.
22. Nielsen LE, Landel RF. Mechanical properties of polymers and composites, 2nd ed. New York: Marcel Dekker, 1994. p. 299.
23. Bassi IW, Corradini P, Fagherazzi G, Valvassori A. Eur Polym J 1970;6:709.
24. Ward IM, Hadley DW. An introduction to the mechanical properties of solid polymers. Chichester: John Wiley & Sons, 1993. p. 221.

25. Ver Strate G. and Wilchinsky ZW. *J Polym Sci: Part A-2* 1971;9:127.
26. Starkweather Jr HW. *J Appl Polym Sci* 1980;25:139.
27. Oshinski AJ, Keskkula H, Paul DR. *Polymer* 1992;33:268.
28. Martuscelli E, Riva F, Sellitti C, Silvestre C. *Polymer* 1985;26:270.
29. Morbitzer L, Kranz D, Humme G, Ott KH. *J Appl Polym Sci* 1976;20:2691.
30. Hill R. *J Mech Phys Solids* 1965;13:213.
31. Brandrup J, Immergut EH, editors. *Polymer handbook*, 3rd ed. New York: John Wiley & Sons, 1989:V/113.
32. Uemura S, Takayanagi M. *J Appl Polym Sci* 1966;10:113.
33. Ward IM, Hadley DW. *An introduction to the mechanical properties of solid polymers*. Chichester: John Wiley & Sons, 1993. p. 63.

## Chapter 6

### Dynamic mechanical properties of blends of nylon 6 and maleated ethylene-propylene rubber

#### 6.1 Analysis of Dickie model

Experimental dynamic moduli were compared to theoretical values by Dickie equations. Dickie showed the following equations<sup>1</sup> for storage modulus,  $E'$ , and loss modulus,  $E''$ , for heterogeneous polymer-polymer composites by application of Kerner equation<sup>2</sup>, if the Poisson's ratio of the matrix is assumed to be real:

$$E' = E_m' (A / C) - E_m'' (B / C)$$

$$E'' = E_m'' (A / C) + E_m' (B / C)$$

where subscript m denotes a matrix property, subscript i denotes an inclusion property, and  $A$ ,  $B$  and  $C$  are the following functions

$$A = (1 - c) (1 + \nu_m) (E_m'^2 + E_m''^2) + (1 - c) (1 + \nu_i)^2 (E_i'^2 + E_i''^2) + [(1 - c)^2 + (1 + \nu_i)(1 + \nu_m)] (E_m' E_i' + E_m'' E_i'')$$

$$B = (1 + \nu_i)^2 c (E_i'' E_m' - E_m'' E_i')$$

$$C = (1 + \nu_m)^2 (E_m'^2 + E_m''^2) + (1 - c)^2 (1 + \nu_i)^2 (E_i'^2 + E_i''^2) + 2 (1 + \nu_m)(1 - c) (E_m' E_i' + E_m'' E_i'')$$

$\nu_m$ ,  $\nu_i$ , and  $\nu$  are functions of Poisson's ratio,  $\nu$ :

$$\nu = 2(4 - 5\nu_m) / (7 - 5\nu_m)$$

$$= (1 + \nu_m) / (1 + \nu_i)$$

$$= (1 + \nu_i) / (1 + \nu_m)$$

It was assumed that  $c$  is a function of volume fraction of inclusion,  $\nu$

$$c = \nu$$

$$= 1 + \nu(1 - \nu_{\max}) / \nu_{\max}^2$$

where  $\nu_{\max}$  is maximum packing fraction.

It was also assumed that

$$= \nu_m$$

$$\text{i.e., } \nu = 1$$

## 6.2 Results

The values of  $E'$  and  $E''$  for the EPR-g-MA blends were calculated as a function of nylon 6 content by assuming that the nylon 6 phase is dispersed phase in the rubber phase matrix for various  $\nu_{\max}$  values as seen in Figure 1. Theoretical curves well described the experimental values in the range of volume fraction of nylon from 0 to 0.3 for both  $E'$  and  $E''$  at  $\nu_{\max} = 0.6$ .

It was also assumed that the rubber is dispersed phase in the nylon matrix phase as seen in Figure 2. The experimental values of  $E'$  and  $E''$  were nearly represented by assuming  $\nu_{\max} = 0.8$ , but some discrepancy between theory and experiment was observed.

$E'$  and  $E''$  data for the blends based on H-EPR-g-MA were calculated in the same way as seen in Figures 3 to 4, respectively. similar results as above were obtained.

Results were summarized in Figure 5. Dickie reported similar values for  $\nu_{\max}$  as seen in the results above. It was reported that the values of  $\nu_{\max}$  for rubbery matrix is 0.6 and  $\nu_{\max}$  for glassy matrix is 0.8<sup>3</sup>. The author suggested that the composite comprises simple glassy inclusions in rubbery matrix at  $\nu_{\max} = 0.6$ . He also pointed out that interaction between soft inclusions in a hard matrix is weaker than that between hard inclusions in a soft matrix; higher value for soft particles may be due to the greater deformability of the inclusions.

In conclusion, the theoretical analysis by Dickie model depends on the polymer matrix and dispersed phase. Dickie model requires two individual  $\nu_{\max}$  for either composition depending on the matrix phase and cannot describe the phase inversion composition for the blends of nylon 6 with maleated rubber. Analysis using Hill model, which is shown in chapter 4 and 5, provides continuous analysis for all composition range and more useful method than that with Dickie model.

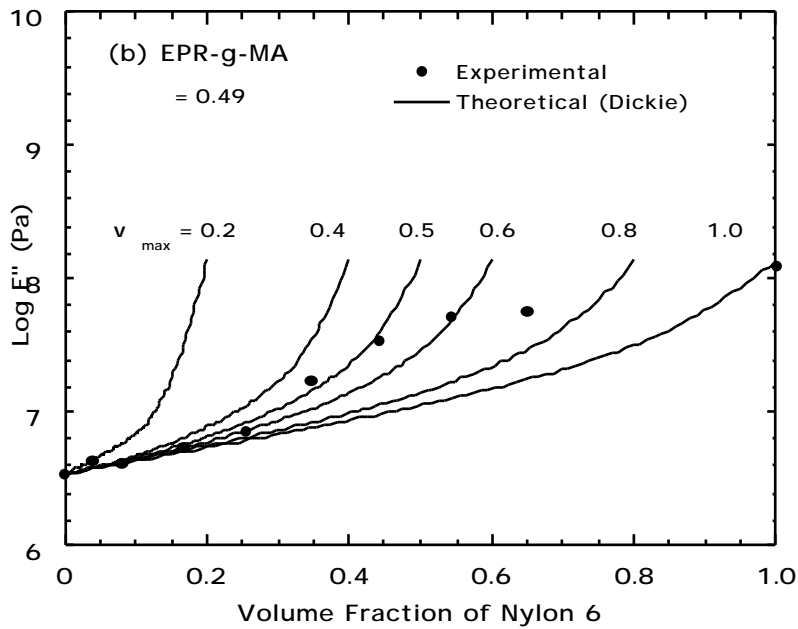
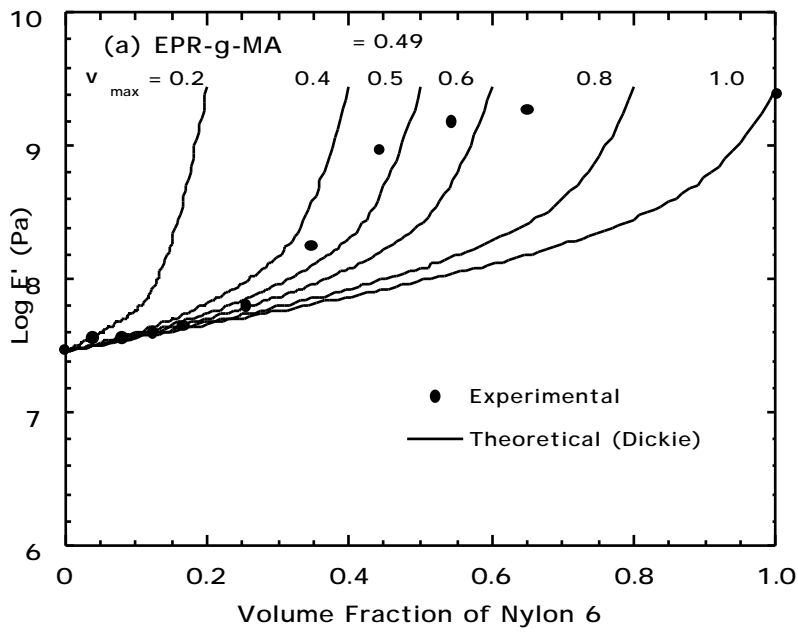


Fig. 1 Effect of nylon 6 content on: (a)  $E'$  and (b)  $E''$  for blends based on EPR-g-MA. Experimental values were compared to theoretical values calculated using Dickie equations by assuming that rubber phase is matrix phase and nylon 6 phase is dispersed phase.

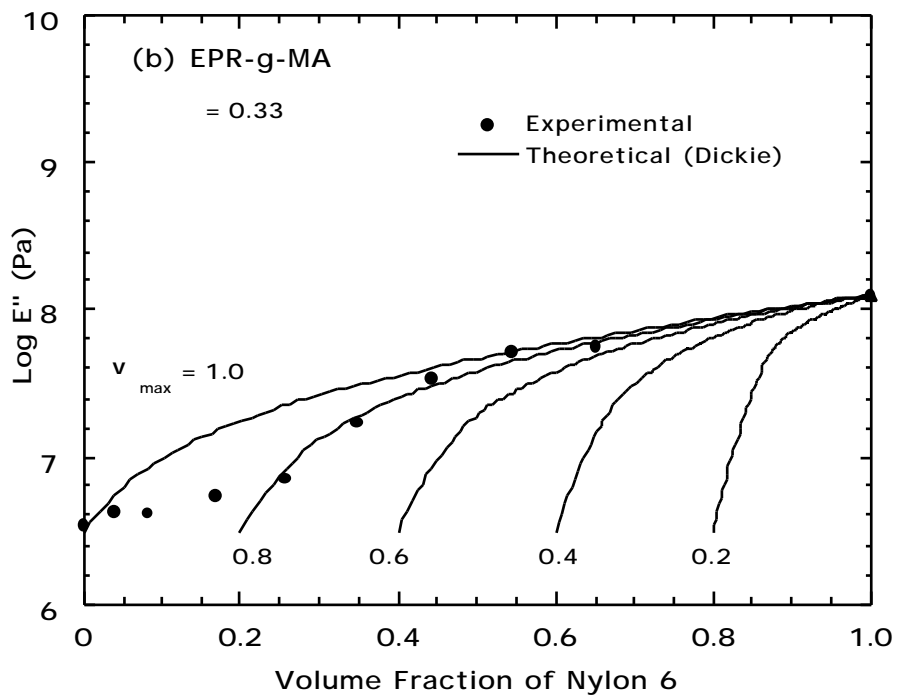
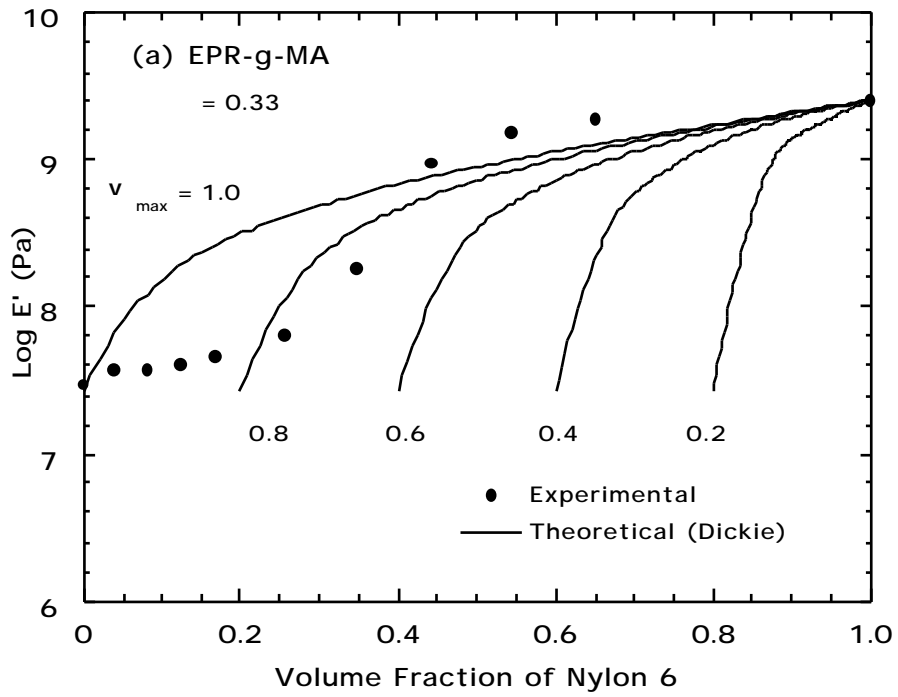


Fig. 2 Effect of nylon 6 content on: (a)  $E'$  and (b)  $E''$  for blends based on EPR-g-MA. Theoretical values were calculated by assuming that nylon 6 phase is matrix phase and rubber phase is dispersed phase.

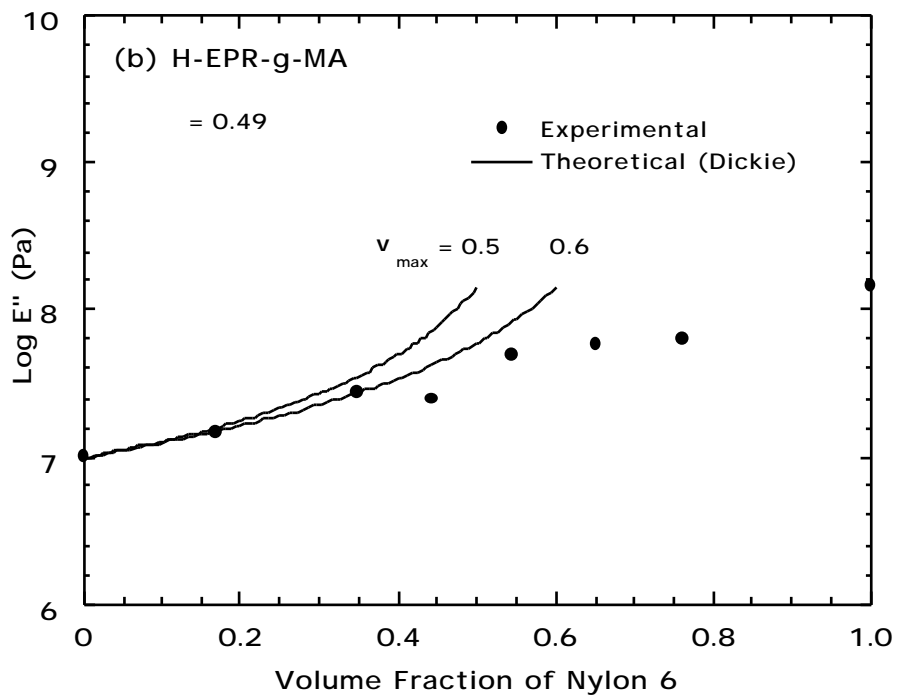
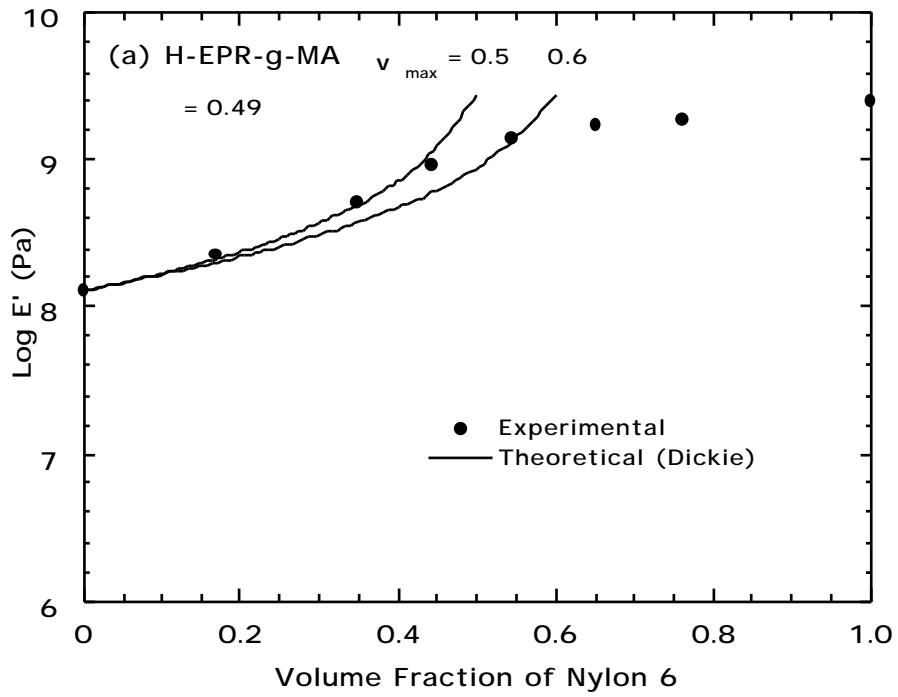


Fig. 3 Effect of nylon 6 content on: (a)  $E'$  and (b)  $E''$  for blends based on H-EPR-g-MA. Theoretical values were calculated by assuming that rubber phase is matrix phase and nylon 6 phase is dispersed phase.

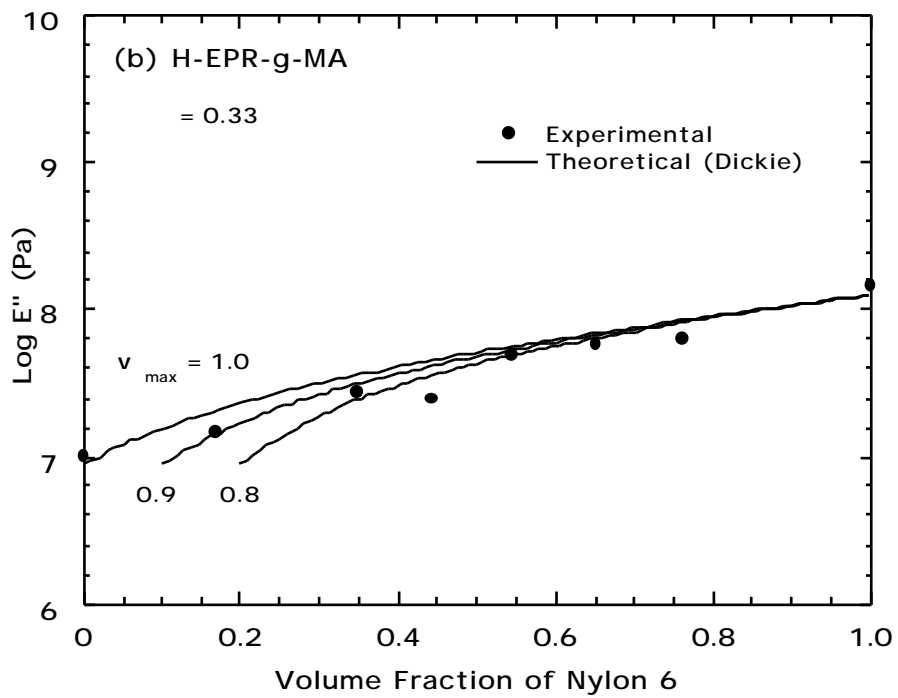
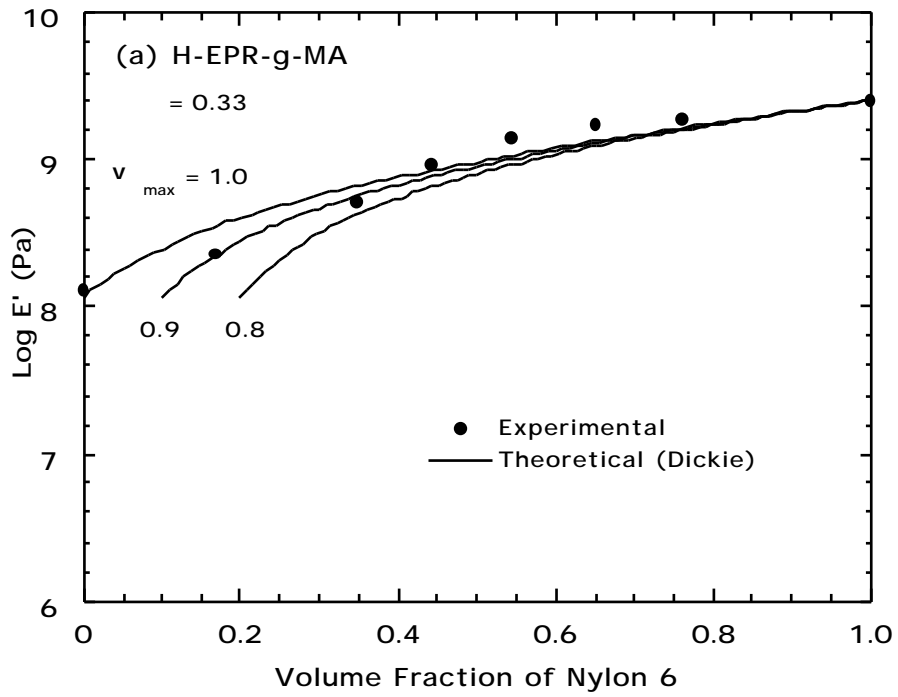


Fig. 4 Effect of nylon 6 content on: (a)  $E'$  and (b)  $E''$  for blends based on H-EPR-g-MA. Theoretical values were calculated by assuming that nylon 6 phase is matrix phase and rubber phase is dispersed phase.

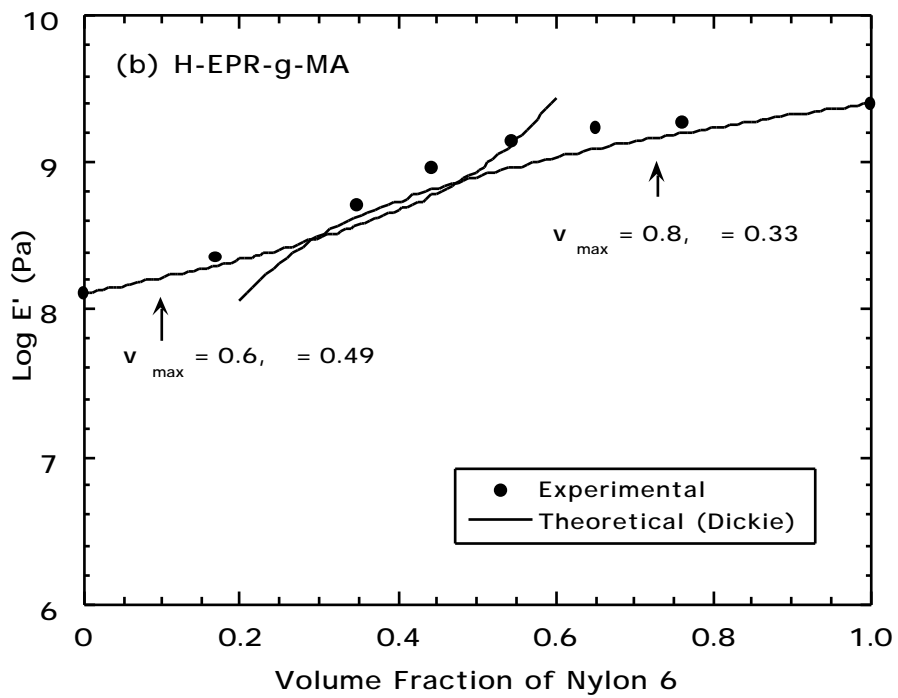
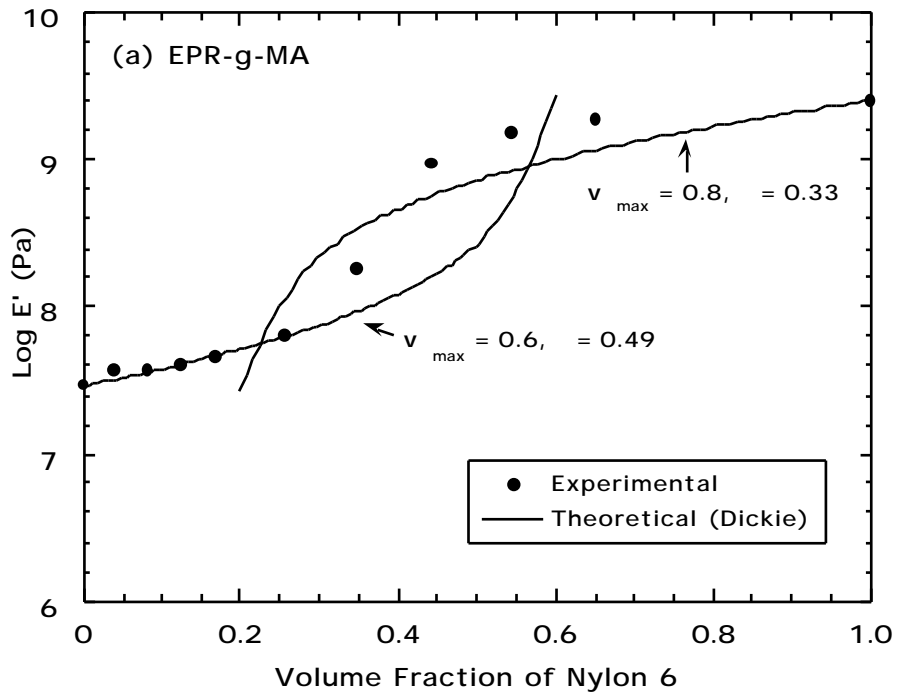


Fig. 5 Dependence of  $E'$  on nylon 6 content for the blends based on: (a) EPR-g-MA and (b) H-EPR-g-MA. Curves were calculated by Dickie equations.

## Reference

1. Dickie, R. A., *J. Appl. Polym. Sci.* **17**, 45 (1973)
2. Kerner, E. H., *Proc. Phys. Soc.*, **69B**, 808 (1956)
3. Dickie, R. A., *J. Appl. Polym. Sci.* **17**, 65 (1973), p. 76

## Chapter 7 Conclusion and development

### 7.1 Thermodynamic criteria for blend miscibility

The Gibbs free energy for mixing a unit volume of monodispersed polymers A and B is expressed by

$$g_{\text{mix}} = B_A B + RT \frac{A}{M_A} \ln \phi_A + \frac{B}{M_B} \ln \phi_B$$

where  $B$  is a binary interaction energy density,  $R$  is the gas constant,  $T$  is the absolute temperature,  $\rho_i$  is the density,  $\phi_i$  is the volume fraction, and  $M_i$  is the molecular weight of component  $i$ . The first term on the right-hand side is Hildebrand-Scatchard- van Laar type heat of mixing and the second term is entropy of mixing of Flory and Huggins.  $B$  is an excess free-energy term when the heat of mixing and other noncombinatorial effects are put together.  $B$  is preferably used rather than the binary interaction parameter,  $\chi$ , because it depends on a reference volume,  $V_{\text{ref}}$  which is arbitrarily defined, as follows:

$$B = \frac{BV_{\text{ref}}}{RT}$$

$g_{\text{mix}}$  must be negative for equilibrium miscibility and its second derivative in terms of composition must be positive for stability.

$$\frac{d^2 g_{\text{mix}}}{d\phi^2} = -2B + RT \left( \frac{A}{M_A} + \frac{B}{M_B} \right)$$

The combinatorial entropy always favors mixing, but the entropy term is almost negligible at high molecular weight of most commercial polymers. Accordingly, the miscibility depends on  $B$  parameter. Miscibility reaches by exothermic interaction, immiscibility typically caused by endothermic interactions.

Critical condition is attained when the third derivative of  $g_{\text{mix}}$  with respect to composition is equal to zero.  $B$  parameter at the critical condition is expressed by the following:

$$B_{\text{critical}} = \frac{RT}{2} \sqrt{\frac{A}{(\overline{M}_w)_A}} + \sqrt{\frac{B}{(\overline{M}_w)_B}}^2$$

where  $(\overline{M}_w)_i$  is the weight-average molecular weight. Overall energetic contribution to mixing,  $B$ , must be less than  $B_{\text{critical}}$  for miscibility.

The example of miscible blends is poly(2,6-dimethyl-1,4-phenylene oxide), PPO, and polystyrene, PS. One phase is observed for the blends because the interaction energy is so favorable.

When the  $B$  parameter exceeds the critical value, a two-phase mixture is observed.

If the difference between  $B$  and  $B_{\text{critical}}$  is not so large, the interfacial tension is small and the fine dispersion can be yielded. Such blends showed strong interface with large interfacial thickness. The example of this immiscible blend is mixture of polycarbonate, PC, and Acrylonitrile-butadiene-styrene copolymer, ABS. When the  $B$  becomes much larger than the critical value, the interfacial tension increases and the size of the domain becomes larger. Interfacial thickness decreases and the interface becomes weaker. The example of such incompatible blends is mixture of nylon and ABS. The properties of incompatible blends are inferior as the dispersion becomes grosser and the interface is weaker. The performance of the incompatible blends can be improved, when finer dispersion and stronger interface is obtained by use of compatibilization.

## 7.2 Prediction and analysis of interfacial properties

### 7.2.1 Interfacial tension and interfacial thickness

Binary interaction energies are important to determine the phase behavior of polymer blends, which is not only miscible but also phase separated. Interface between phases is strongly affected by interaction energies: morphology in the melt is determined by interfacial tension using  $B$ , adhesion in the solid state is determined by interfacial thickness through  $B$ . Helfand and Tagami proposed a quantitative expression of interfacial properties by thermodynamic interaction energy. The interfacial thickness is described by Helfand and Sapse as follows:

$$= \sqrt{\frac{2RT}{B} \left( \frac{1}{A} + \frac{1}{B} \right)} \quad (\text{A})$$

where  $B$  is the interaction energy density, and is related to the dimension of the polymer coil as followings:

$$= \sqrt{\frac{1}{6} \left( \langle r_i^2 \rangle / M_i \right)^{1/2}} \quad (\text{B})$$

where  $\langle r_i^2 \rangle$  is the mean-square unperturbed end-to-end chain distance and  $M_i$  is the molecular weight.

The interfacial tension is expressed as follows:

$$= \sqrt{\frac{RTB}{2} \left( \frac{1}{A} + \frac{1}{B} \right)} \left[ 1 + \frac{1}{3} \left( \frac{A - B}{A + B} \right)^2 \right] \quad (\text{C})$$

infinite molecular weight for both components is assumed for Eqs. (A) and (B). However, theory was extended to finite molecular weight by Broseta.

Predictions of and have been compared to the experimental values. The measurements are difficult and require extreme care in experiments. For example, predictions of and for blends of PC and SAN were compared to the experimental values from neutron reflectivity and capillary thread instability. Prediction of for PPO/SAN blends agrees with experimental results from neutron reflectivity. Merfeld et al [1] studied interfacial thickness

in bilayers of poly(phenylene oxide) and styrenic copolymers of styrene-acrylonitrile (SAN) and styrene-maleic anhydride (SMA) based on the theory of Helfand and Tagami. The theoretical predictions using a mean field binary interaction model agree with experimental values from neutron reflectivity.

### 7.2.2 Theory of droplet deformation and breakup

Taylor observed that the drops break, when the radius of drops is great enough or when the rate of distortion is high for the mixtures where Newtonian liquids is suspended in another Newtonian liquid. Droplet breakup is affected by viscosity ratio,  $p$ , (the viscosity of the dispersed phase)/(the viscosity of the matrix), the type of flow, and the capillary number,  $C_a$ . The capillary number,  $C_a$ , is the ratio between the deforming stress  $\dot{\gamma}_m$  imposed by the flow and the interfacial forces  $\sigma/R$ , where  $\sigma$  is the interfacial tension and  $R$  is the radius of the drop.  $C_a$  is expressed as:

$$C_a = \dot{\gamma}_m R / \sigma$$

If  $C_a$  is small, the interfacial forces dominate and a steady drop shape develops. The drop becomes unstable and breaks, if  $C_a$  becomes larger than a critical value,  $C_{a,crit}$ . Taylor also defined a dimensionless group  $E$  as follows:

$$E = C_a [(19p + 16) / (16p + 16)]$$

where  $p$  is viscosity ratio (the viscosity of the dispersed phase)/(the viscosity of the matrix,  $\dot{\gamma}_m$ ).

When breakdown and coalescence are balanced at equilibrium, the particle size at equilibrium,  $d_e$ , is expressed by Tokita as follows:

$$d_e = \left( \frac{24P_r}{12} \right)^{1/2} + \left( \frac{4P_r E_{DK}}{12} \right)^{1/2} \frac{1}{d}$$

where  $\tau_{12}$  is the shear stress,  $\sigma$  is the interfacial tension,  $E_{DK}$  is the bulk breaking energy,  $\phi_d$  is the volume fraction of the dispersed phase, and  $P_r$  is the probability that a collision will result in a coalescence. As the shear stress increases, the interfacial tension decreases, and the volume fraction of the dispersed phase decreases, the particle size decreases.

Elmendorp and Van der Vegt described the shear-induced coalescence of spherical droplets. The critical coalescent time,  $t_c$ , which is defined as the time between arrival of a droplet and breakup of an intervening film, is expressed as follows:

$$t_c = \left( \frac{3}{2} \frac{R}{h_c} \right) \ln \left( \frac{R}{2 h_c} \right)$$

where  $h_c$  is the critical separation distance.

Two mechanisms are proposed for dispersion of one liquid to another by Rumscheidt. One is stepwise equilibrium mechanism of steady and repeated breakup at  $C_a$  crit. And the other, which is known as capillary instability, is the disintegration of a deformed fine thread into a series of fine droplets. The capillary instability is observed under transient shear conditions or after cessation flow.

### 7.3 Theory of interfacial properties for compatibilized blends

Noolandi and Hong studied interfacial properties of immiscible homopolymer blends in the presence of block copolymers [2]. They studied the emulsifying effect of block copolymer in immiscible homopolymer blends, using a general formalism for inhomogeneous multicomponent polymer systems. The calculation shows the reduction in interfacial tension with increasing the block concentration for a range of copolymer and homopolymer molecular weights. It is clear that the calculated interfacial density profiles

show much exclusion of homopolymer from the interphase region when the molecular weight of the block copolymer is used. The critical concentration of block copolymer required for micellar aggregation in homopolymer phase is also estimated.

Vilgis and Noolandi demonstrated theory of homopolymer-blockcopolymer blends based on thermodynamic behavior of a blend containing homopolymer A, homopolymer B, and arbitrary block copolymer CXY, and solvent [3]. The behavior of the diblock copolymer near the interface was studied in detail. It is demonstrated that the longer copolymers localize more strongly at the interface. The interfacial tension decreases and the width of the interface increases if special relationship between the parameters are chosen. Under such circumstances, CXY can be considered as a universal compatibilizer, if the concentration is below the critical micelle concentration. They suggested the design of a universal compatibilizer, which makes use of preferential repulsive interactions between the homopolymers and the different blockcopolymer.

#### **7.4 Conculusions**

In Chapter 2, the fracture of blends of nylon 6 and maleated ethylene-propylene rubber was examined by both the Izod impact test and a single-edge notch three-point bend (SEN3PB) instrumented Dynatup test. The effects of EPR-g-MA content, ligament length, method of fracture surface measurement, sample thickness and fracture position in the molded bar on the fracture behavior were investigated. The data were analyzed by plotting the specific fracture energy ( $U/A$ ) as a function of ligament length. The blends containing a high portion of EPR-g-MA in the rubber phase were found to be super tough over the whole range of ligament lengths and under all test conditions. However, a ductile-to-brittle

transition was observed with ligament length for marginally tough blends which contained a low content of EPR-g-MA in the rubber phase and had a ductile-brittle temperature near or above room temperature; the specimens with short ligament length fractured in a ductile manner, while the specimens with long ligaments showed brittle fracture. The transition ligament lengths were found to be dependent on the rubber particle size. The dual mode of fracture was rationalized by equations for ductile yielding and brittle crack propagation; values of yield stress and critical intensity factor were estimated from these model equations. The dissipative energy density,  $u_d$ , was more sensitive to rubber particle size, sample thickness and location in the molded bar than the limiting specific fracture energy,  $u_o$ . There is a good correlation between the standard Dynatup impact strength and the parameter  $u_d$  for the gate end specimens.

In Chapter 3, fracture toughness for blends of nylon 6 with maleated ethylene-propylene rubber (EPR-g-MA) and maleated styrene-hydrogenated butadiene-styrene triblock copolymer (SEBS-g-MA) was investigated using a single-edge notched three-point bend (SEN3PB) instrumented Dynatup test. The effects of rubber particle size and ligament length on the fracture behavior were examined. The blends in which the rubber particles size is less than 0.7  $\mu\text{m}$  fracture in a ductile manner over the whole range of ligament lengths while blends with particles larger than 0.7  $\mu\text{m}$  show a ductile-to-brittle transition with ligament length. In this regime, ductile fracture was observed for specimens with short ligaments while brittle fracture was seen for those with long ligaments. The ductile fracture behavior was analyzed using the essential work of fracture (EWF) model. The limiting specific fracture energy,  $u_o$ , for EPR-based blends was higher than that for SEBS-based blends, while the dissipative energy density,  $u_d$ , for the latter was larger than that for the

former. Larger fracture energies for the SEBS-based blends than the EPR-based blends can be explained by larger  $u_d$  of the SEBS-based blends. The critical strain energy release rate,  $G_{IC}$ , and the plane-strain critical stress intensity factor,  $K_{IC}$ , were obtained from the brittle fracture behavior. Both of these fracture parameters increase with decreasing the rubber particle size for either blend systems. The  $G_{IC}$  and  $K_{IC}$  parameters have similar values regardless of rubber type where the rubber particle size is fixed. The transition ligament length, which increases with decreasing rubber particle size, was found to be near the size criterion for plane-strain conditions for both blend systems. This suggests that the ductile-to-brittle transition along the ligament length corresponds to the size criterion for plane-strain conditions based on the fracture mechanics parameters.

In Chapter 4, blends of nylon 6 and ethylene-propylene rubber, grafted with maleic anhydride, (EPR-g-MA) were prepared using a melt blending process. For certain compositions, nylon 6 forms finely dispersed particles due to the reaction of the polyamide amine end groups with the grafted maleic anhydride, that have potential to reinforce elastomer matrix. This study focuses on the effects of the content of nylon 6 on the rheological, morphological and mechanical properties of such blends where nylon 6 is the dispersed phase. Transmission electron microscopy was used to determine blend morphology. Mechanical properties were examined by stress-strain measurements and dynamic mechanical thermal measurements; the modulus is compared to values calculated from theory. The addition of magnesium oxide causes significant improvement in tensile properties of these blends.

In Chapter 5, blends of nylon 6 with maleated ethylene-propylene rubber (EPR-g-MA) were prepared by melt blending over the whole composition range. The reaction of the polyamide amine end groups with the grafted maleic anhydride has the potential to form thermoplastic elastomers (TPE) with controlled morphology and chemical bonding between the phases. This study focuses on the effects of nylon 6 content and crystallinity of the maleated rubber on morphological, thermal and mechanical properties of these blends. Maleated EPR with some ethylene crystallinity (H-EPR-g-MA) results in blends which have better mechanical properties than those based on amorphous EPR-g-MA. Strain-hardening and cold-drawing were observed for both blend systems in the intermediate and polyamide-rich composition range. These effects are found to be enhanced by ethylene crystallinity in the blends. Modulus values from stress-strain measurements and dynamic mechanical thermal measurements are compared to predictions using a model by Hill for composite materials. Blends based on rubber with high ethylene crystallinity give better agreement with the model than those based on amorphous rubber. Phase inversion compositions derived from TEM observation, modulus measurements are compared to those calculated from the model of Avgeropoulos.

In Chapter 6, the theoretical analysis by Dickie model depends on the polymer matrix and dispersed phase. Dickie model requires two individual  $v_{\max}$  for either composition depending on the matrix phase and cannot describe the phase inversion composition for the blends of nylon 6 with maleated rubber. Analysis using Hill model, which is shown in chapter 4 and 5, provides continuous analysis for all composition range and more useful method than that with Dickie model.

## **7.5 Future development**

Polymer blends will be developed scientifically and commercially for various fields such as high-performance materials with various functionalities, recycling plastics, and biodecomposite materials, and so on. Technologies of polymer blends will be sophisticated by combination of several other immerging technology i.e., nano-technology, supramolecules, biology, and so on.

## **References**

- [1] Merfeld GD, Karim A, Majumdar B, Satija SK, Paul DR. J. Polym. Sci.:part B: Polymer Physics 1998;36:3115.
- [2] Noolandi J, Hong KM. Macromolecules 1982;15:482.
- [3] Vilgis TA, Noolandi J. Macromolecules 1990;23:2941.

## **ACKNOWLEDGMENTS**

The author wishes to express the greatest acknowledgment to Prof. Dr. Donald R. Paul and Dr. Henno Keskkula for their sincere direction, discussion and encouragement. The author also would like to express sincere gratitude to Prof. Dr. Hiroyuki Nishide, Prof. Dr. Hiroyuki Kawada and Associate Prof. Dr. Shinji Takeoka for their helpful suggestion and their advice as members of judging committee for the dissertation.

This work was supported by Bridgestone Corporation. The author would like to express sincere appreciations to Mr. Akeshi Noda, Dr. Yoshihide Fukahori, Dr. Hideo Nakauchi, Mr. Tsuyoshi Hamanaka, Mr. Shingo Kato and Mr. Toshiki Takizawa for their permission to make research and to write the dissertation.

This work has been performed at the University of Texas at Austin (UT). Grateful acknowledgment is made to Dr. Yoshihiro Kayano, Dr. Ryan Kudva, Dr. Gregg Wildes, Dr. Wes Hale, Dr. Toru Harada, Dr. Matt Laura and Dr. Thomas Pressly for their helpful and valuable discussions at UT.

Finally, the author expresses his gratitude to his parents, Mr. Heiichi Okada, Mrs. Kouko Okada, wife Mayumi and daughter Haruka for their continuous help.

Osamu Okada

June 2003